2F

BNWL-2127
UC-70
UC-32

MULTICOMPONENT MASS TRANSPORT MODEL: THEORY AND NUMERICAL IMPLEMENTATION (DISCRETE-PARCEL-RANDOM-WALK VERSION)

by

S. W. Ahlstrom
H. P. Foote
R. C. Arnett(a)
C. R. Cole
R. J. Serne

May 1977

This report is based on work sponsored by the Atlantic Richfield Hanford Company under Energy Research and Development Administration Contract EY-76-C-06-1830

Battelle, Pacific Northwest Laboratories
Richland, Washington 99352

(a) Atlantic Richfield Hanford Company, Richland, Washington

BLANK PAGE

SUMMARY

The Multicomponent Mass Transfer (MMT) Model is a generic computer code, currently in its third generation, that was developed to predict the movement of radiocontaminants in the saturated and unsaturated sediments of the Hanford Site. This model was designed to use the water movement patterns produced by the unsaturated and saturated flow models coupled with dispersion and soil-waste reaction submodels to predict contaminant transport.

This report documents the theoretical foundation and the numerical solution procedure of the current (third) generation of the MMT Model. The present model simulates mass transport processes using an analog referred to as the Discrete-Parcel-Random-Walk (DPRW) algorithm. The basic concepts of this solution technique are described and the advantages and disadvantages of the DPRW scheme are discussed in relation to more conventional numerical techniques such as the finite-difference and finite-element methods. Verification of the numerical algorithm is demonstrated by comparing model results with known closed-form solutions. A brief error and sensitivity analysis of the algorithm with respect to numerical parameters is also presented. A simulation of the tritium plume beneath the Hanford Site is included to illustrate the use of the model in a typical application.

ACKNOWLEDGMENTS

The authors wish to express their gratitude to the Scientific Research Programs Section of the Atlantic Richfield Hanford Company (ARHCO) for the funding that made this document and much of the model development possible. The review and comments of R. A. Deju, R. G. Baca, and G. S. Barney of ARHCO, J. R. Eliason, J. R. Raymond and D. B. Cearlock of Battelle and R. W. Nelson of Boeing Computer Services are also gratefully acknowledged.

CONTENTS

FIGURES

BLANK PAGE

SYMBOLS

Symbol	Description	Section
a	Dispersion length scalar [L]	II
A,B,C	Unspecified elemental species in solution	III
a,b	Experimentally determined combined rate constants [variable units]	III
AW	Atomic weight of a given species	III
b	Number of backward steps in a random walk [Dimensionless]	II
D	Dispersion coefficient of component of the hydrodynamic dispersion tensor [$L^2 T^{-1}$]	II
$\bar{D}$	Hydrodynamic dispersion tensor [L^2T^{-1}]	II
d_{rms}	Root-mean-square distance moved by parcel ensemble with respect to the advective flow system by dispersive mechanisms [L]	III
$E(n_i)$	Expected number of parcels within a given interval Δx [Dimensionless]	IV
f	Number of forward steps in a random walk [Dimensionless]	II
G	A factor to convert from system units to user desired concentration units [Dimensionless]	III
H	Aquifer thickness [L]	II
J(x)	Vertically-averaged horizontal diffusive flux [$ML^{-2}T^{-1}$]	IV
$\bar{j}$	Mass flux relative to $\bar{v}$ (diffusive flux) [$ML^{-2}T^{-1}$]	II
K_1, K_2	Experimentally determined chemical equilibrium constants [Dimensionless]	III
ℓ	Random walk step length [L]	II
m	Random walk position index	II

n	Number of particle displacements per unit time $[T^{-1}]$	II
M	Mass constant of a given elemental species within a cell [Moles L^{-3}]	III
$M(x)$	Mean position of $\zeta(x_2 t)$	II
N	Number of steps	II
N_p	Total number of parcels released in system [Dimensionless]	III,IV
N_t	Number of steps in time	III
$P(m,N)$	Probability of residing at location m after N steps of a random walk [Dimensionless]	III
P	Probability distribution function [Dimensionless]	III,IV
Q	Total mass released in a system or assigned to a particle set [M]	II,IV
$\bar{q}$	Darcian velocity of groundwater $[L\ T^{-1}]$	II
$[R]_g^h$	A random number in the range g to h	III
r	Source/sink term $[ML^{-3}T^{-1}]$	II,IV
r	Reaction rate expression $[ML^{-3}T^{-1}]$	III
S.E.	Standard error	IV
t	Time [T]	II
u	Particle diffusion velocity = $1/2\ n\ell$ $[L\ T^{-1}]$	II
u	Advective velocity component in the x direction $[L\ T^{-1}]$	III
V	Volume of a given cell $[L^3]$	III
v	Advective velocity component in the y direction $[L\ T^{-1}]$	III
v	Advective velocity $[LT^{-1}]$	IV
$\bar{v}$	Mass average pore velocity of groundwater $[L\ T^{-1}]$	II

Δt	Computational time increment [T]	III
$VAR(\eta_i)$	The variance of the expected value [Dimensionless]	IV
X,Y,Z	Fixed orthogonal coordinate system	II,III
X',Y',Z'	Orthogonal lagrangian coordinate system moving with advective flow	III
x',y',z'	Spatial coordinate locations with respect to to lagrangian system [L]	III
x,y,z	Spatial coordinate locations with respect to fixed system [L]	II,III
$\bar{x}$	Mean value of parcel displacements [L]	IV
x_j	Displacement of parcel j [L]	IV
Δx	Grid spacing used to resolve the concentration distribution	IV
w	Mass fraction of solute [Dimensionless]	II
w	Advective velocity component in the z direction [L T^{-1}]	III
α,γ	Experimentally determined exponents indicating the reaction rate order [Dimensionless]	III
∇	Del operator	II,III,IV
δ	Dirac delta function [Dimensionless]	IV
ε_σ	Relative standard deviation error = $1-\sigma_m/\sigma$	IV
ε_v	Error variance or variance of the computed function about the true function	IV
λ	First order decay constant [Dimensionless]	III
η_{ijl}	Number of parcels within cell (i,j,l)	III
η_i	Number of parcels between $x_i-\Delta x/2$ and $x_i+\Delta x/2$ [Dimensionless]	IV
ϕ	Angle between XZ plane and the advective displacement vector	III

ρ	Mass density or concentration of the transport solution [M L^{-3}]	II,III,IV
ρ_{io}	Expected concentration from the analytical solution of the convection-diffusion equation [M L^{-3}]	IV
ρ_i	Computed concentration at x_i; $\rho_{io} = \eta_i / N_p \Delta x$	IV
θ	Angle between the XY plane and the advective displacement vector	III
σ	Convection diffusion equation length parameter [L] or standard deviation of a normal distribution	IV
σ_m	Standard deviation of computed distribution [L]	IV
$\xi_p^{k,n}$	Mass of a given constituent, k, associated with a particular parcel, p, at time level n [M] or [Curies] for radionuclides	III
ν	Volumetric moisture content or porosity in the case of saturated flow [Dimensionless]	II,III
$-\zeta,+\zeta$	Lower and upper limit of a random number population used in determining dispersion [L]	III

Superscripts

k	The transported species index (k= 1,2,3...K) where K is the total number of constituents present in the system	III
k'	Radioactive decay daughter of species k	III
n	Time level index (n = 1,2,3...N_t) where N_t is the number of time increments to be compared	III
s	Number of times data has been passed through a moving average filter	IV
*	An intermediate value indicator	III

Subscripts

b	Recharge boundary indicator	II
i,j,l	Nodal position index in the X,Y,Z directions respectively	III
i	Location index along the x axis	IV
L	Indicator of direction with the flow	II,III
p	Parcel index (p = 1,2,3...N_p) where N_p is the total number of parcels used to represent a given quantity of matter	III
rms	root-mean-square indicator	II,III
T	indicator of direction transverse to flow	II,III

BLANK PAGE

I. INTRODUCTION

Since 1944 the Hanford Site located in south-central Washington, has been a location for radioactive waste storage, reactor development, and chemical separation facilities for the production and purification of plutonium needed in the development of nuclear weapons.[1] These activities have involved the disposal of some radioactive waste to surface or near surface disposal sites with a consequent contamination of some of the aquifers underlying the Hanford Site. An extensive groundwater monitoring program conducted over the years at Hanford indicates that the movement of radioactive contaminants through the groundwater flow system toward biosphere uptake points (primarily the Columbia River) is limited.[2] Nevertheless, a program is being conducted to assure continued isolation of such contaminants from the biosphere both now and in the future.

At present, the Atlantic Richfield Hanford Company operates the waste management activities at Hanford under contract to the U.S. Energy Research and Development Administration. A Groundwater Management program has been instituted in support of the waste management activities to:

1. identify potential ways in which groundwater can come in contact with high-level radioactive wastes;
2. assess data gathering and computer modeling requirements needed for long-term prediction of subsurface contaminant migration from high-level radioactive wastes areas into and through the groundwater flow system;
3. examine the potential impact to the high-level radioactive waste areas resulting from past, present, and projected activities at Hanford, potentially hazardous incidents, and potential or existing water use activities adjacent to or within the Hanford Site; and
4. improve the management of the Hanford flow regime and identify methods of controlling accidental contaminant releases and preventing the contaminant from reaching the biosphere.

The procedure used in technical evaluation and management of the Hanford groundwater system is shown in Figure 1. System characterization is established through data collection and interpretation which lead to a conceptual model of the system. Such a conceptual model may be used directly for environmental assessment and management decision purposes or it may first be translated into mathematical form amenable to analytical or computer solution methods.

The conceptual model of the Hanford groundwater system and the mathematical modeling capabilities needed for better understanding of possible contaminant movement are discussed in detail in a report by Arnett et al.[3] In that report the groundwater predictive models are divided into the major categories of fluid flow and contaminant transport. The point was made that except perhaps for extreme cases the fluid flow patterns could be assumed independent of the concentration of any solutes that might be present. This allows the formulation of a decoupled transport model. In practical terms, this means that a mass conservative fluid flow field can be determined over the entire simulation period and the resultant information preserved and input to the transport model at a later time.

Early in the Hanford Groundwater Modeling Program, three independent but interrelated models were developed by Battelle, Pacific Northwest Laboratories:

1. the Partially-Saturated-Transient (PST) Flow Model,[4]
2. the Variable-Thickness-Transient (VTT) Flow Model,[5] and
3. the Multicomponent-Mass-Transfer (MMT) Transport Model.

The PST Model was designed to predict moisture movement in the partially saturated zone as a function of time and space. Although the PST Model effort was valuable in obtaining insight into partially or unsaturated flow phenomena certain limitations in the numerical solution methods and the applicability of the formulation to the entire range of Hanford unsaturated flow problems prevented PST from becoming an operational management model. Work is underway both at Battelle and at the Atlantic Richfield Hanford Company to develop a set of operational flow models applicable to the unsaturated flow regime.

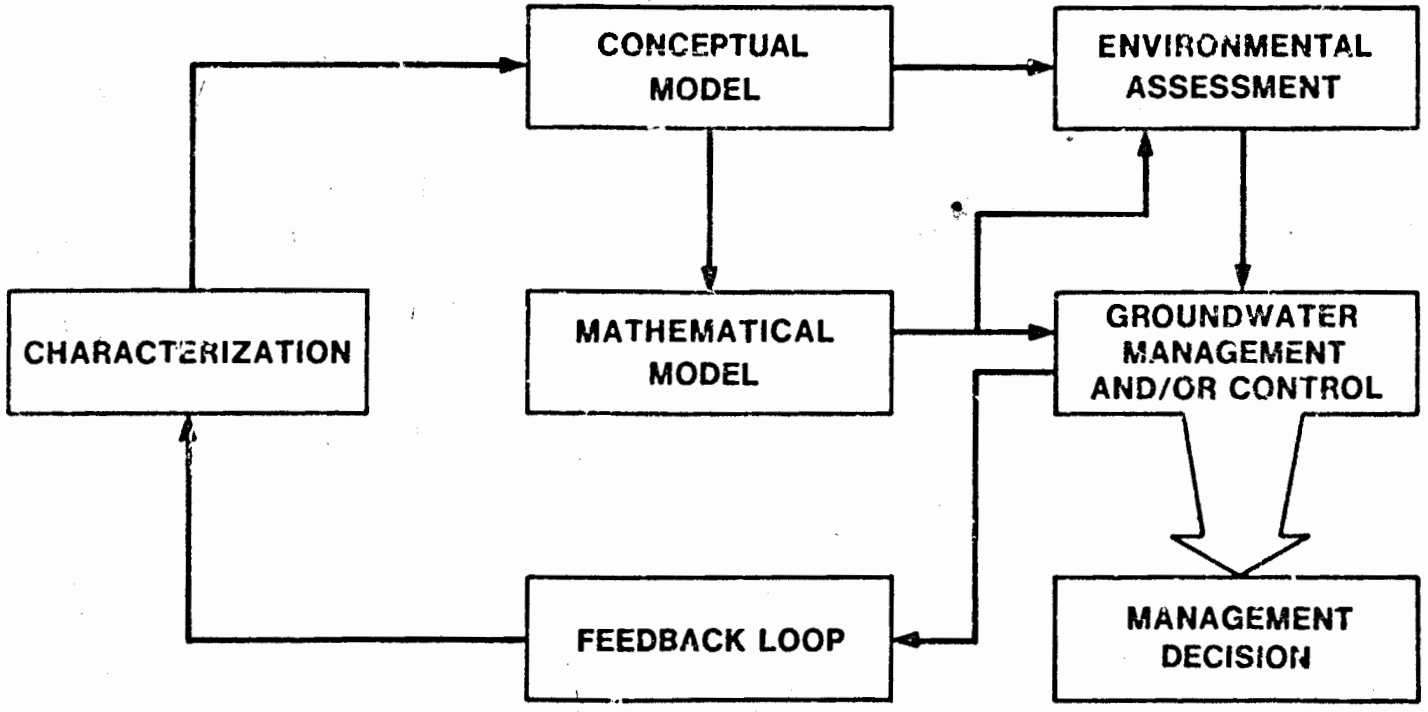

FIGURE I-1. Hanford Groundwater System Technical Evaluation and Management Procedure

The VTT Model predicts the two-dimensional flow patterns of groundwater in the unconfined aquifer. The MMT Model is designed to combine either the moisture movement rates generated by an unsaturated flow model or the groundwater movement data generated by a saturated flow model (VTT) with dispersion and pertinent soil-waste reactions to predict the spatiotemporal distributions of important radiocontaminants in either the saturated or unsaturated regime.

This report describes the theoretical basis and the numerical implementation of the third developmental generation of the MMT Model. This generation of the model differs from previous versions primarily in the type of numerical procedure used to create the simulation. The new numerical algorithm is called the Discrete-Parcel-Random-Walk (DPRW) technique. The mnemonic selected for this version of the model to differentiate it from previous generations is MMT-DPRW.

The MMT chemical submodel assumes that all dissolved or suspended material can be segregated into two categories: 1) minerals naturally present in relatively large quantities in groundwater systems (macroions) and 2) species that are present only in trace quantities (microions). Macroion species, by definition, exist in concentrations large enough to significantly affect the chemical behavior of each other and any microions present. Microion species are assumed to exist only in minute quantities relative to macroion concentrations and do not appreciably affect the chemistry of the macroions or other microions in the system. Important radiocontaminants can usually be assumed to be present in microion concentrations.

In order to be compatible with the VTT Flow Model, the MMT code was initially formulated to handle two-dimensional vertically-averaged systems. Although this assumption neglects vertical flow components in the Hanford unconfined aquifer, it does consider the varying aquifer thickness (as does the VTT Flow Model). The current formulation can easily and economically be extended to three dimensions, but this modification is presently awaiting the completion of an operational three-dimensional Hanford groundwater flow model and sufficient field data for calibration and verification. The MMT-DPRW

Model has yet to be applied to a partially saturated test case so that adjustments may still be needed. Partially saturated applications of MMT-DPPW are planned for the near future.

The conceptual design of the MMT-DPRW Model is discussed in the following section. In subsequent sections the DPRW computational scheme is detailed; the numerical verification, error and sensitivity analysis of the new algorithm are discussed; and a preliminary application of the model to the Hanford system is given. Some details of the chemical submodel are discussed in the appendix.

BLANK PAGE

II. THEORETICAL DEVELOPMENT OF THE MODEL

The development of a mathematical model of a given physicochemical system or process may be approached using two different methods. One approach first attempts to describe the system with a representative mathematical equation and then tries to solve this equation with appropriate boundary conditions, thereby creating the simulation. The other approach attempts to simulate reality more directly by defining numerical structures that represent specific constituents or physical structures of the system and by allowing these numerical representations to react and interact as determined by the physical driving forces or constraints that are active in the real system.

The first approach is termed the "model-equation" method and usually leads to complex partial-differential equations which must be solved numerically, most often by using finite-difference or finite-element techniques. The second or "direct-simulation" method normally requires only that an efficient bookkeeping structure be established to control the response of the numerical representations so that all physical constraints are satisfied. Each approach, if properly implemented, can yield an adequate simulation of reality, but each approach has certain inherent advantages and disadvantages.

Initially, the development of a subsurface transport code for Hanford was based on the traditional model-equation type of approach. A preliminary model was developed that used a finite-difference, alternating-direction-implict (ADI) numerical solution technique, but it was soon recognized that the numerical dispersion properties of this method prohibited its widespread use. Next, the particle-in-a-cell (PIC) numerical algorithm used by Pinder and Cooper[6] was investigated. This method eliminated some numerical dispersion problems, but it tended to have some stability and mass-conservation problems for many required applications.

In 1973, developmental emphasis shifted toward adopting a direct-simulation type of transport analog originated by Eliason and Foote[7] for modeling thermal transport in coastal waters. A version of this numerical technique was adapted to operate in subsurface flow regimes and subsequently formed the basis of the current version of the MMT model. Its primary advantages are:

- always mass-conservative
- no cumulative numerical dispersion
- inherent numerical stability
- facilitates handling of multicomponent systems.

The conceptual development of workable mathematical models using both the model-equation and direct-simulation approaches is outlined below. Although the model equation based viewpoint was not used in the formulation of the current model, a discussion of this approach is included to provide a point of reference and a basis of comparison for the following explanation of the direct-simulation analog.

Although the current computerized version of MMT is a two-dimensional vertically average formulation, the conceptual model development is presented in three-dimensions in anticipation of future model updates. Assumptions specific to the vertically averaged version are discussed when necessary. A brief analysis of the advantages and disadvantages of the direct approach follows the two conceptual descriptions.

Fundamentally, the MMT Model and all other mass transport models are based on the law of conservation of mass. This law can be expressed in non-mathematical terms as:

The rate of change of mass concentration of chemical species k within a given control volume	=	the net advective flux of the species k into the control volume
	+	the net diffusive flux of species k into the control volume

+ the net rate of production of species k within the control volume. (II-1)

THE MODEL-EQUATION APPROACH

A mathematical statement of Equation II-1 is usually referred to as an equation of continuity. The general form of the equation of continuity for a nonisothermal multicomponent fluid consisting of k chemical species can be written as:[3]

$$\frac{\partial \rho^k}{\partial t} = -(\nabla \cdot \rho^k \bar{v}) - (\nabla \cdot \bar{j}^k) + r^k \qquad k = 1,2,3\ldots k \qquad \text{(II-2)}$$

where

ρ^k = the mass concentration of species k [M/L^3]
t = time [T]
∇ = the Del operator
$\bar{v}$ = the mass average pore velocity of the fluid [L/T]
$\bar{j}^k$ = the mass flux of k relative to $\bar{v}$ (diffusive flux) [M/L^2T]
r^k = the net rate of production of species k within the control volume [M/L^3T].

The addition of k equations of this kind gives the equation of continuity for a mixture. Each term of Equation II-2 corresponds directly with the terms of Equation II-1. Equation II-2 is written in general terms and applies to both liquid and gaseous mixtures containing an arbitrary number of components in any ratio at any temperature and pressure. Practical models are by necessity much more limited. Before the simplifying assumptions necessary for a practical Hanford groundwater model are investigated, it may be instructive to discuss the significance and contribution of each term of Equation II-2.

Transport Equation Terms

The term on the left-hand side of Equation II-2 is called the transient term. It may be interpreted as the total rate of change of mass concentration of species k at a point in space at a given instance in time. The rate of change of concentration is generally assumed to be a function of temperature, pressure, and location as well as the concentration of any other species that might be present. If ρ^k does not change with time, this term is identically zero and Equation II-2 reduces to what is commonly called a steady-state mass balance. In the groundwater system beneath Hanford, solute distributions have been observed to be changing over a number of years. Since the primary function of a transport model is to predict and quantify these changes in solute concentrations, the steady-state assumption cannot be made. However, a hypothetical steady-state case can be postulated assuming that all artificial discharges are eliminated and that all natural sources of groundwater and solutes remain relatively constant.

The first term on the right-hand side of Equation II-2 is the advective term. This term represents a change in concentration of the system resulting from the gross movement of fluid in which species k is transported. The mass average velocity vector of the fluid mixture, $\bar{v}$, is a function of time, space, temperature, and the chemical composition of the mixture. If $\bar{v}$ is constant with respect to time, the flow field is said to be steady. For applications at Hanford, the assumption of a steady-flow field may be adequate for short-term simulations in the range of a few years because the changes that occur in the flow field are relatively slow in most locations. For longer simulations, the velocity field cannot reasonably be assumed to be constant. The assumption of stagnant groundwater conditions (i.e. stationary fluid, $\bar{v} = 0$) has very limited application within the Hanford system.

The second term on the right-hand side of Equation II-2 is the diffusive or relative flux term. This term represents the change in concentration at a point in the system resulting from molecular diffusion and mechanical dispersion.[9] Molecular diffusion is caused by the random motion of

molecules when a concentration gradient is present. Mechanical dispersion results from the irregular porous structure and other larger nonhomogeneities in a subsurface flow system. The contribution of molecular diffusion is believed to be very minor for regional transport analyses, but the contribution of mechanical dispersion is usually large enough to make the relative flux term significant. The types of mechanical dispersion mechanisms that are important depend upon the scale of a given problem. These mechanisms are discussed in more detail later in this section.

The last term is usually called the source/sink, reactive or nonconservative term. It represents all internal processes that tend to change the net amount of species k present in a control volume including injection, withdrawal, radioactive decay, and chemical reaction. The reactivity of a chemical system may be a function of temperature and any or all of the k mass concentrations in the mixture. Ideally, this term should consist of a series of rate expressions that represent all known mechanisms by which species k can react with its immediate environment. Species for which r^k is zero are referred to as conservative substances because they are neither produced nor consumed within a control volume. Nitrate is an example of a conservative species in groundwater systems, because it is essentially nonreactive and is simply carried along with the water. An example of a nonconservative species is ^{106}Ru which is lost from the system as a result of radioactive decay.

Simplifying Assumptions

Equation II-2 serves as the starting point to explain assumptions made to create a practical model for the Hanford subsurface system. These simplifications were made for one or more of the following reasons:

- A portion of the general equation, based on an analysis of the best available information, appeared to be relatively insignificant for the anticipated applications of the model.
- The quality of existing data or additional data that can be reasonably obtained does not justify considering anything above a certain level of complexity.
- A reduction in complexity was required to allow a computer simulation within reasonable time and economical constraints, based on present-day computing hardware limitations.

Each simplifying assumption will be denoted by italics when it appears in the text.

First, *it is assumed that the effects of changing atmospheric pressure will be negligible.* This should be a valid assumption for sub-surface water systems everywhere except within a few feet of the ground surface or near a well.

The velocity distributions required for a transport simulation can be derived from a flow model simulation or by analysis of the data produced by a fairly extensive field measurement program. Regardless of the method used the velocity field is determined prior to computing the transport simulation. *The assumption inherent in this practice is that the advection patterns are not dependent on the chemical composition or temperature of the solution.* In other words, the momentum, mass, and energy transport processes are decoupled. This assumption is valid for systems that are nearly isothermal and that contain relatively low concentrations of contaminants.

The decoupling simplification should usually be valid in the groundwater zone, but is probably not satisfactory near the ground surface where large temperature gradients are present or when some of the species present in the mixture are reacting and producing significant amounts of heat. For example, the heat producing decay of radionuclides and the high salt concentrations near a possible leak from a high-level waste storage tank may invalidate this assumption.

Resolution of flow patterns below a certain scale in large-scale environmental flow systems is usually not feasible when calculating or measuring advective fields. In surface water systems, the small-scale unresolved motion is usually referred to as turbulence. In porous media systems, analogous small-scale advective motion is called mechanical dispersion.[9]

Mechanical dispersion is often subdivided into micro- and macroscopic dispersion mechanisms.[10] Micro-dispersion occurs because the complicated network of interconnected passages that comprise the microstructure of soil causes a continuous division and re-division of a fluid mass as it flows

though the ground. Variations in local velocity, both magnitude and direction, along the tortuous flow paths and the velocity distribution within each pore then cause a contaminant to spread and occupy an ever increasing volume of the porous media.

Macro-dispersion is the apparent mixing produced by unresolved variations in the porous medium, such as local variations in lithologic units which cause changes in the direction and speed of groundwater flow. The magnitude of this mechanism is therefore often a function of the scale of porous material property identification[10] and it becomes more significant as the degree of nonhomogeneity of the medium increases. In a regionally sized heterogeneous groundwater system such as the Hanford unconfined aquifer, there is a strong likelihood that macroscopic dispersion is considerably more important than dispersion caused by micro-processes.

These two dispersion mechanisms achieve essentially the same result (i.e., spreading material) as molecular diffusion, but much more rapidly. In some respects the tortuous movement of fluid through the soil can be thought of as a random process, occurring on a larger scale, but having many characteristics in common with molecular scale diffusion. *Because of these similarities, it was assumed that the mechanical dispersion processes can be included with the molecular diffusion in the relative mass flux term,* $\bar{j}$. The combined effect of all dispersive and diffusive mechanisms is called hydrodynamic dispersion.[9]

If it is assumed that the relative mass flux can be adequately described by expressions having the form of Fick's First Law, then it can be expressed for species k as:

$$\bar{j}^{k} = -\rho \bar{\bar{D}}^{k} \nabla w^{k} \qquad \text{(II-3)}$$

where

ρ = total mass density of the solution $[M/L^3]$
$\bar{\bar{D}}^{k}$ = hydrodynamic dispersivity tensor $[L^2/T]$
w^{k} = the mass fraction of species k (ρ^{k}/ρ).

Inherent in Fick's First Law formulation are the assumptions that the mixture is an ideal solution and that only binary interactions at the molecular level are significant.

The dispersivity tensor, $\bar{\bar{D}}^k$, is generally a function of both space and time. *If the dispersion is assumed to be isotropic in the directions longitudinal and transverse to the direction of flow*, then the component of $\bar{\bar{D}}^k$ can be represented by:

$$D^k_{xx} = D^k_L \cos\theta^2 \cos\phi^2 + D^k_T (\sin^2\phi + \sin^2\theta \cos^2\phi) \quad \text{(II-4a)}$$

$$D^k_{xy} = (D^k_L - D^k_T) \sin\phi \cos\phi \cos^2\theta \quad \text{(II-4b)}$$

$$D^k_{xz} = (D^k_T - D^k_L) \sin\theta \cos\theta \cos\phi \quad \text{(II-4c)}$$

$$D^k_{yx} = D^k_{xy} \quad \text{(II-4d)}$$

$$D^k_{yy} = D^k_L \cos^2\theta \sin^2\phi + D^k_T (\cos^2\phi + \sin^2\theta \sin^2\phi) \quad \text{(II-4e)}$$

$$D^k_{yz} = (D^k_T - D^k_L) \cos\theta \sin\theta \sin\phi \quad \text{(II-4f)}$$

$$D^k_{zx} = D^k_{xz} \quad \text{(II-4g)}$$

$$D^k_{zy} = D^k_{yz} \quad \text{(II-4h)}$$

$$D^k_{zz} = D^k_L \sin^2\theta + D^k_T \cos^2\theta \quad \text{(II-4i)}$$

where

ϕ = angle between the direction of flow and the (X,Y,Z) coordinate system in the X-Y plane measured from the X axis (See Figure III-2, page III-5)

θ = vertical angle between the direction of flow and the X-Y plane, measured from the X-Y plane. (See Figure III-2)

D_L^k = dispersion coefficient in the direction of flow [L^2/T]

D_T^k = dispersion coefficient in the direction transverse to flow [L^2/T]

D_L^k and D_T^k *are commonly*[9] *assumed to be represented by:*

$$D_L^k = a_L|\bar{v}| \qquad \text{(II-5a)}$$

$$D_T^k = a_T|\bar{v}| \qquad \text{(II-5b)}$$

where a_L and a_T are dispersion length scalars that are characteristics of a given porous medium. This implies that $\bar{\bar{D}}$ is only a function of soil type not of each species, k. Hence, the k superscript is dropped. *Inherent in the form of Equations II-5a and II-5b is the assumption that the contribution of the molecular diffusion is negligible or at least constant for all species.*

The advective term can be expanded giving:

$$\nabla\cdot\rho^k\bar{v} = \rho^k(\nabla\cdot\bar{v}) + (\bar{v}\cdot\nabla\rho^k) \qquad \text{(II-6a)}$$

The pore velocity, $\bar{v}$, can be expressed as $\bar{q}/\nu$ where $\bar{q}$ is the Darcian velocity and ν is the volumetric moisture content or porosity in the case of saturated flow. Substituting this expression in Equation II-6a and expanding again gives:

$$\nabla\cdot\rho^k\bar{v} = \rho^k\frac{\bar{q}}{\nu^2}\cdot\nabla\nu + \frac{\rho^k}{\nu}(\nabla\cdot\bar{q}) + \bar{v}\cdot\nabla\rho^k \qquad \text{(II-6b)}$$

If the transporting medium (water) is assumed to be incompressible, which is valid except near the boiling point:

$$\nabla\cdot\bar{q} = 0 \qquad \text{for saturated systems}$$

and

$$\nabla \cdot \bar{q} = - \frac{\partial \nu}{\partial t} \quad \text{in unsaturated systems.}$$

In the Hanford subsurface the only anticipated regions where the fluid may be hot enough to invalidate this assumption would be in the immediate vicinity of a leak of high-level waste from a subsurface storage tank.

If all of the above assumptions are incorporated into Equation II-2, *and also assuming that the total mass density, ρ, of the mixture remains relatively constant.* The equation for saturated systems becomes:

$$\frac{\partial \rho^k}{\partial t} + \rho^k \frac{\bar{v}}{\nu} \left(\nabla \nu\right) + \bar{v} \cdot \nabla \rho^k = \nabla \cdot \bar{\bar{D}} \nabla \rho^k + r^k \qquad \text{(II-7a)}$$

and for partially saturated flow systems:

$$\frac{\partial \rho^k}{\partial t} - \frac{\rho^k}{\nu} \left(\frac{\partial \nu}{\partial t}\right) + \rho^k \frac{\bar{v}}{\nu} \cdot \nabla \nu + \bar{v} \cdot \nabla \rho^k = \nabla \cdot \bar{\bar{D}} \nabla \rho^k + r^k \qquad \text{(II-7b)}$$

In either of these forms with the exception of the reactive term, the continuity equation is amenable to a numerical solution.

In groundwater systems the reactive term r^k is a complex function:

$$r^k = f^k(\rho^1, \rho^2, \rho^3 \ldots \rho^k) \qquad \text{(II-8)}$$

consisting of a series of rate expressions which describe the influence of all the species present on the reactivity of species k. However, for most problems of practical interest the chemical kinetics are simply not known, nor are these relationships likely to be obtained soon because of overwhelming experimental problems inherent in this type of determination. If the kinetics are known for a given system, the problems associated with obtaining a stable numerical solution still place a stringent constraint on the utility of the model.

Consequently, an alternate chemical submodel was developed based on *the assumption that most groundwater systems are at or near chemical equilibrium at all times.* At the end of each numerical time step all constituents are constrained to be in equilibria with each other. The dissolved or suspended material is segregated into two classifications: 1) *macroions which are defined to exist in concentrations large enough to affect the chemical behavior of each of the other species present, and 2) microions that are assumed to exist in only minute quantities relative to macroions and do not appreciably affect the chemistry of each other or the macroions.*

A more complete discussion of the techniques used to simulate the reactive term is available in the Appendix. Details of the development and rationale of this scheme are given by Routson and Serne.[11]

Two-Dimensional, Vertically Averaged Formulation

The model equation that describes the existing vertically averaged model can be derived using basically the same assumptions that were discussed above.[12] This equation, which is representative of the current computerized version of the model and is suitable for use in simulating transport in saturated *uniform porosity* systems, is:

$$\frac{\partial \rho^k}{\partial t} + \left(\bar{v} - \frac{\bar{\bar{D}}}{H} \nabla H \right) \cdot \nabla \rho^k = \nabla \cdot \bar{\bar{D}} \nabla \rho^k + r^k \qquad \text{(II-9)}$$

where H is *the aquifer thickness which is allowed to vary spatially but is assumed to remain nearly constant in time.* The del operators, ∇, are in this case 2-D operators and $\bar{\bar{D}}$ is a second order tensor.

Boundary Conditions

Only two boundary types need to be defined for a transport simulation of the Hanford region (Figure II-1). The first boundary type is the no-flow or impervious condition which is specified by:

$$(\nabla \cdot \rho^k)\Big|_{\text{no-flow boundary}} = 0 \qquad \text{(II-10)}$$

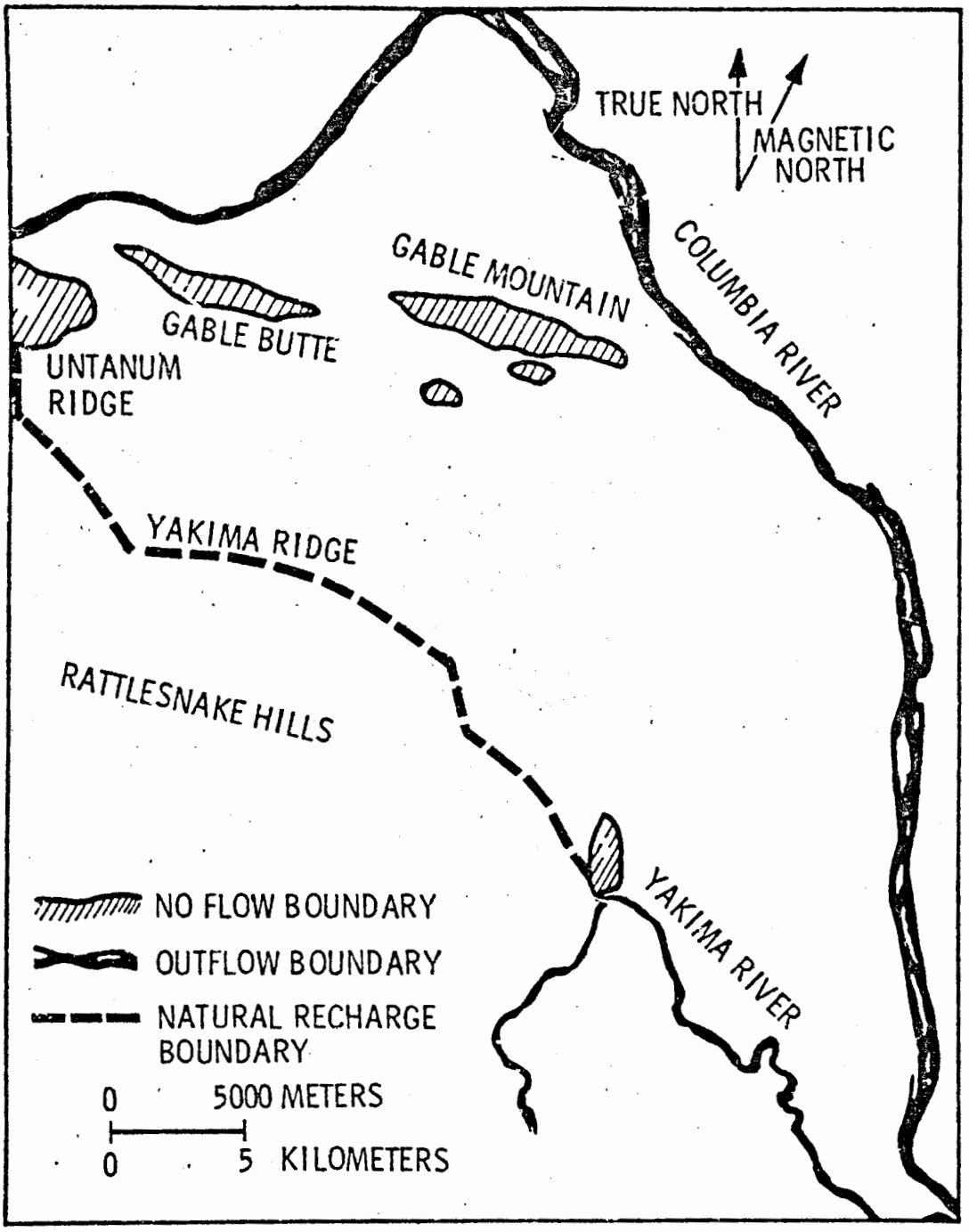

FIGURE II-1. Hanford Site Unconfined Aquifer Boundary Test

The other type of boundary is an outflow or recharge flow boundary. At the point where the aquifer flows into the Columbia River, the following condition is applied:

$$\rho^k\Big|_{\text{river boundary}} = 0 \qquad \text{(II-11a)}$$

Because of the extremely high ratio of Columbia River flow versus the rate of discharge of the unconfined aquifer, the river is assumed to be an infinite sink of zero concentration. At a recharge boundary:

$$\rho^k\Big|_{\text{recharge boundary}} = \rho_b^k(x,y,z,t) \qquad \text{(II-11b)}$$

where ρ_b^k is the mass concentration of species k in the recharge stream. This concentration is in general a function of time and location. No significant levels of radioactive contaminants above natural groundwater levels have been identified in the recharge flow to the Hanford aquifer. Consequently, Equation II-11b reduces to:

$$\rho^k\Big|_{\text{recharge boundary}} = 0. \qquad \text{(II-11c)}$$

for these species. All additions or withdrawals of material inside these boundaries are assumed to be included in the source/sink term, r^k.

THE DIRECT SIMULATION APPROACH

The intent of the direct-simulation approach is to create a numerical analog that directly represents the physical behavior of a system. Besides satisfying the principle of conservation of mass, all other important physical constraints or driving forces that are present in the model system must be accounted for. A direct-simulation approach applicable to Hanford subsurface transport problems is outlined below. Each important assumption will again be indicated by italics.

Particles of Mass

An important first step in creating a direct analog of a mass transport system is to define a numerical construct with which to represent the

chemical species of interest. Engineering-oriented approaches to mass transfer processes traditionally have tended to view chemical solutions as continuums that are defined with respect to a fixed or 'Eulerian' frame of reference. It can also be useful to view material systems as being comprised of a large number of discrete particles of matter. Carried to the molecular or atomic level, this concept has been established as a reliable description of the nature of matter.

It is not feasible at present to consider molecular-scale subdivisions when attempting to model large environmental systems, but the same concept can be used to create a workable analog. *The direct approach assumes that the material that is dissolved or suspended in subsurface water can be represented as an ensemble of a finite number of discrete particles of matter.* Computational restrictions usually limit the number of particles that can efficiently be used to something on the order of 10^4 or 10^5. *The water mass that is carrying the material is assumed to be a continuum subject only to laminar flow. All particles are assumed to move with the continuum and at its velocity.*

Each particle has a defined location and a finite mass quantity associated with it. *The particles are assumed to be independent of one another,* or in other words any one particle is not affected by the proximity or behavior of others. This assumption is strictly valid only for dilute solutions, but is approximately true for all except very highly concentrated systems. The particles occupy zero volume by definition. *Because of their relatively large mass, the motion of the particles is assumed to be governed by Newtonian rather than relativistic mechanics.*

Advective Transport

The advective motion of the particles is controlled by the host medium in which they are immersed. *It is assumed that the flow properties of the host medium (water) are not significantly affected by the number or type of particles present.* This simplification is analogous with the assumption that the momentum and mass balance equations are decoupled in the equation-based approach. This also implies that the advective motion of each particle is only a function of the physical properties of the carrier and the geometry of the system.

The flow properties of the host water body usually are represented as a matrix of velocity components. This matrix must represent a mass conservative flow field if a proper transport simulation is to take place. Of course, this requirement is also necessary when the model is developed from an equation-based approach. Several methods are available for constructing the required flow fields, but most commonly they are the result of a flow model simulation. Each particle is allowed to move for a time interval, Δt, as determined by its location in the flow field. For best results the time-step size should be restricted so that the maximum distance moved by a particle is not larger than the matrix spacing of the flow field.

Dispersive Transport

The next transport process that must be accounted for is the readily observable property usually referred to as diffusion or dispersion, which results in a net flux relative to the ambient velocity. A qualitative discussion of the mechanisms causing mechanical dispersion was given in the section on the model-equation approach. Molecular diffusion which also contributes to dispersion will take place in the absence of fluid motion when mechanical dispersion ceases. However, both have the same net result of causing foreign material to spread throughout the medium as the result of apparently random movements.

The particles of mass used to simulate dissolved or suspended material are subject to *the various dispersive mechanisms which are assumed to cause statistically random displacements*. Consider a single particle at position x at t = 0 which has moved to x' at a later time, t, viewed from a Lagrangian frame of reference moving with the fluid. Its displacement x'-x is then a random function of time which can be described in terms of a spatial probability distribution function, P(x'-x,t). As more steps are taken, the particle trajectory can be described as having the properties of a process known in statistics as a random walk. The probability distribution of a particle executing random steps is a standard problem of probability theory.[13-17] The following discussion is based on a summary of random walk theory given by Bear[9] and Csanady.[18]

The main features of the problem can be understood most simply by the analysis of a random walk in one dimension with each step having a unit length and the probability of a step in either direction being exactly one half. Thus, assuming a particle is released at the origin of an arbitrary coordinate system, it could be at any of the points:

$$-N, -N+1, -N+2, \ldots N-2, N-1, N$$

after N steps.

The problem then is determining with what probability a particle reaches a given point m where $-N<m<+N$. That probability, denoted by $P(m,N)$, can be calculated by enumerating all of the possible outcomes of a random walk consisting of N steps and determining which ones of those will result in the particle finishing up at point m.

The probability of any one sequence of N backward and forward steps is given by $(1/2)^N$. The required probability is therefore this value times the number of distinct sequences which will lead to the point m after N steps. If the number of forward steps taken is f and the number of backward steps b, in order for the particle to arrive at m after N steps, the following relationships must be true:

$$f + b = N \tag{II-12a}$$

$$f - b = m \tag{II-12b}$$

which yields

$$f = (N + m)/2$$

$$b = (N - m)/2$$

The number of different sequences consisting of exactly f forward and b backward steps is:

$$\frac{N!}{(f!b!)} \tag{II-13}$$

therefore:

$$P(m,N) = \frac{N!}{[1/2(N+m)]![1/2(N-m)]!}(1/2)^N \tag{II-14}$$

which is known as a Bernoulli distribution.[19]

For modeling large-scale groundwater flow the case of most interest occurs for very large N. For this case the result for P(m,N) can be simplified by making use of Stirling's formula:[19]

$$\ln(N!) = (N+1/2)\ln(N) - N + \ln(2\pi) \qquad \text{(II-15)}$$

After some algebraic manipulation,[19] Equation II-14 reduces to:

$$P(m,N) = \sqrt{\frac{2}{\pi N}}\, e^{-(m^2/2N)} \qquad \text{(II-16)}$$

which is a Gaussian or normal distribution with standard deviation $\sqrt{N}$. The convergence of the Bernoulli to the Gaussian distribution is quite rapid as N increases. For example, the differences are within a few percent for N=10 except at the extremes of the distributions.

The "discrete" distribution expressed by Equation II-16, can be made continuous by *assuming that the individual steps are small compared to the length Δx over which we may want to define particle concentrations. If the step length is ℓ, which is assumed to be characteristic of a particular medium, then*:

$$m = x/\ell \qquad \text{(II-17)}$$

where x is the displacement from the origin. The total probability of finding a particle over a range Δx, centered at x, is then approximately:

$$P(m,N)\cdot(\Delta x/2\ell) \qquad \text{(II-18)}$$

The factor 2 is in the denominator because the discrete neighboring probability points are always separated by two step lengths. In a diffusing cloud of independent particles, having total mass Q, the fraction of the material contained within the range Δx is then given by:

$$\text{total mass}\Big|_{x-1/2\Delta x}^{x+1/2\Delta x} = \Delta m = Q\cdot P(m,N)\,\frac{\Delta x}{2\ell} \qquad \text{(II-19)}$$

which can be expressed in terms of concentration as:

$$\rho = \frac{\Delta m}{\Delta x} = \frac{Q}{2\ell}\sqrt{\frac{2}{\pi N}}\, e^{-\left(\frac{x^2}{2N\ell^2}\right)} \qquad [M/L] \qquad \text{(II-20)}$$

The total number of steps, N, may be related to a diffusion time, t, if the particle is assumed to undergo n displacements per unit time:

$$t = \frac{N}{n} \qquad \text{(II-21)}$$

and a "diffusion velocity," u, can be defined as:

$$u = \tfrac{1}{2} n\ell \qquad [L/T] \qquad \text{(II-22)}$$

Defining a dispersion coefficient, D, as:

$$D = \tfrac{1}{2} n\ell^2 = u\ell \qquad [L^2/T] \qquad \text{(II-23)}$$

yields:

$$\rho(x,t) = \frac{Q}{2\sqrt{\pi D t}}\, e^{-\left(\frac{x^2}{4Dt}\right)} \qquad \text{(II-24)}$$

This equation is recognizable as a Gaussian distribution with standard deviation $\sqrt{2Dt}$ and also as a solution to the classical one-dimensional diffusion equation.[20,21] The above arguments have been extended to three dimensions for a homogeneous isotropic system by Scheidegger,[16] yielding:

$$\rho(x,y,z,t) = \frac{Q}{(2\sqrt{\pi D t})^3}\, e^{-\left(\frac{x^2}{4Dt} + \frac{y^2}{4Dt} + \frac{z^2}{4Dt}\right)} \qquad \text{(II-25)}$$

which is a solution to the three-dimensional diffusion equation. Chandrasekhar[17] has shown for a general, three-dimensional Markovian random walk that this probablistic approach can be connected directly to the diffusion equation without having to enumerate all possible sequences of displacements. A brief summary of Chandrasekhar's arguments is presented by Csanady[18] showing that the asymptotic ($N \to \infty$) temporal transition probability of the random walk problem has a form identical to the classical diffusion equation.

In Scheidegger's[16] formulation *the motion of a particle through a specific medium was assumed to be made up of a sequence of straight elementary displacements of equal duration in which the direction and length of each displacement take on random values.* However, his model does not take into account the observed difference in rate of dispersion with respect to the directions longitudinal and transverse to flow. De Jong[22] shows that for a homogeneous system the longitudinal dispersion can generally be expected to be five to seven times larger than the transverse component because of the shorter residence times in the pores oriented in the direction of flow. However, when irregularities are present in the system this ratio is not readily predictable or quantifiable.

The most important point to be gained from this very brief discussion of the statistical description of dispersion is that the rms (root-mean-square) distance that an ensemble of parcels which are undergoing a random walk will move during a time step, Δt, can be expressed (for the one-dimensional case) as:

$$\Delta x_{rms} = \sqrt{2D\Delta t} \qquad \text{(II-26)}$$

based upon the result shown in Equation II-24. Similar displacements will also occur in the other spatial directions. The numerical analog adopted for the dispersion portion of the direct simulation model approach is based on Equation II-26 and is similar to Scheidegger's approach with the extension that the rates of dispersion are allowed to differ with respect to the longitudinal and transverse flow directions.

Total Particle Movement

To summarize particle movement, a particle of mass is defined that is assumed to be subject to displacements resulting from both advective and dispersive mechanisms during a given time step. If a large number of particles are released at a concentrated location after several time steps, an ellipsoidal cloud will result with a center point moving with the average flow velocity and the major semi-axis coincident with the direction of flow.

Another significant point to note is that based upon the assumptions presented above, the motion of a particle is dependent only on the nature of the flow system and not on the type of species being transported. This suggests that each particle can be tagged with more than one mass quantity, each representing a different species. By computing the movement of one set of particles, the transport of several species can be simulated simultaneously with considerable savings in computer time.

Concentration Distribution

At the end of any desired time step, the solution can be halted and the amount of mass residing within any defined volume can be tabulated yielding an average concentration value for the volume. The solution can then continue transporting each particle from where it was halted, stopping again to compute another concentration distribution when desired. This procedure is completely mass conservative as opposed to some earlier Lagrangian solution techniques such as the PIC method[6] which tagged each particle with a concentration rather than a mass. Averaging a set of concentrations to calculate an overall cell concentration can often lead to serious mass conservation problems.

Source/Sink Terms

The simple injection or withdrawal of contaminants from the system is easily simulated by adding or removing particles at appropriate locations. Other types of source/sink mechanisms such as radioactive decay or chemical reaction require that the mass quantities associated with each particle be adjusted or redistributed. All of these types of source/sink contributions are important for simulations of the Hanford subsurface.

Prior to the computation of one of the more complex types of non-conservative mechanisms it is usually most convenient to convert the particle location distributions into a set of concentration distributions. New concentrations for each subdivision are calculated from a reaction rate or equilibrium type of reactive submodel. The concentration change within each summation interval ($\Delta x, \Delta y, \Delta z$) for each species is accounted for by appropriately adjusting the mass quantities associated with each parcel within the interval.

The current MMT soil-waste reaction chemical model uses the equilibrium constraint approach which assumes that all species within a summation interval must be in equilibrium at the end of each time step. This model is discussed briefly in the Appendix and is explained in detail by Routson and Serne.[11]

Boundary Conditions

The boundary conditions for the direct approach model can be specified quite easily. Two distinct types can be identified:

1. Free flow boundary - any particle transported out of the system across this type of boundary is assumed to have exited from the system. New particles with appropriate mass are created at inflow boundaries.

2. Reflecting or no flow boundary - any particle encountering this type of boundary is reflected back into the system.

Assumptions for the Vertically Averaged Version

The preceding discussion accurately describes the assumptions in the current vertically averaged version of MMT-DPRW with one exception. Local reductions on aquifer thickness should hinder horizontal spreading and increases in thickness should increase the spreading rate. In a fully three-dimensional model this is taken care of by specifying the aquifer top and bottom as reflecting boundaries. However, in the 2-D vertically averaged version the particles do not have a vertical coordinates associated with them that could make use of this boundary condition.

Fortunately, it is still relatively easy to account for this phenomenon in the 2-D model. In Equation II-9 this spreading rate adjustment is computed by the $-\frac{\bar{D}}{H} \nabla H \cdot \nabla \rho^k$ term. Careful examination of Equation II-9 indicates that the net result of this term is to increase or decrease the pore velocity, $\bar{v}$. Consequently, *the vertically averaged model formulation approximates these spreading rate pertubations by adding a* $-\frac{\bar{D}}{H} \nabla H$ *component to each velocity vector of the flow field.* This assumption is discussed further with appropriate examples in Section IV.

ADVANTAGES AND DISADVANTAGES OF THE DIRECT SIMULATION APPROACH

Advantages

The direct approach to model development has been found to have the following significant advantages over more traditional model-equation based approaches:

- Always Mass Conservative - The fundamental approach of the algorithm is inherently mass conservative in contrast to the somewhat similar PIC technique.
- Inherent Stability - The response of this numerical analog is inherently stable with respect to time step size and other model parameters such as the dispersion coefficient and the magnitude of the velocity (see Trent[23]).
- No Cumulative Numerical Dispersion - Most of the numerical smearing problems often found in other numerical schemes are eliminated (see Trent[23]). The main reason for this is the Lagrangian approach to advection computation. Many of the stability and numerical dispersion problems of Eulerian methods arise from the approximations made to the advective term. This property was one of the primary motivating factors for development of the direct approach. The only numerical dispersion in this approach occurs when concentrations are computed. This results from calculating an average concentration for each grid cell. However, this numerical dispersion is not carried forward in time since particle positions and associated masses are not affected by this averaging process.
- Ease of Control of Solution Accuracy - The accuracy of the solution can be easily controlled by specifying the number of particles to be used in the simulation. This allows a rough preliminary debug solution to be computed for the full length of a simulation using only a few particles at a substantial reduction in cost compared to a more accurate run using a large number particles (see Sensitivity and Error Analysis Section).

- Solution Stacking - If nonlinear source/sink terms are not present in a given simulation (based upon the previously stated assumption this is the only way nonlinearity can enter the problem), the results of one solution for a given problem may be averaged with subsequent solutions of the same case to give more accurate results. For instance, suppose that after computing a simulation it was apparent that too few particles had been used, the entire simulation need not be re-computed using more particles. Instead, an additional run of the same simulation can be computed (making sure the random number generator continues where it left off) and its results averaged with the previous run. This process effectively increases the particle density in each cell and can be repeated as many times as necessary to achieve the desired solution accuracy.

- Adaptability to Small Economical Computer Systems - The fact that each particle is independent of any other makes this solution technique particularly easy to program for small computers with limited addressable memory but with fairly large mass storage (disk) resources. Only a few sets of particle data need to be in memory at any one time with the remainder of the data residing on disk. The smaller machines, although somewhat slower than most larger systems, are usually much more cost effective and allow real-time user interaction. The independence of the particle trajectory calculations also makes this model attractive for use on computers designed with a high degree of parallelism.

- Ease of Coupling New Source/Sink Models - The capability of being able to simply re-distribute particle mass as a means of responding to an externally defined reaction scheme and the simplicity of adding or removing particles to simulate injection or withdrawal allow a great deal of flexibility.

- Complicated Mathematical Structures are Avoided - The direct, discrete-particle solution approach is basically simple. The entire scheme can be described with a few simple algebraic expressions. The main task in implementing this algorithm is concerned with creating an

efficient bookkeeping structure for keeping track of particles. This type of code is much easier for nonprofessional computer technicians to understand than complex numerical solution schemes necessary for solving the differential equations upon which models are usually based. This allows more rapid program development and debugging as well as making the resulting code easier to maintain and modify.

- Easy to Use for Three-Dimensional Applications - Assuming the accuracy is to remain constant, computation time increases linearly with the number of vertical levels used. This is a much less rapid increase in computation time than is the case with other methods. Also, problems that often arise from very high aspect ratios (the ratio of the horizontal size of a system to its vertical extent) are nonexistent.

- Complex Boundaries are Easily Handled - All that is necessary to account for boundaries is a knowledge of the coordinates of the boundaries and the location of each particle. When a boundary is encountered by a particle, appropriate action, as discussed above, is taken based on the boundary type.

Disadvantages

In addition to these advantages three primary disadvantages of the discrete particle method have been noted:

- Computation Speed - The primary drawback of the particle-based method outlined above is the computational speed. For circumstances where model parameters have values that are within the stability range of a finite-difference or finite-element solution schemes, these types of algorithms are usually faster for a given degree of accuracy except perhaps for some three-dimensional cases. This problem is most acute when high accuracy solutions are required, and nonlinear terms are present. The convergence of the discrete particle scheme improves only as the square root of computation time. (Four times as many particles must be used to double the accuracy.) When the problem is nonlinear the entire solution set of particles must be brought forward in time before the next time step can be computed. This eliminates many of the advantages gained from the assumed independence of each particle.

The relatively large computation times are partially offset by the reliability of the algorithm for any combination of values of model parameters, and by the compatibility of this method with small economical computer systems. However, this approach very likely is not the best method to use for problems requiring a solution with a very high degree of accuracy. Fortunately, most environmental simulation problems are not of this type. For most large-scale environmental simulations the required input data are usually not known within an accuracy of better than a few percent. Consequently a simulation using a relatively small number of particles is usually acceptable.

- Presence of Random Noise - A certain amount of statistical random noise is always present in solutions computed with the direct simulation scheme. As more particles are added, the amplitude of the noise decreases, but because of the statistical nature of the random walk analog, it is always present to some degree. The random noise portion of the solution can be reduced, quite markedly in some intances, by post-processing the results with various smoothing or filtering methods (see the section on Error and Sensitivity Analysis).

- Number of Particles - A general criterion has yet to be developed for selecting the number of particles needed to obtain acceptable solution accuracy. Although the solution stacking procedure can be helpful in this regard, much depends upon the experience of the user.

Although the discrete particle approach has been shown to have several advantages and commendable properties, it should not be viewed as the best method for all problems. The possible applications of this scheme are quite broad, but it probably should not be used when the computed solution accuracy must be within 5% of the true value. However, for environmental simulations, where predictions that might be in error by a few percent are totally acceptable, this method holds a great deal of promise.

BLANK PAGE

III. NUMERICAL IMPLEMENTATION

The numerical scheme resulting from the direct simulation approach is the Discrete-Parcel-Random-Walk (DPRW) method. The basic device or numerical tool employed by this procedure is a hypothetical entity referred to as a computational "parcel". The term "parcel" was chosen to distinguish the numerical tool from the more general but slightly vague "particles" referred to in the previous section. The continuum of dissolved or suspended matter to be modeled is represented as consisting of a finite ensemble of these parcels. The parcels have, by definition, zero size, but each has associated with it a set of Cartesian spatial coordinates (x_p^n, y_p^n, z_p^n) and a set of discrete quantities of mass $\xi_p^{k,n}$, where:

p = the parcel index (p = 1,2,3...N_p) where N_p is the total number of parcels used to represent a given quantity of matter.

k = the transported species index (k = 1,2,3...K) where K is the total number of constituents present in the system.

n = the time level index (n= 1,2,3,...N_t) where N_t is the number of time increments to be computed.

For example, the location of parcel 3 after five time steps is (x_3^5, y_3^5, z_3^5). If the problem is concerned with five distinct constituents, this parcel would have associated with it five separate mass quantities $\xi_3^{1,5}$ $\xi_3^{2,5}$ $\xi_3^{3,5}$ $\xi_3^{4,5}$, and $\xi_3^{5,5}$.

During a given time step a new location for each parcel is computed as determined by advective and dispersive mechanisms, and the weights associated with each parcel are adjusted to account for any source/sink processes. The sequence of these computations is as follows:

1) First, the new location as determined by advective motion is calculated.
2) This new location is then modified by a random step to simulate dispersion.
3) If necessary, parcel weights are adjusted to account for first-order source/sink mechanisms such as radioactive decay.
4) A matrix of concentrations is calculated for a specified cell matrix (Figure III-1) by adding the mass of the particles within each cell and dividing by the cell volume.

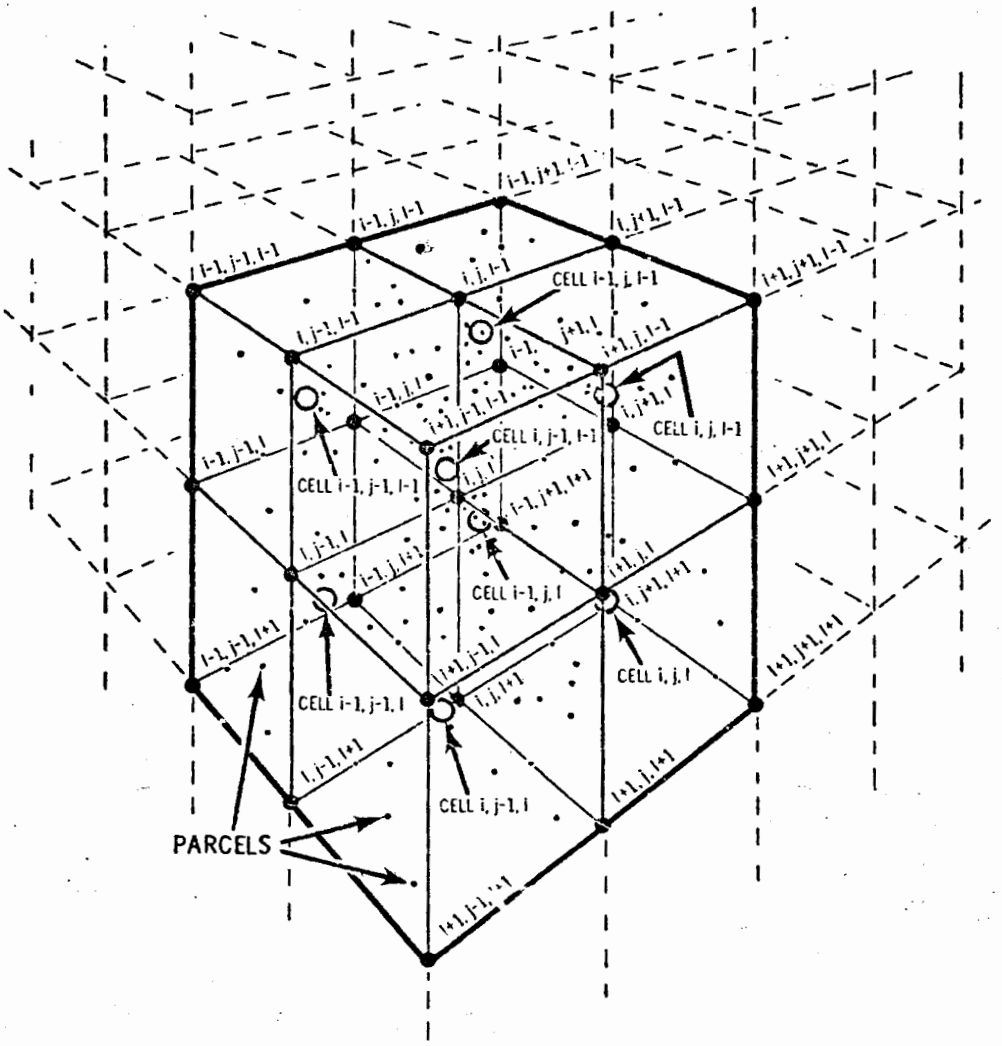

FIGURE III-1. DPRW Nodal-Cell Network
• - Nodes
o - Cell Centers

5) Concentration changes within each cell during the time interval resulting from higher order source/sink mechanisms are computed.

6) The parcel weights are then adjusted to reflect the concentration changes.

Each of these steps is discussed in more detail in the following subsections.

ADVECTIVE COMPONENT

The MMT-DPRW transport code requires as input a set of mass conservative velocity components that describe the flow patterns of the host groundwater system. These velocity components must be arranged in a regularly spaced, rectangular matrix that remains stationary although the magnitude and directions of the vectors are allowed to vary with space and time. Three velocity components (u, v, w) are defined at each nodal point of the matrix (see Figure III-1). The individual parcels are then advected through this network as determined by the velocity vectors immediately surrounding their present location. The three spatial velocity components at the location of parcel "p", (u_p^n, v_p^n, w_p^n), are linearly interpolated from the surrounding matrix of values. The advective transport contribution is then computed by:

$$x_p^* = x_p^n + \Delta t^n u_p^n \qquad \text{(III-1a)}$$

$$y_p^* = y_p^n + \Delta t^n v_p^n \qquad \text{(III-1b)}$$

$$z_p^* = z_p^n + \Delta t^n w_p^n \qquad \text{(III-1c)}$$

where Δt is the computational time increment, and * denotes an intermediate value. In order to ensure a smooth continuous solution, the value of Δt is limited such that the maximum distance that any parcel is transported during a given time step is less than or equal to the distance between surrounding nodal points of the velocity matrix.

DISPERSIVE COMPONENT

A dispersive transport component is then calculated for each parcel by assuming that the ensemble of parcels is subject to Brownian-like random

motion resulting from the tortuous path that the host fluid takes through a complex medium such as soil. Equation III-2 shows rms distance moved by the ensemble of parcels, with respect to the advective flow of the system, for a given time step, Δt, in a homogeneous one-dimensional system: (See Equation II-26)

$$d_{rms} = \sqrt{2D\Delta t} \qquad \text{(III-2)}$$

with the direction of motion of each parcel assumed to be random. The current version of the model allows two options for determining the dispersion coefficient D. It can be input directly and used as a constant, or it can be calculated by:

$$D = a|\bar{v}|$$

where a is a characteristic length parameter that is read in. "D" and "a" are the same variables used in the dispersion discussion in Section II with the subscripts omitted.

In three-dimensional porous media systems it has been generally observed that the rate of dispersion is higher in the direction of flow than in the direction lateral to the flow.[9,22] The rms step size coincident with the flow is expressed as:

$$d_{L,rms} = \sqrt{2D_L \Delta t} \qquad \text{(III-3a)}$$

and in both transverse directions as:

$$d_{T,rms} = \sqrt{2D_T \Delta t}. \qquad \text{(III-3b)}$$

If an ensemble of parcels initially concentrated at a point is allowed to disperse in this type of environment for a time Δt, an ellipsoid shaped cloud, such as that illustrated in Figure III-2, will be formed. The major semi-axis of the ellipsoid will be coincident with the direction of flow and the rms value of the parcel displacements in this direction are given by Equation III-3a.

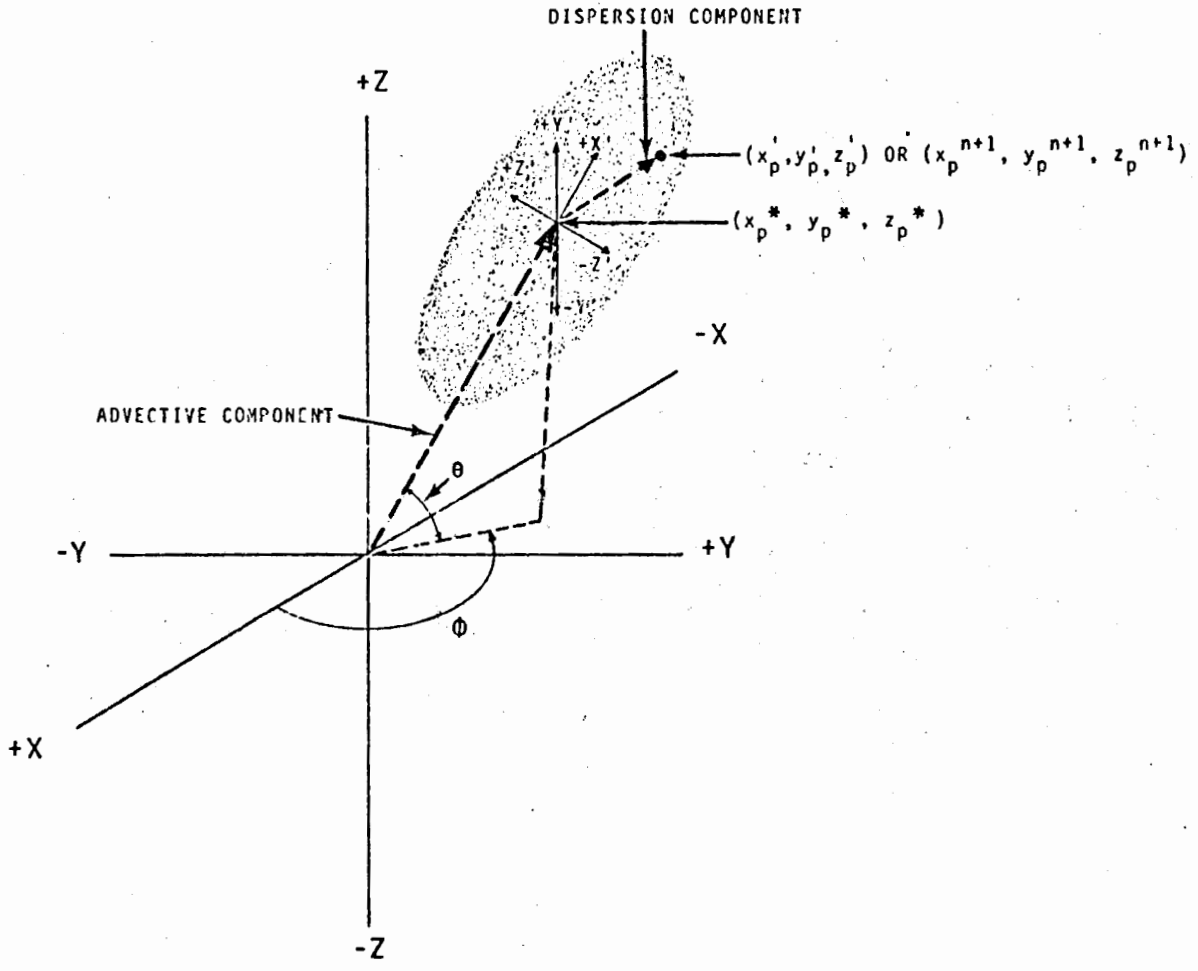

FIGURE III-2. Sample Parcel Trajectory During Time Step n

The other two semi-axes of the ellipsoid are perpendicular to the flow. The rms parcel displacement in the transverse directions is specified by Equation III-3b. This spreading process is numerically simulated in the DPRW algorithm as follows.

A second set of right-hand coordinate axes (X', Y', Z') is defined having its origin at (x_p^*, y_p^*, z_p^*) with the positive X-axis oriented in the direction of the velocity vector, $\bar{v}_p^n$. The transformation to the new coordinate system can be made by rotating the base coordinate system (X,Y,Z) through a horizontal angle ϕ and vertical angle θ (Figure III-3) and then translating the origin.

A dispersive step length for parcel p is generated by selecting a value from a distribution of step lengths having the proper rms value (Equations III-3a or III-3b) and a zero arithmetic mean. The exact shape of the chosen distribution is not critical; however, some types of distributions are much more convenient and economical to generate than others. Regardless of the shape of the distribution, if it has a zero mean and the proper rms value after a few time steps, the shape of a diffusing cloud of parcels will be statistically equivalent. This is a result of the well-known central limit theorem which states that the distribution of the sums of a series of sets of random samples from any arbitrary probability distribution will always approach a normal distribution.[19]

For convenience the MMT-DPRW code uses a uniform probability distribution from which to select dispersive step sizes. The generation of a dispersive step in the x'-direction can then be expressed by:

$$x'_p = [R]_{-\zeta_L}^{\zeta_L} \qquad \text{(III-4)}$$

where $[R]_{-\zeta_L}^{+\zeta_L}$ indicates a random number from a population that is uniformly distributed in the range $-\zeta_L$ to $+\zeta_L$, with ζ_L selected so that the constraint $x'_{rms} = d_{L,rms}$ is satisfied.

To determine ζ_L, the rms value of parcel step sizes in this range must be calculated. The mean of the square of the step size is given by:

$$x'_{rms} = \int_{-\zeta_L}^{+\zeta_L} P(x)x^2 dx \qquad \text{(III-5)}$$

where P(x) is a probability distribution function. For a uniform distribution in the interval $(-\zeta_L, +\zeta_L)$:

$$P(x) = \frac{1}{2\zeta_L} \qquad \text{(III-6)}$$

Evaluating the integral in Equation III-5 and taking the square root yields:

$$x'_{rms} = \frac{\zeta_L}{\sqrt{3}}$$

Equating this expression to the required dispersive step length, $d_{L,\,rms}$, given in Equation III-2 yields:

$$\zeta_L = \sqrt{6D_L \Delta t} \qquad \text{(III-7)}$$

which allows Equation III-4 to be rewritten as:

$$x'_p = [R]_{-\sqrt{6D_L \Delta t}}^{+\sqrt{6D_L \Delta t}} \qquad \text{(III-8)}$$

The random number generator routines available on most computer systems commonly return values uniformly distributed in the range [0,1]. Adapting Equation III-8 to use this type of random number generator gives:

$$x'_p = \sqrt{24D_L \Delta t}\left(.5-[R]_0^1\right) \qquad \text{(III-9a)}$$

Similarly, it can be shown that in the lateral directions:

$$y'_p = \sqrt{24D_T\Delta t}\left(.5-[R]_0^1\right) \qquad \text{(III-9b)}$$

$$z'_p = \sqrt{24D_T\Delta t}\left(.5-[R]_0^1\right) \qquad \text{(III-9c)}$$

The only remaining computation in the dispersive portion of the code involves transforming the current parcel location from the (X', Y', Z') coordinate system to the base system (X, Y, Z):

$$x_p^{n+1} = x_p^* + x'_p\cos\theta\cos\phi - y'_p\sin\phi - z'_p\sin\theta\cos\phi \qquad \text{(III-10a)}$$

$$y_p^{n+1} = y_p^* + x'_p\cos\theta\sin\phi + y'_p\cos\phi - z'_p\sin\theta\sin\phi \qquad \text{(III-10b)}$$

$$z_p^{n+1} = z_p^* + x'_p\sin\theta + z'_p\cos\theta \qquad \text{(III-10c)}$$

Parcel "p" has thereby been transported by advection and dispersive mechanisms from (x_p^n, y_p^n, z_p^n) to $(x_p^{n+1}, y_p^{n+1}, z_p^{n+1})$ during time step n. A trace of a parcel during this time step is illustrated in Figure III-2.

To clarify the system geometry examples are given in Figures III-3, III-4 and III-5. These figures are photographs taken from a cathode ray tube display of an ellipsoidal distribution of parcels calculated by the model. A total of 3000 parcels were released at a point in a uniform flow field with the direction of flow at $\phi = 45°$ and $\theta = 45°$ as indicated by the arrow pointing toward the center of the ellipsoid. Figures III-3, III-4 and III-5 are projections in the Y-Z, X-Y and X-Z planes, respectively. All views are from the positive side of the plane.

CONVERSION TO INTENSIVE VALUES

When the advective and dispersive computations have been completed for every parcel in the system, a grid network can be superimposed upon the spatially distributed ensemble of parcels (Figure III-1). The nodal points of the grid are labeled with i,j,l indices where

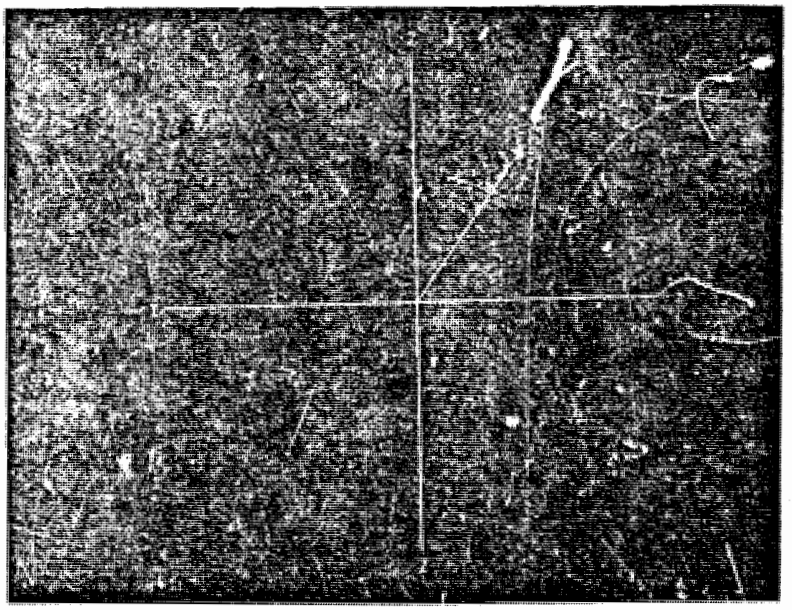

FIGURE III-3. Computed Ellipsoidal Parcel Cloud, Y-Z Planar View

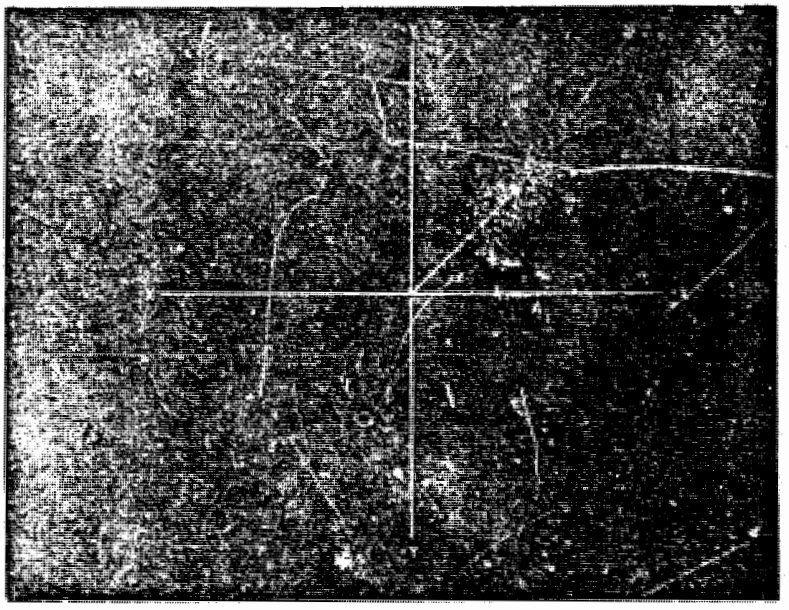

FIGURE III-4. Computed Ellipsoidal Parcel Cloud, X-Y Planar View

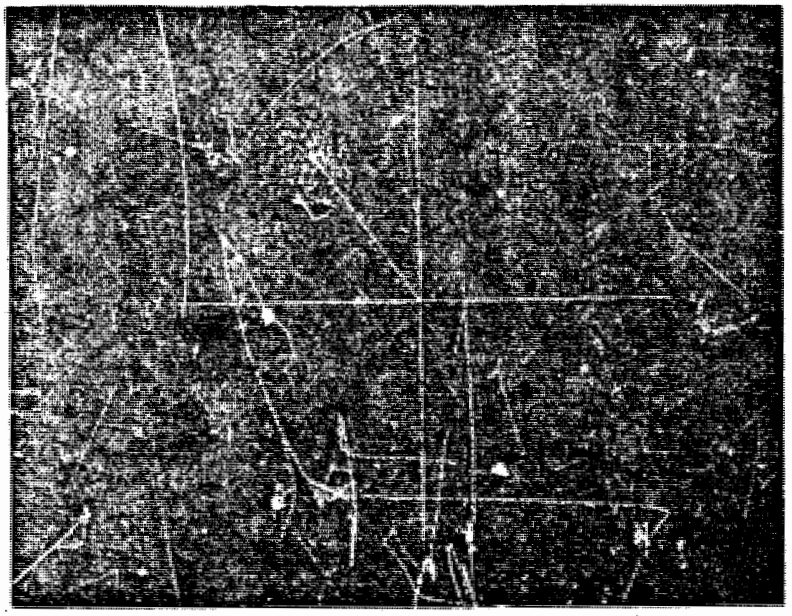

FIGURE III-5. Computed Ellipsoidal Parcel Cloud, X-Z Planar View

$i = 1,2,3...I$, I = number of nodal points in x-direction

$j = 1,2,3...J$, J = number of nodal points in y-direction

$l = 1,2,3...L$, L = number of nodal points in z-direction

The nodal points form the vertices for $(I\text{-}1) \times (J\text{-}1) \times (L\text{-}1)$ rectangular solids which are referred to as cells. The dimensions of cell (i,j,l) are Δx_i by Δy_j by Δz_l:

where

$$\Delta x_i = x_{i+1} - x_i$$

$$\Delta y_i = y_{j+1} - y_j$$

$$\Delta z_l = z_{l+1} - z_l$$

Parcel "p" is said to lie within cell (i,j,l) if:

$$x_i \leq x_p^{n+1} < x_{i+1} \tag{III-11a}$$

$$y_j \leq y_p^{n+1} < y_{j+1} \tag{III-11b}$$

$$z_l \leq z_p^{n+1} < z_{l+1} \tag{III-11c}$$

The total amount of mass of each species within cell (i,j,l) is computed by summing the mass quantities, $\xi_p^{k,n}$, for all parcels that lie within the cell:

$$\xi_{ijl}^{k,*} = \sum^{\eta_{ijl}} \left(\xi_p^{k,n}\right)_{ijl} \tag{III-12}$$

η_{ijl} = number of parcels within cell (i,j,l)

In this case the asterisk (*) again indicates an intermediate value. Here it denotes a value obtained after parcel movement, but prior to source/sink adjustment within a given time step computation.

The volume of each cell, V_{ijl}, is a known quantity ($\Delta x_i \times \Delta y_j \times \Delta z_l$). Consequently, an average intensive quality variable, usually a concentration, can be computed for each constituent in each cell by the equation:

$$\rho_{ijl}^{k,*} = \frac{G^k \xi_{ijl}^{k,*}}{V_{ijl} \nu_{ijl}} \tag{III-13}$$

where

G^k = an appropriate conversion factor to convert ξ^k to the units desired by the user (e.g., the factor for converting from Ci/ft^3 to pCi/ml).

ν_{ijl} = volumetric moisture content or effective porosity of cell (i,j,l).

The concentrations, ρ_{ijl}, are defined at the center of each cell (Figure III-1).

SOURCE/SINK CONTRIBUTIONS

To complete the numerical scheme the contributions of the source/sink term must be accounted for. The method used to model these contributions varies depending upon the type of mechanisms represented by $r^{k'}$. If the source/sink mechanism is simply a discharge of material into the system or a removal of material from it, parcels are either added to or removed from appropriate areas of the solution matrix.

Decay Losses

Some simple source/sink mechanisms such as first order decay processes can be computed very simply by adjusting each parcel's associated weights by:

$$\xi_p^{k,n+1} = \xi_p^{k,n} e^{-\lambda^k \Delta t} \qquad \text{(III-14)}$$

where λ^k is the first-order decay constant for species k. If the daughters of the decay process are among the species that are being considered by a simulation their weights must be incremented by:

$$\xi_p^{k',n+1} = \xi_p^{k',n} + \left(\xi_p^{k,n} - \xi_p^{k,n+1}\right)\left(\frac{AW^{k'}}{AW^{k}}\right) \qquad \text{(III-15)}$$

where k' indicates a daughter of species k and AW is the atomic weight.

Most source/sink mechanisms in real systems, however, are of a more complicated type incorporating simultaneous interactions among many of the solutes present as well as their interactions with the surrounding soil matrix. The MMT-DPRW code allows these complex mechanisms to be approximated by reaction rate expressions or as a set of equilibrium constraints.

Rate Expressions

A reaction rate expression is a predefined function that describes the rate of change of ρ^k as a function of the concentration of all constituents present. Typically the rate expression for species k in cell (i,j,l) of an isothermal system is of the form:

$$r^k = a^k \left[\prod_{m=1}^{K} (\rho_{ijl}^m)^{\alpha^m} \right] - b^k \left[\prod_{m=1}^{K} (\rho_{ijl}^m)^{\gamma^m} \right] \qquad \text{(III-16)}$$

where a and b are experimentally determined combined rate constants and α and γ are experimentally derived exponents that indicate the order of dependence of r^k on the concentration of each species. For example, the rate equations in cell (i,j,l) for a three-component system might be expressed by:

$$r^1 = a_1 (\rho_{ijl}^2)(\rho_{ijl}^3) - b_1 (\rho_{ijl}^1) \qquad \text{(III-17a)}$$

$$r^2 = a_2 (\rho_{ijl}^1)^2(\rho_{ijl}^3) - b_2 (\rho_{ijl}^2)(\rho_{ijl}^3)^3 \qquad \text{(III-17b)}$$

$$r^3 = a_3 (\rho_{ijl}^1)^2(\rho_{ijl}^2)^2 - b_3 (\rho_{ijl}^3)^2(\rho_{ijl}^1)(\rho_{ijl}^2)^{1/2} \qquad \text{(III-17c)}$$

The new concentration in a cell at the end of a time step, $\rho^{k,\,n+1}$, can be calculated explicitly by substituting the $\rho^{k,*}$ values into the rate expression, multiplying by Δt, and then adding this value to $\rho^{k,*}$.

Equilibria Constraints

The MMT-DPRW model code provides an alternate method for simulating simultaneous chemical reaction by requiring the system to be at equilibria within each cell at the end of each time step. The approach is justified only when the rates of reaction are very fast with respect to the flow rate of the system and the numerical time step size. If a portion of the source/sink term is to be computed using this assumption, a solution of a set of simultaneous nonlinear algebraic equations is usually required for each cell. These equations represent mass and charge balances and either mass-action expressions or functions that specify the minimization of the Gibbs Free Energy.

As an example, consider the reactions of three elemental species A, B and C within cell (i,j,l) where the following reactions occur very rapidly with respect to the numerical time step size:

$$A + 2B \rightleftarrows AB_2 \qquad \text{(III-18a)}$$

$$3B + 2C \rightleftarrows C_2B_3 \qquad \text{(III-18b)}$$

The system will then contain five distinct chemical species. To determine the equilibrium state of this cell it is necessary to solve a set of five equations that describe equilibrium requirements. Two of these equations may be mass-action expressions derived from Equation III-18:

$$K_1 = \frac{[AB_2]}{[A]\,[B]^2} \qquad \text{(III-19a)}$$

$$K_2 = \frac{[C_2B_3]}{[B]^3\,[C]^2} \qquad \text{(III-19b)}$$

where the brackets, [ ], denote the activity of the components, and K_1 and K_2 are equilibrium constants that are measurable in the laboratory.

Three additional relationships are provided by forming a mass balance for species A, B, and C:

$$M_A = (A) + (AB_2) \qquad \text{(III-19c)}$$

$$M_B = (B) + 2(AB_2) + 3(C_2B_3) \qquad \text{(III-19d)}$$

$$M_C = (C) + 2(C_2B_3) \qquad \text{(III-19e)}$$

where the parentheses indicate molar concentrations. The volume of the cell, V_{ijl}, which is constant, is included in each of the mass constants, M_A, M_B and M_C.

Systems of equations of the above type (Equation III-19) are usually solved by a Newton-Raphson iteration or some other alternative type of iterative procedure. The concentration values obtained immediately following the advection-dispersion computations (indicated by an *) are used to provide starting values for the iterative procedure. The reactive submodel in the current MMT-DPRW model is of this type and is discussed in some detail in the Appendix.

Once the concentration at the next time level, $\rho_{ijl}^{k,n+1}$, has been determined by a set of rate expressions or equilibria constraints, the mass associated with each parcel is adjusted by the ratio of this value to the initial or asterisk value:

$$\left(\xi_p^{k,n+1}\right)_{ijl} = \left(\frac{\rho_{ijl}^{k,n+1}}{\rho_{ijl}^{k,*}}\right)\left(\xi_p^{k,*}\right)_{ijl} \qquad \text{(III-20)}$$

The conversion of ξ (mass) to ρ (concentration) does not necessarily have to be made prior to computing some types of source/sink term contributions (Equation III-14), but concentration is usually a much more convenient quantity to work with than mass.

The entire procedure is repeated for as many time steps (N_t) as required to reach the desired simulation length. If non-zero concentrations of material are present at the beginning of a simulation, a specified number of parcels, η^0, are allocated to each distributed randomly within each cell and an initial mass is assigned to each parcel by:

$$\left(\xi_p^{k,0}\right)_{ijl} = \frac{\rho_{ijl}^{k,0}\, V_{ijl}}{G^{\zeta}\, \eta^0} \qquad \text{(III-21)}$$

Although the discussion has been directed towards computing the transport of mass, the computer code is also capable of simulating the transport of heat. If the words, heat and temperature, are substituted for mass and concentration in the development of the model and analogous assumptions made, the functional form of the mathematical analog is identical to that developed for mass transport calculation. This property allows heat to be treated as another species of groundwater contaminant that can be considered simultaneously with other chemical constituents.

IV SENSITIVITY AND ERROR ANALYSIS

The general characteristics of a DPRW solution can be illustrated by considering a particular test problem which is simple enough to analyze in detail, i.e., diffusion from an instantanous point source. The important numerical parameters associated with the DPRW numerical model will be varied to show how they affect the solution.

For this discussion the region of interest is assumed to be sufficiently restricted so the flow field can be considered constant in space and time. The general transport equation reduces to simple diffusion with respect to a coordinate system moving with the transporting fluid. The governing equation then becomes the classical diffusion equation:

$$\frac{\partial \rho}{\partial t} = D_x \frac{\partial^2 \rho}{\partial x} + D_y \frac{\partial^2 \rho}{\partial y^2} + D_z \frac{\partial^2 \rho}{\partial z^2} + r \qquad \text{(IV-1)}$$

where

ρ = concentration $[M/L^3]$
D = dispersion coefficient $[L^2/T]$
t = time [T]
r = source/sink term $[M/L^3T]$

The source term is a Dirac delta function, δ, in time and space:

$$r = Q\delta(x - x_o)\ \delta(y - y_o)\ \delta(z - z_o)\ \delta(t - t_o)$$

which states that an amount of material Q is released at time t_o at location (x_o, y_o, z_o). The analytical solution to this problem is:[20,29]

$$\rho = \frac{Q}{(2\pi)^{3/2}\sigma_x\sigma_y\sigma_z} e^{-\left[\frac{(x - x_o)^2}{2\sigma_x^2} + \frac{(y - y_o)^2}{2\sigma_y^2} + \frac{(z - z_o)^2}{2\sigma_z^2}\right]} \qquad \text{(IV-2)}$$

where

$$\sigma_x = \sqrt{2D_x(t-t_o)}$$
$$\sigma_y = \sqrt{2D_y(t-t_o)}$$
$$\sigma_z = \sqrt{2D_z(t-t_o)}$$

In order to simplify the presentation and clarify the parametric relationships only a one-dimensional case will be considered. For one dimension, Equation IV-2 reduces to:

$$\rho = \frac{Q}{(2\pi)^{\frac{1}{2}}\sigma} e^{\left[\frac{-(x - x_o)^2}{2\sigma^2}\right]}, \sigma = \sqrt{2D(t-t_o)} \qquad \text{(IV-3)}$$

which will be used as a reference in the subsequent discussion. Equation IV-3 is also recognizable as a normal distribution with standard deviation σ. For the numerical simulation a number of parcels, N_p, were released at $x_o = 0$ at $t_o = 0$, and were allowed to diffuse by a random walk process with characteristic root ~~mean~~ square step length Δx_{rms} and time step Δt. The relation between Δx_{rms}, Δt and the desired dispersion coefficient was shown in Equation II-26 to be given by:

$$\Delta x_{rms} = \sqrt{2D\Delta t} \qquad \text{(IV-4)}$$

Figure IV-1 shows a typical plot of a parcel distribution for the point source spreading problem resolved on a grid with unit spacing. For this simulation 500 parcels were used. The analytic solution (Equation IV-3) has been plotted as a solid line for comparison. The accuracy was quantified in two ways. First, the standard deviation of the computed distribution, σ_m, was calculated:

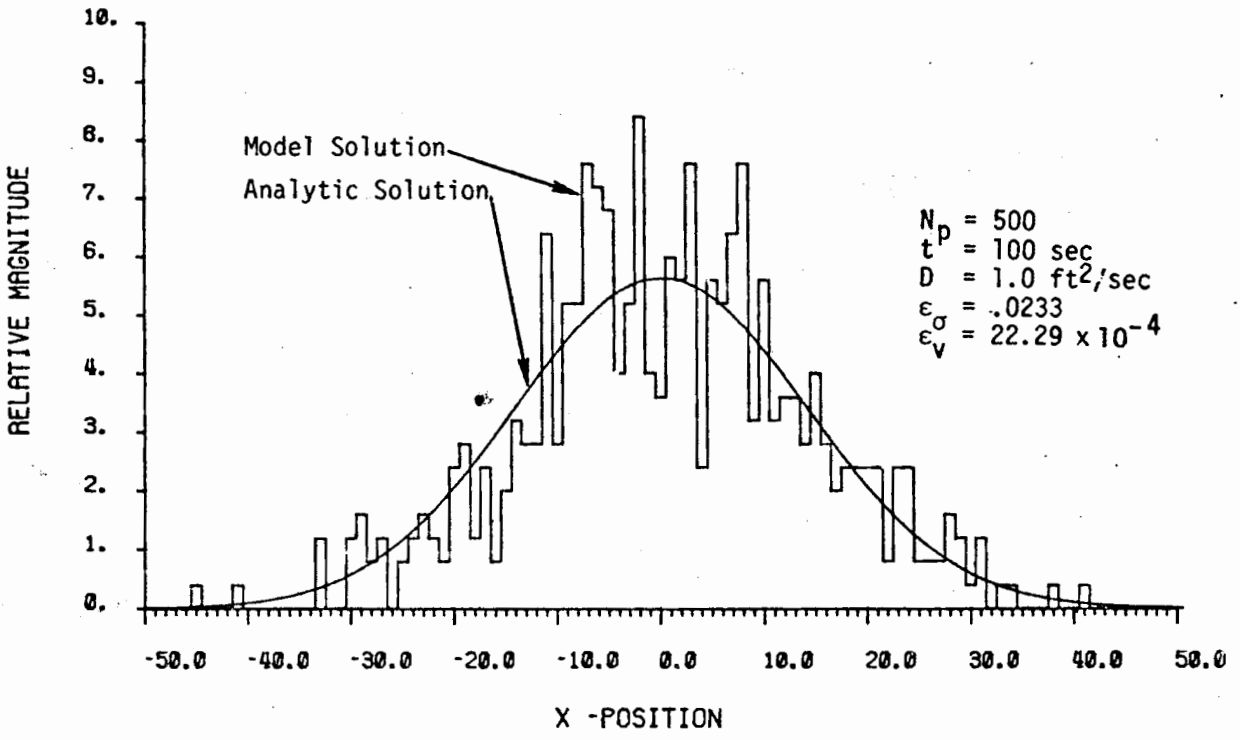

FIGURE IV-1. Comparison of 500 Parcel Model Solution Resolved on a 1 ft Grid, Bar Graph, with the Analytic Solution, Solid Line

$$\sigma_m = \left[\frac{1}{N_p} \sum_{j=1}^{N_p} (x_j - \bar{x})^2 \right]^{1/2} \qquad \text{(IV-5)}$$

where

x_j = displacement of parcel j

N_p = total number of parcels

$\bar{x}$ = mean value of parcel displacements

A relative standard deviation error, ε_σ, is then computed by:

$$\varepsilon_\sigma = 1 - \frac{\sigma_m}{\sigma} \qquad \text{(IV-6)}$$

In this example, σ_m = 13.81 when its expected value, σ, at this time is 14.14 from Equation IV-3. The standard deviation can be considered a measure of the width of the distribution. Consequently, this is a good parameter for checking the spreading rate of the numerical solution. The second check on the solution is the variance about the true function. Here it is called the "error variance" ε_v and is calculated by the formula:

$$\varepsilon_v = \Delta x \sum_{i=-\infty}^{\infty} (\rho_i - \rho_{io})^2 \qquad \text{(IV-7)}$$

where

Δx = grid spacing used to resolve the concentration distribution

ρ_i = expected concentration from Equation IV-3

ρ_{io} = computed concentration at x_i; $c_{io} = n_i/N_p \Delta x$

n_i = number of parcels between $x_i - \Delta x/2$ and $x_i + \Delta x/2$

i = location index along the x axis

The error variance is a measure of the roughness or noisiness of the numerical solution. Figure IV-2 shows the same case as Figure IV-1 but with 2000 parcels or four times as many. Both the values of ε_σ and ε_v have improved. This result indicates that the quality of a solution can be expected to improve as the number of parcels is increased. Figure IV-3 shows the effect of increasing the size of the summation interval to 5 ft. The solution shows an improved accuracy over Figure IV-2 but a lower spatial resolution.

These empirical results can be understood in a more general sense through the following arguments. Let $P(x,t)$ be the probability distribution function over the range of parcel displacements. The probability that a parcel will reside within the interval Δx at time t is given by:

$$P_i = P(x_i,t)\Delta x \qquad \text{(IV-8)}$$

When N_p parcels are released simultaneously, the expected number of parcels, $E(n_i)$, within the Δx interval will be:

$$E(n_i) = N_p P_i = N_p P(x_i,t)\Delta x \qquad \text{(IV-9)}$$

where n_i is the number of parcels within Δx. The variance of the expected value, $VAR(n_i)$, is given by:[19]

$$VAR(n_i) = N_p P_i (1-P_i) \qquad \text{(IV-10)}$$

When Δx is small with respect to the range of $P(x,t)$, $P_i \ll 1$ and Equation IV-10 can be rewritten as:[19]

$$VAR(n_i) = N_p P_i = N_p P(x_i,t)\Delta x \qquad \text{(IV-11)}$$

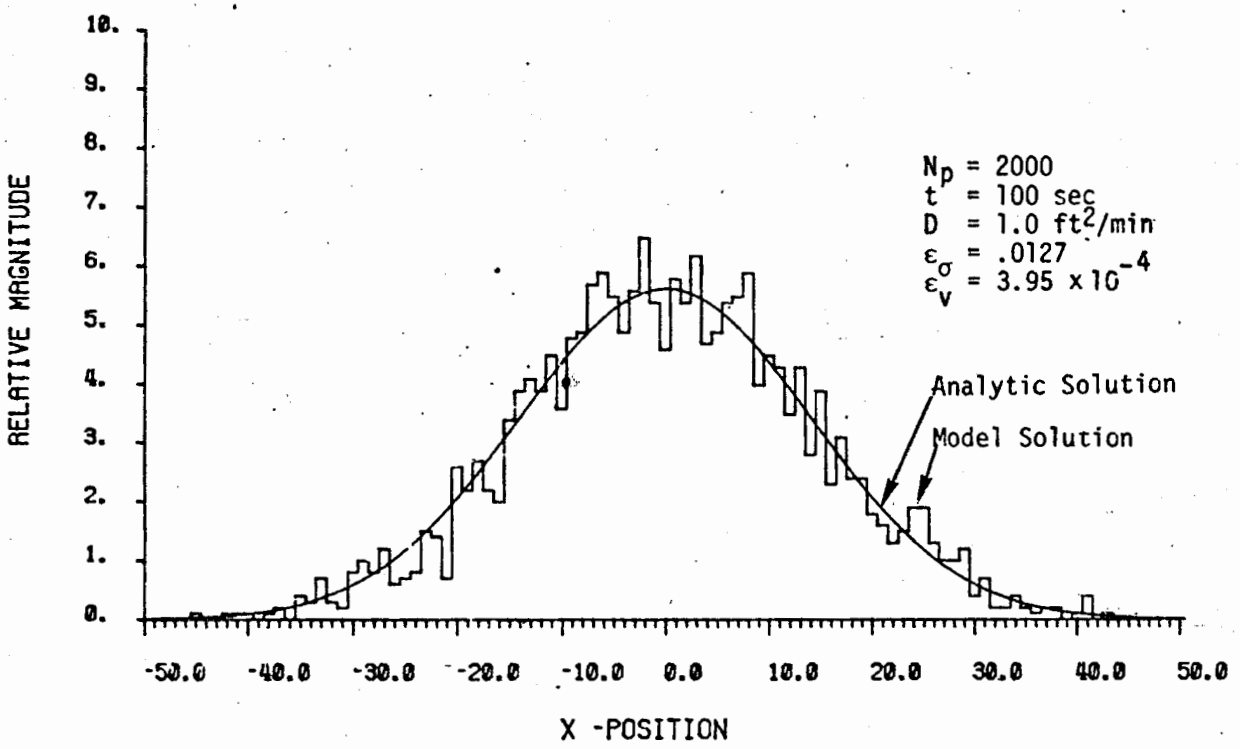

FIGURE IV-2. Comparison of 2000 Parcel Model Solution Resolved on a 1 ft Grid, Bar Graph, with the Analytic Solution, Solid Line

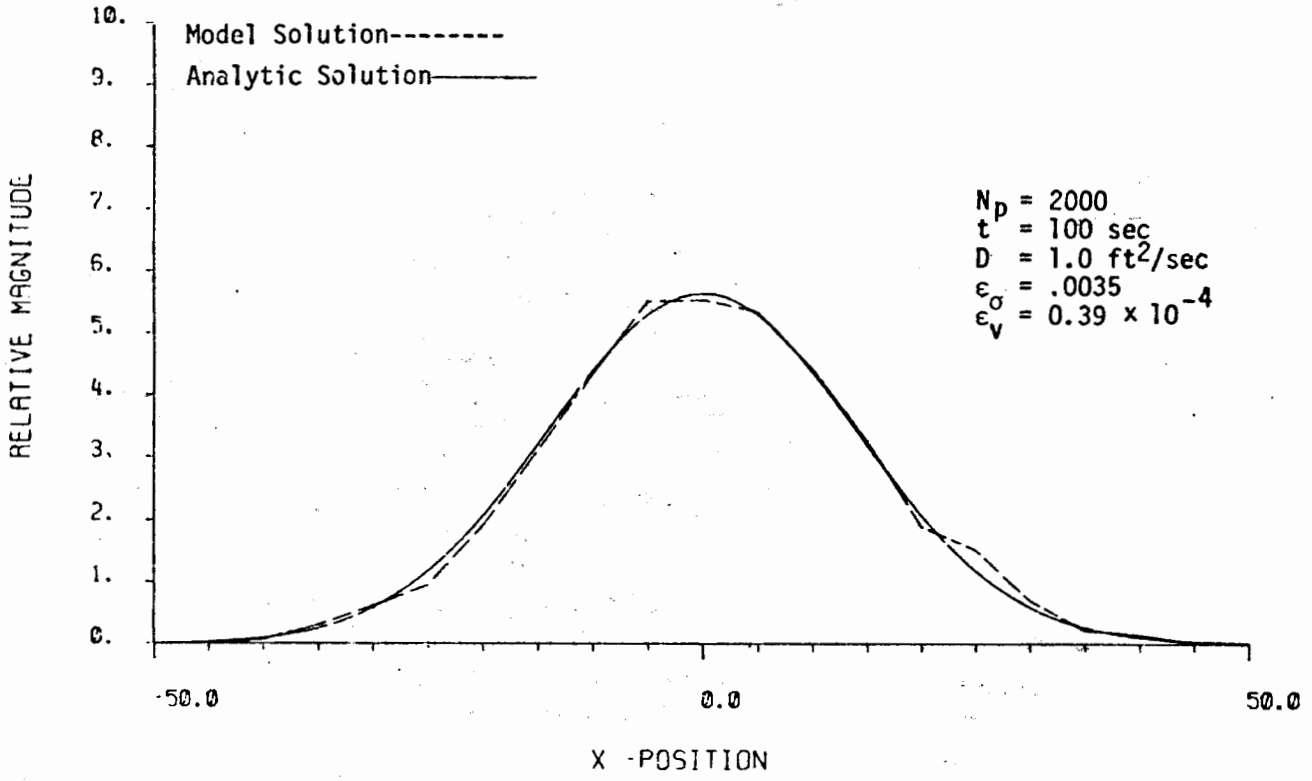

FIGURE IV-3. Comparison of 2000 Parcel Model Solution Resolved on a 5 ft Grid, Dashed Line, with the Analytic Solution, Solid Line

As discussed in Section III, a concentration (in one dimension) can be computed as:

$$\rho_i = \frac{G\eta_i}{\Delta x N_p} \qquad \text{(IV-12)}$$

where η_i is the number of parcels in the interval Δx and G is a proportionality constant used to express ρ_i in any desired units. The expected value and variance of ρ_i can then be expressed as:

$$E(\rho_i) = E(\frac{G\eta_i}{\Delta x N_p}) = \frac{G}{\Delta x N_p} E(\eta_i) = GP(x_i,t) \qquad \text{(IV-13)}$$

$$VAR(\rho_i) = VAR(\frac{G\eta_i}{\Delta x N_p}) = (\frac{G}{\Delta x N_p})^2 VAR(\eta_i) = \frac{G^2}{\Delta x N_p} P(x_i,t) \qquad \text{(IV-14)}$$

The squared term in Equation IV-14 results from a property of variances that can be expressed as:

$$VAR(bx) = b^2 VAR(x)$$

where b is a constant.

From the definition of variance the expression for the variance in the interval Δx can also be written as:

$$VAR(\rho_i) = \Delta x(\rho_i - \rho_{io})^2 \qquad \text{(IV-15)}$$

where ρ_{io} is the expected concentration at x_i given by Equation IV-3. The total squared error or error variance for the distribution is given by:

$$\varepsilon_v = \Delta x \sum_{i=-\infty}^{i=\infty} (\rho_i - \rho_{io})^2 \qquad \text{(IV-16)}$$

Equation IV-14 can be used to express the variance in the interval Δx. This substitution allows ε_v to be expressed in terms of Δx, N:

$$\varepsilon_v = \Delta x \sum_{i=-\infty}^{\infty} \frac{G^2}{\Delta x N_p} P(x_i,t) = \frac{G^2}{\Delta x N_p} \sum_{i=-\infty}^{\infty} P(x_i,t)\Delta x = \frac{G^2}{\Delta x N_p} \qquad \text{(IV-17)}$$

since in the limit

$$\lim_{\Delta x \to 0} \sum_{-\infty}^{\infty} P(x_i,t)\Delta x = 1 \qquad \text{(IV-18)}$$

In the following tests the internal spacing Δx is small enough that the error introduced is small compared to the variance.

Equation IV-17 was checked by running cases where grid spacing Δx was held constant and the number of parcels N_p varied (Figure IV-4). Also the cases are plotted with N_p constant and a variable Δx (Figure IV-5). In both plots the error variance was calculated from Equation IV-16. Each data point represents one run made with the parameters set at the values specified and analyzed at the indicated time. The data points were plotted on a log-log scale and a least squares straight line fit was made and plotted. The slope of the fitted line is indicated on each plot. Clearly, the points lie fairly close to the straight line on both plots. Moreover, the slope in both cases is within a few percent of -1. Thus an inverse relationship is indicated between error variance and number of parcels (Figure IV-4) and grid size (Figure IV-5). This is the result expected from Equation IV-17 where ε_v is proportional to $1/\Delta x N_p$. The standard error is equal to $\sqrt{\varepsilon_v}$:

$$\text{S.E.} = \sqrt{\varepsilon_v} = \sqrt{\frac{k}{\Delta x N}} \qquad \text{(IV-19)}$$

From this equation the general behavior of two of the important trade-offs in the numerical model are apparent. In order to reduce the statistical error component to half of its original value an increase by a factor of 4 in N_p is required. The same error reduction could be achieved by increasing the grid

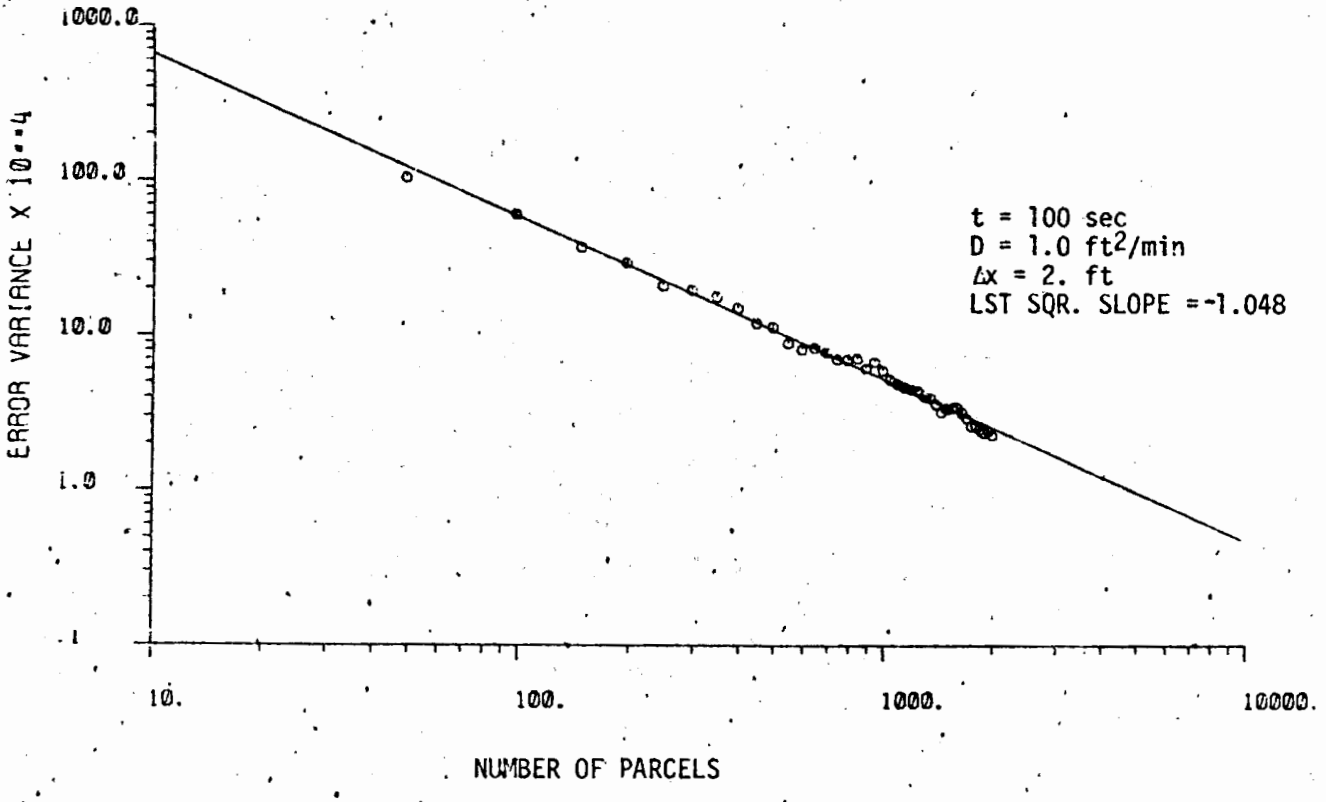

FIGURE IV-4. A Log Plot of the Inverse Relationship Between the Error Variance and the Number of Parcels Used in the Solution

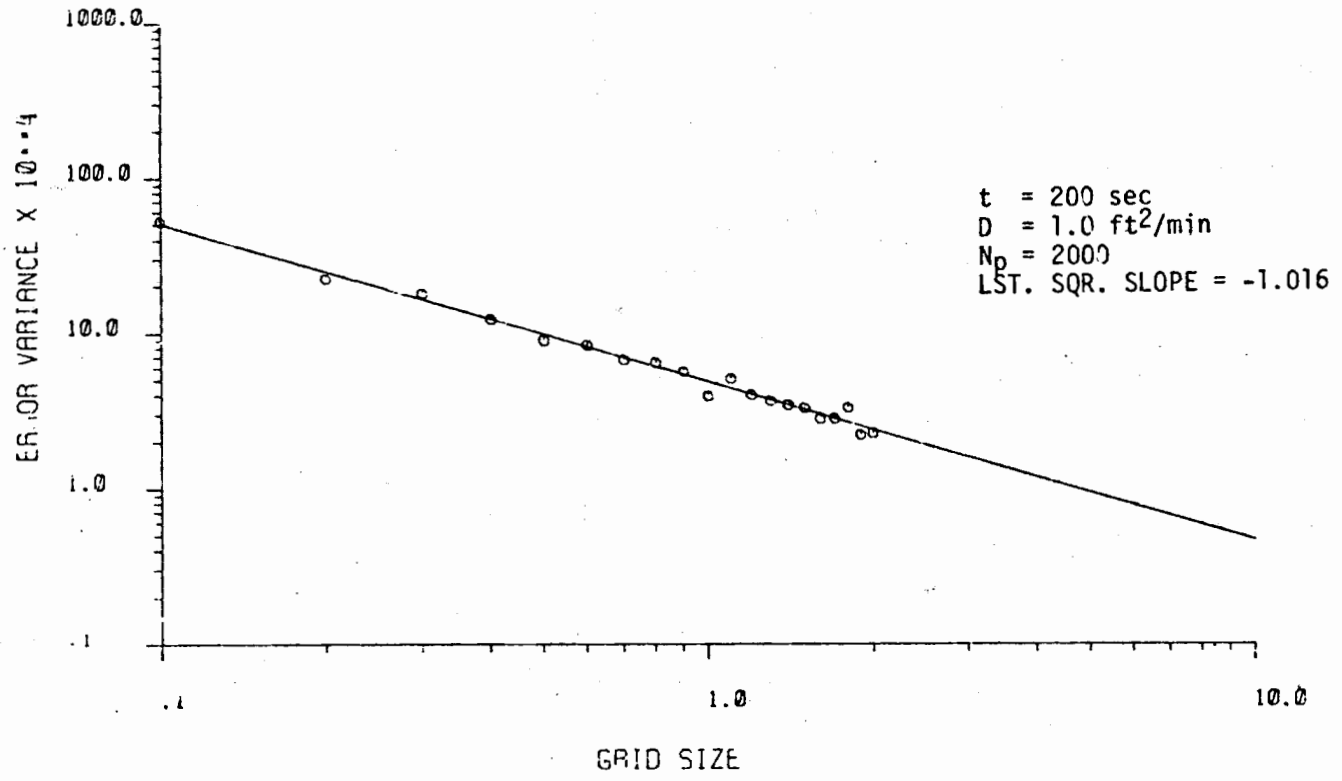

FIGURE IV-5. A Log Plot of the Inverse Relationship Between the Error Variance in a Solution and the Grid Size Used to Resolve that Solution

spacing Δx by a factor of 4. In a typical problem this means that the grid spacing should be made no smaller than the spatial resolution requirements of the problem demand. In regions where the concentration gradient is low a larger grid spacing could be used to advantage.

This slow convergence property of a solution means that it is unreasonable in most cases to reduce the relative error below 1%. A typical two-dimensional problem might use from 2×10^4 to 2×10^5 parcels and have an error range of 2-10%.

With most large-scale simulations the uncertainty in the input data is at least 5%. Thus, the practical numerical accuracy is usually not a serious limitation. However, if the data will permit a more accurate solution and the case in question requires it, then the trade-offs should be examined more carefully. It may be practical to run the model long enough to achieve the desired accuracy range or it might be necessary to consider a different type of model. In a particular case the practical accuracy limits can usually be estimated from a fairly short trial simulation.

Another way of checking the solution is to look at its spreading rate measured by the rate change of the variance of the particle distribution, $\frac{d(\sigma^2)}{dt}$. From the one-dimensional diffusion equation it can be shown that:

$$\frac{d(\sigma^2)}{dt} = 2D \qquad \text{(IV-20)}$$

Thus we can see if the solution is spreading at the proper rate by computing the rate of change of its variance. The rate of change was computed for two cases as depicted in Figures IV-6 and IV-7. In Figure IV-6 the variance of the distribution of a group of 100 parcels was calculated and plotted at each of 20 equally spaced time intervals. A least squares fit of the points was computed and plotted as a solid line. One half the slope of this line should be equal to the diffusion constant D. In this case the error was 8.78%. The same procedure was used for Figure IV-7 with 2000 parcels. The error in the slope was reduced to 2.22%. The residual variance, σ_r^2, is a measure of the quality of the least squares fit.

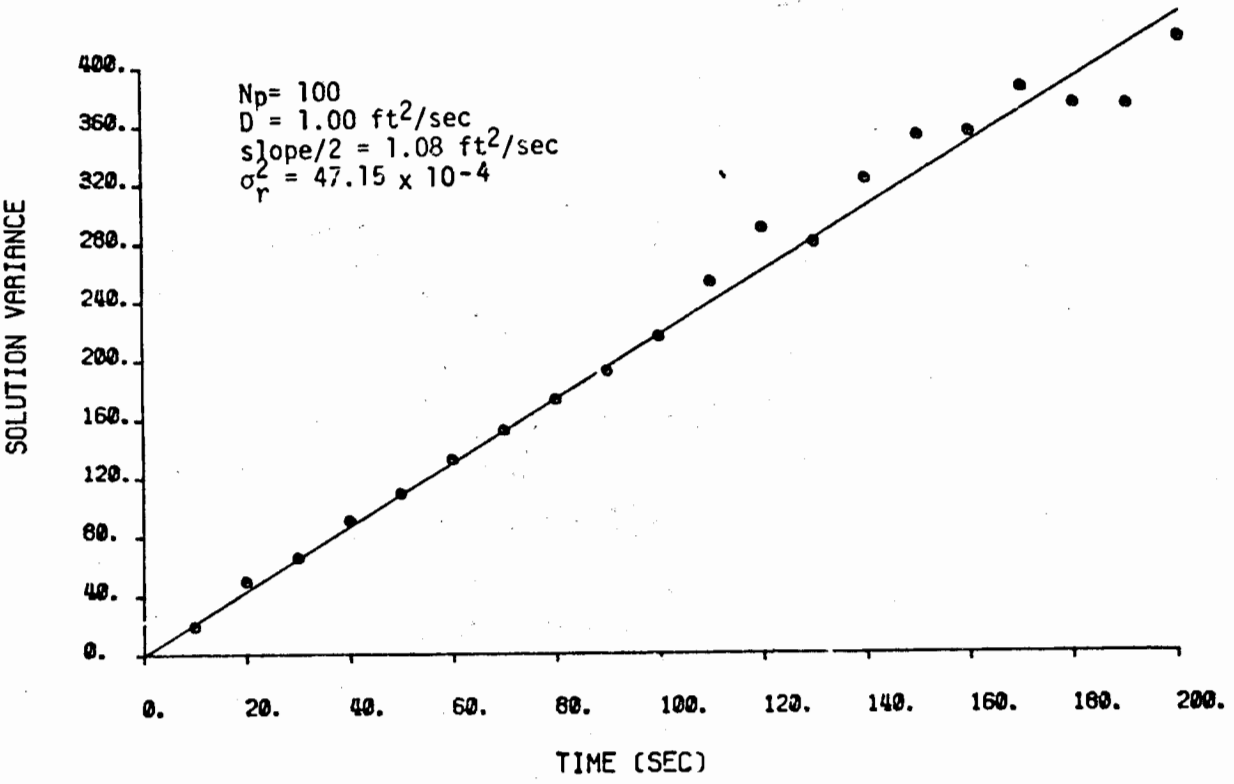

FIGURE IV-6. A Least Squares Plot of the Increase in the Variance of the Distribution with Time for 100 Parcels

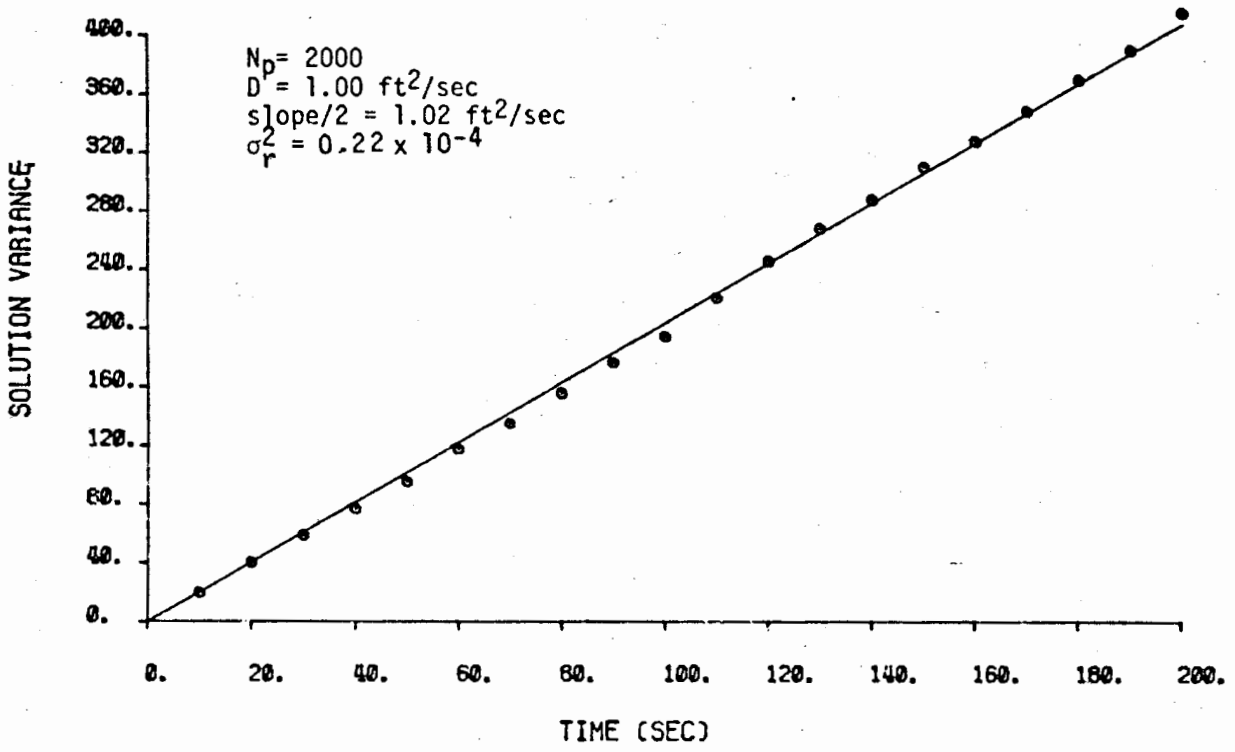

FIGURE IV-7. A Least Squares Plot of the Increase in Variance of the Distribution With Time for 2000 Parcels

SMOOTHING AND FILTERING FOR VARIANCE REDUCTION

It is often helpful to think of a DPRW solution as being exact but contaminated with random noise. The process of running a solution with more parcels improves the "signal to noise ratio" since the coherent part of the solution adds linearly and the incoherent or noisy part adds only as $\sqrt{N_p}$. This occurs because added noise tends to partially cancel itself while the signal adds coherently. Thus, the signal to noise ratio improves as $\sqrt{N_p}$.

Another way to improve the signal to noise ratio is by preferentially filtering the noise. Many times the solution is fairly smooth and slowly varying in space, and superimposed upon the solution is the random short period statistical "noise". Thus, by taking advantage of the predominatly high frequency nature of this portion of the solution the noise may be removed by low pass filtering.

The simplest type of filter to apply is a moving average filter in the space domain. The one used most often to smooth DPRW results has the form:

$$\rho_i^{s+1} = \frac{\rho_{i-1}^{s} + \rho_i^{s} + \rho_{i+1}^{s}}{3} \qquad \text{(IV-21)}$$

where the s superscripts indicate the number of times the data has been passed through the filter. When s=0 the c^s values are the raw unfiltered concentrations. Filtering can also be accomplished in the frequency domain.

The smoothing filter of Equation IV-21 was applied to the solutions of Figures IV-1 and IV-2 to produce the improved solutions in Figures IV-8 and IV-9. The 500 point case was smoothed 15 times and the 2000 point case 5 times. The error variance has been considerably reduced in both cases and the standard deviation slightly increased. To achieve the same reduction by increasing the parcel count would have required about a factor of 10 increase in the number of parcels and consequently 10 times the computer time.

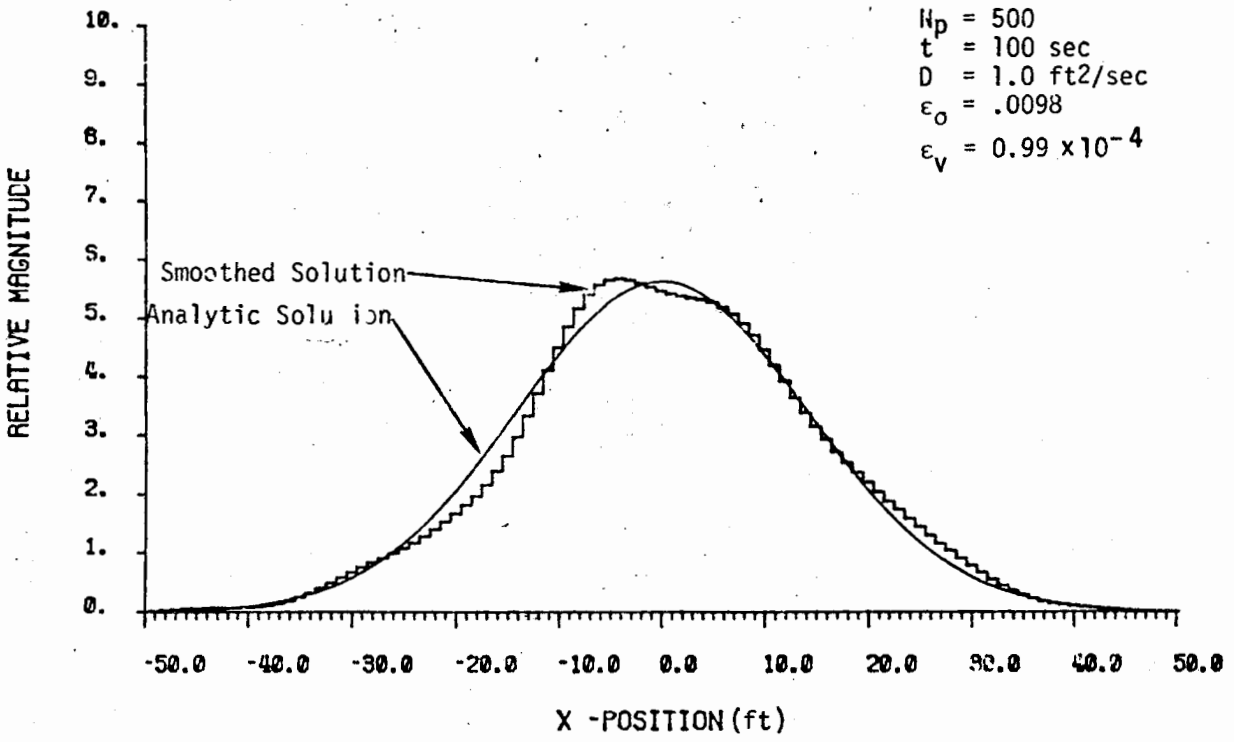

FIGURE IV-8. A Plot of the Parcel Distribution Shown in Figure IV-1 Smoothed 15 Times With a 3 Point Moving Average Filter

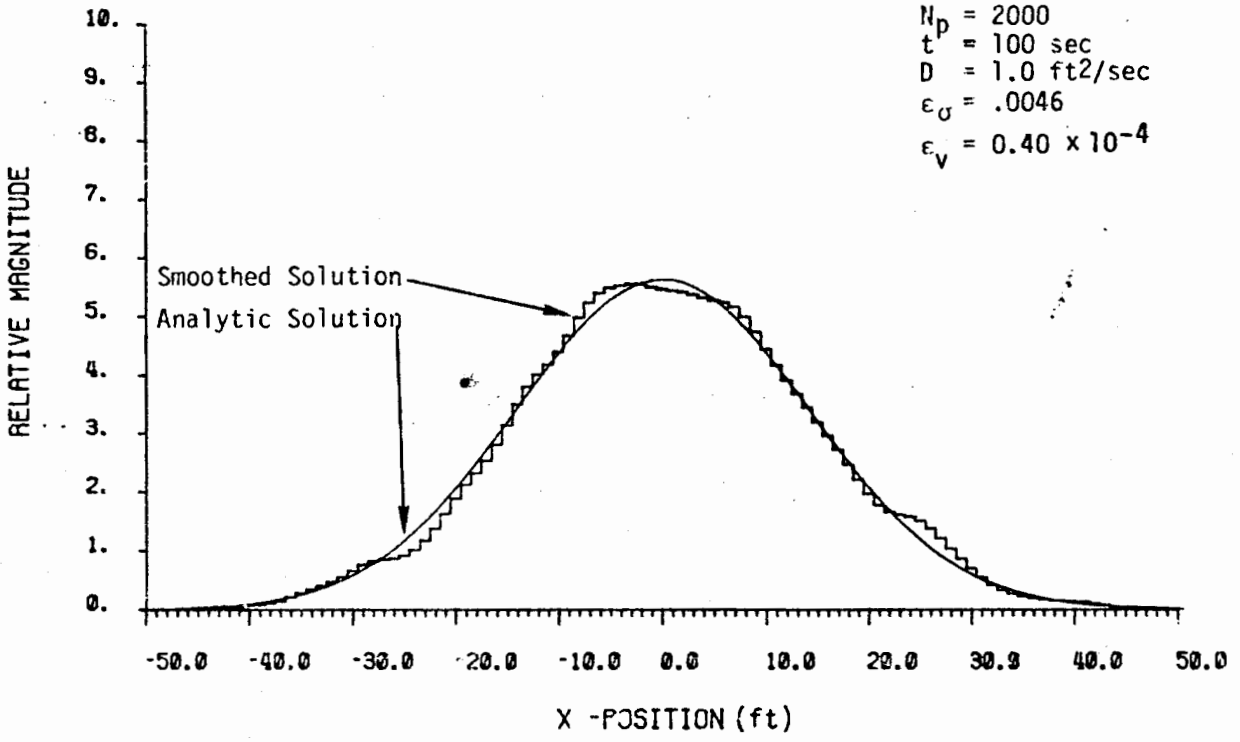

FIGURE IV-9. A Plot of the Distribution Shown in Figure IV-2 Smoothed 5 Times With a 3 Point Moving Average Filter

Figures IV-10 through IV-12 depict the frequency domain filtering of the same two cases. Figure IV-10 shows the long high frequency tail containing most of the noise in the solution, which can be eliminated by low pass filtering to considerably improve the accuracy of the solution. The comparison of results is shown in Figure IV-12. The error variance has been reduced by an order of magnitude. The same procedure has been applied to the 2000 point case in Figures IV-13 through IV-15. Here the high frequency component is smaller and the filtering more successful. The variance was reduced by a factor of 20.

Generally it can be seen that when the desired solution does not contain high spatial frequencies, filtering may be successfully applied to reduce error. The savings of computer time over the alternative of using more parcels can be considerable. A moving average filter will work nearly as well as exact frequency domain low pass filter and is much less time consuming to apply. In these examples the Fast-Fourier-Transform (FFT) was used for frequency filtering. However, when applied in two or more dimensions this type of filter would consume a significant portion of the computer time it was attempting to save.

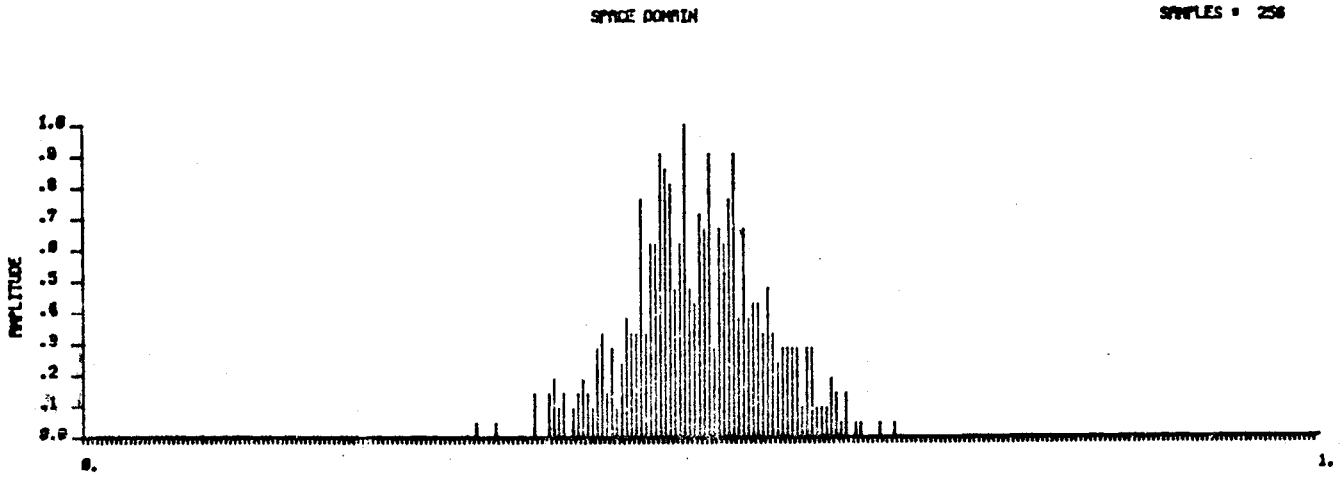

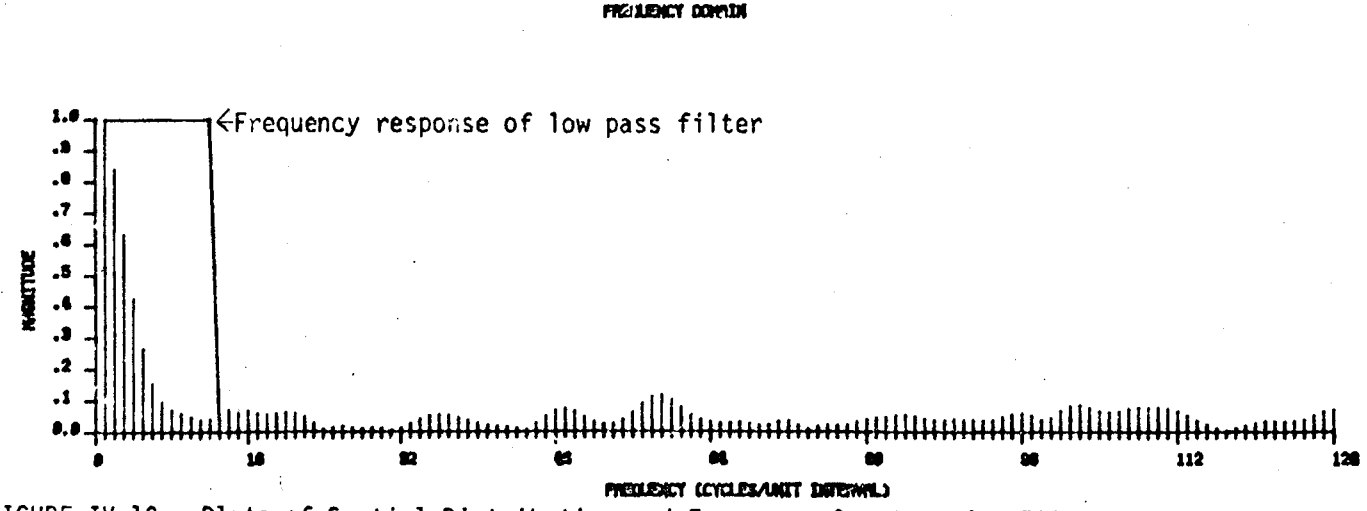

FIGURE IV-10. Plots of Spatial Distribution and Frequency Spectrum for 500 Parcel Solution Depicted in Figure IV-1

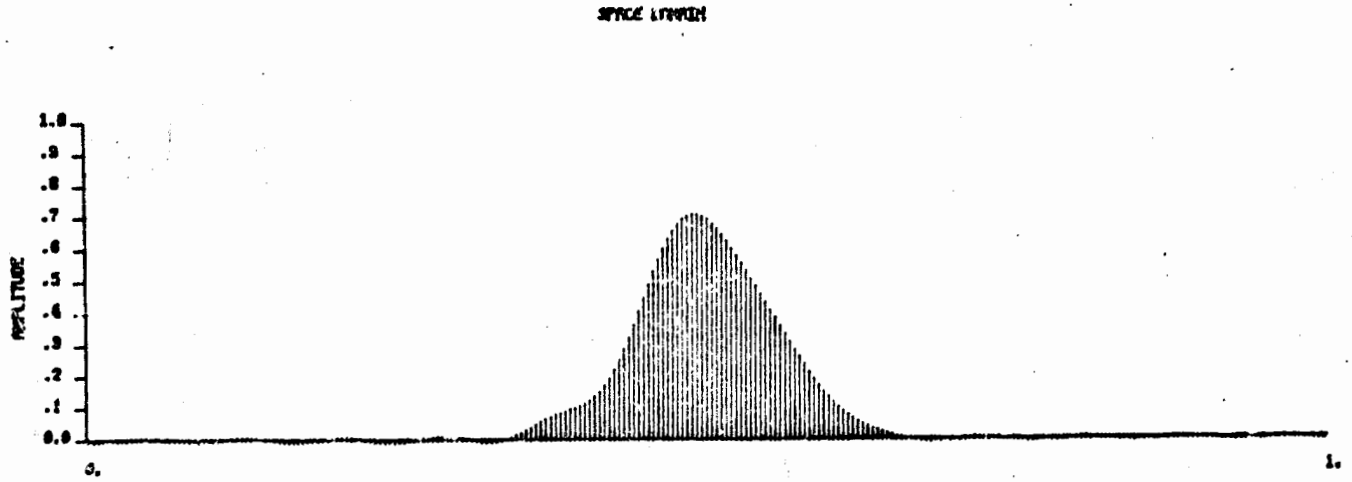

FIGURE IV-11A. Plot of Inverse Fourier Transform of the Filtered Frequency Spectrum in IV-11B

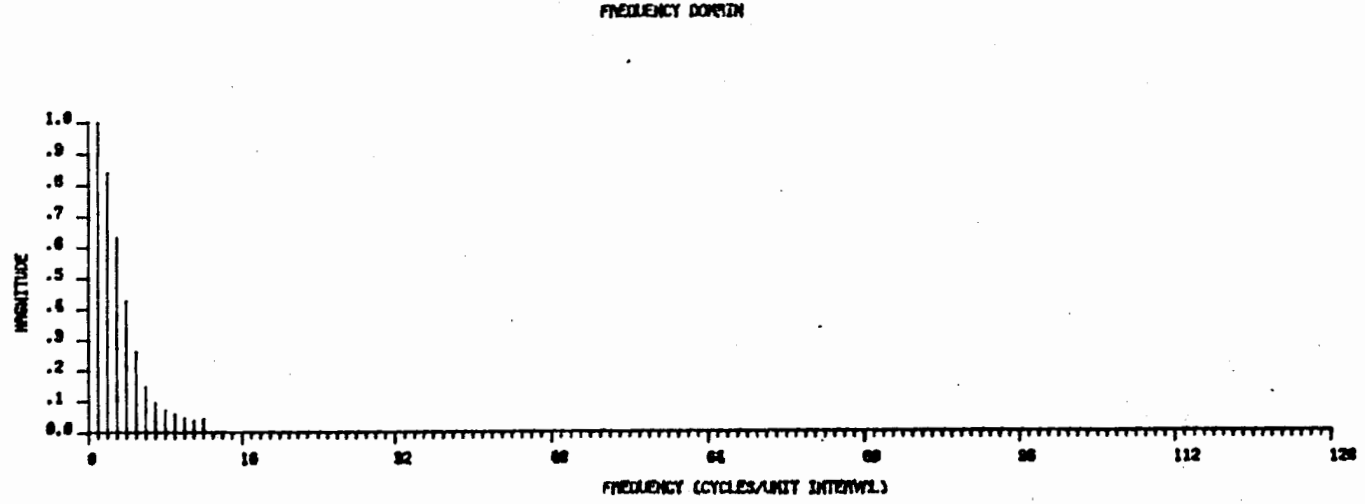

FIGURE IV-11B. Plot of the Frequency Spectrum of Figure IV-10 After Low Pass Filtering

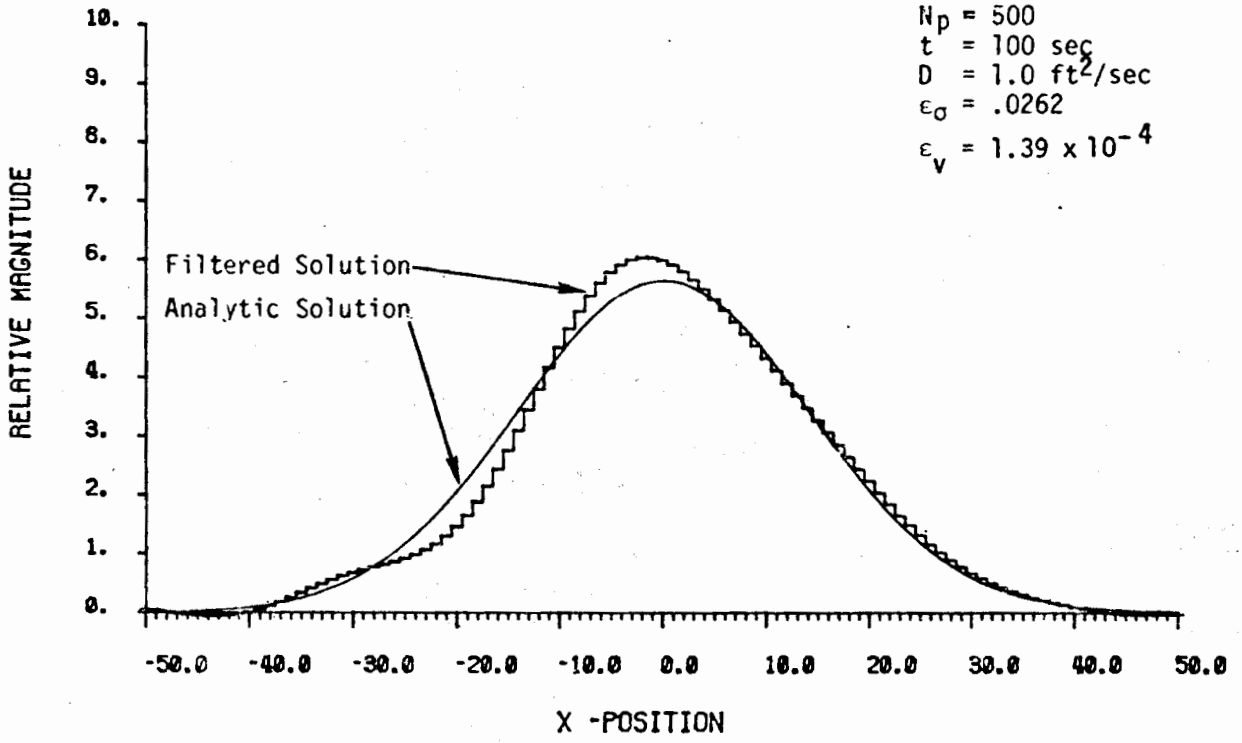

FIGURE IV-12. Frequency Domain Low Pass Filtered Version of the Distribution From Figure IV-1

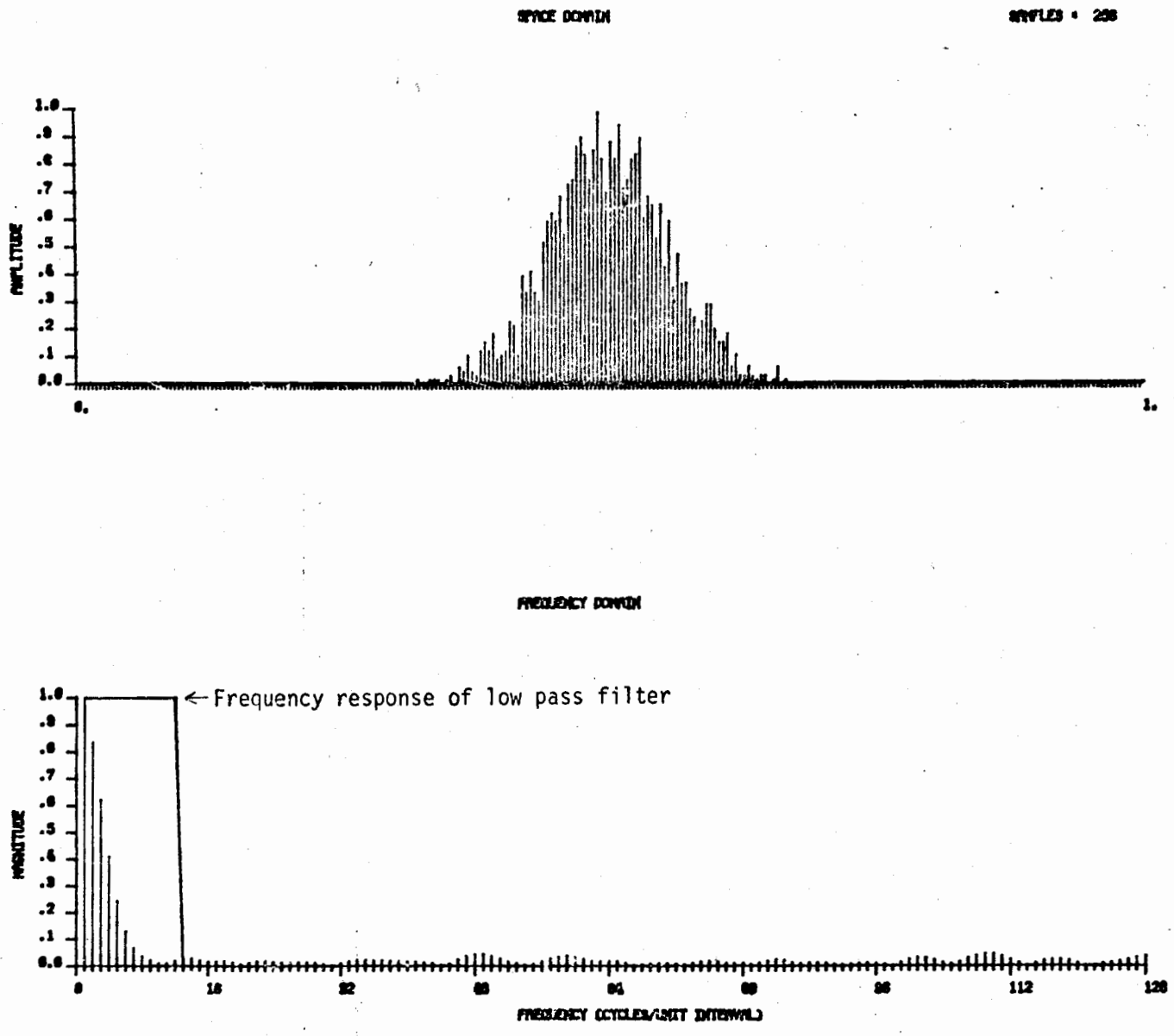

FIGURE IV-13. Plots of Spatial Distribution and Frequency Spectrum for 2000 Parcel Solution Depicted in Figure IV-2

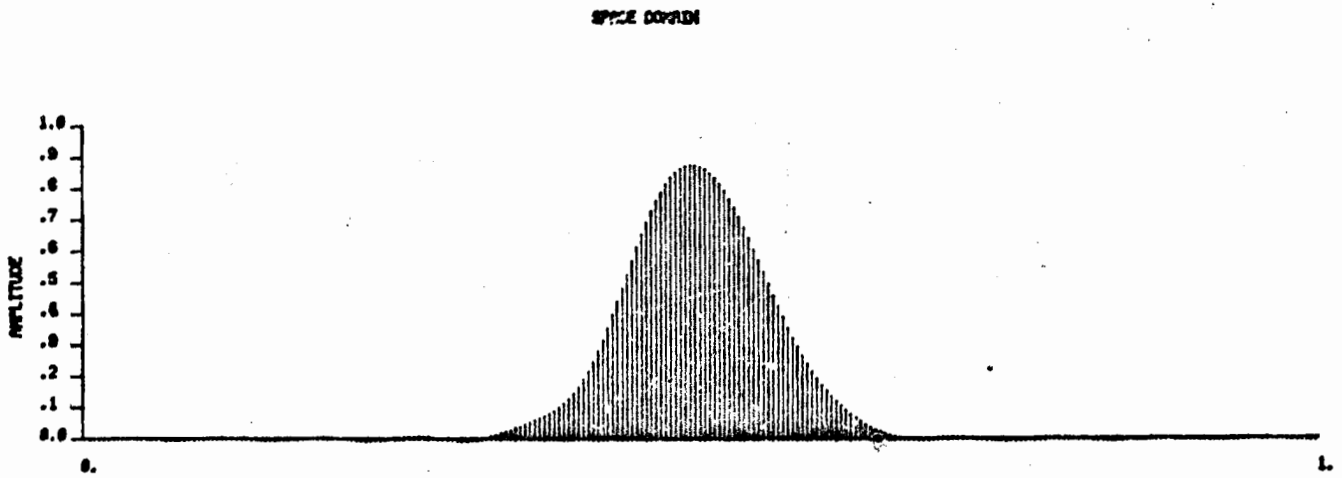

FIGURE IV-14A. Plot of Inverse Fourier Transform of the Filtered Frequency Spectrum in Figure IV-14B

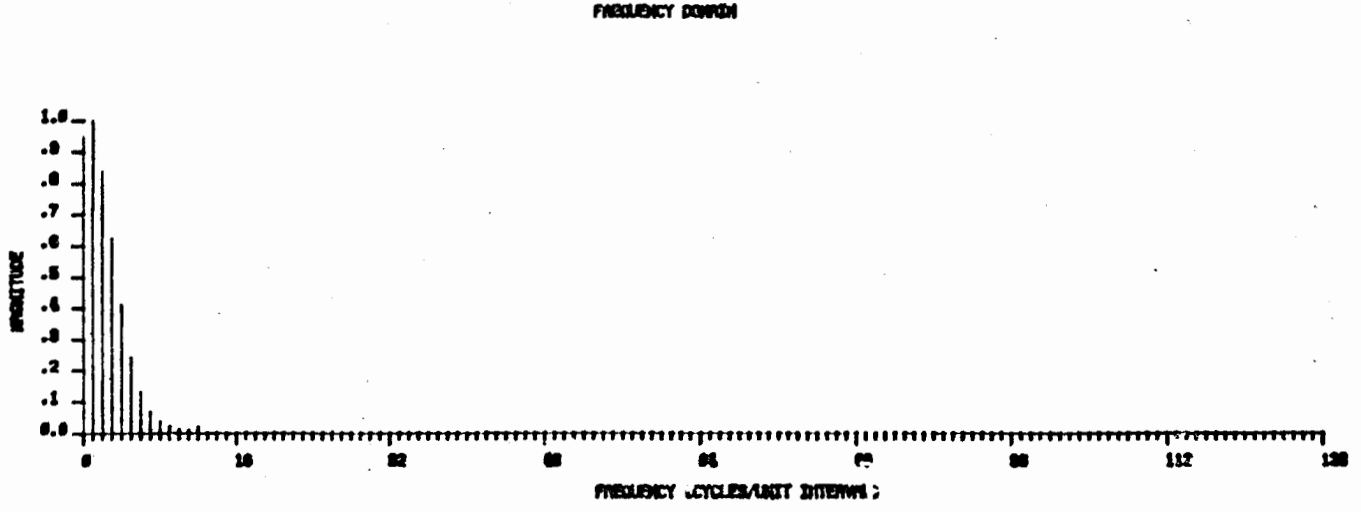

FIGURE IV-14B. Plot of the Low Pass Filtered Frequency Spectrum of Figure IV-13

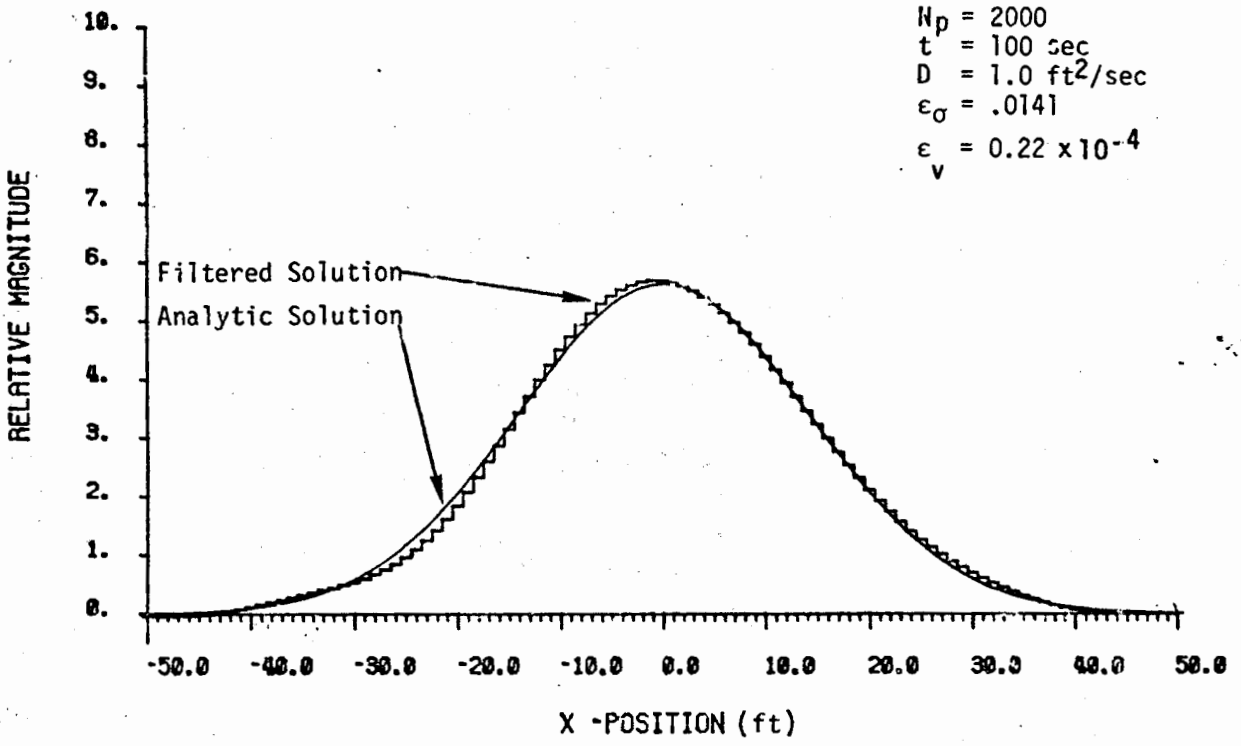

FIGURE IV-15. The Frequency Domain Low Pass Filtered Version of the Distribution From Figure IV-2

VERTICALLY AVERAGED TRANSPORT EQUATION

This section considers the modifications required in the previously described solution techniques for the special case of the vertically averaged transport equation. Again for simplicity the one-dimensional case will be examined. In one-dimension, Equation II-9 reduces to:

$$\frac{\partial \rho}{\partial t} + \left(v - \frac{D}{H}\frac{dH}{dx}\right)\frac{\partial \rho}{\partial x} = \frac{\partial}{\partial x}\left(D\frac{\partial \rho}{\partial x}\right) + r \qquad \text{(IV-22)}$$

where

ρ = concentration [M/L^3]
v = advective velocity [L/T]
D = dispersion coefficient [L^2/T]
H = aquifer thickness [L]
r = source/sink term [M/T]

All that distinguishes this equation from the transport equation for uniform thickness is the term $\frac{D}{H}\frac{dH}{dx}$. The effect and origin of this term will be detailed in the following text. Because this term has units of velocity (ft/day) and depends directly on the rate of change of aquifer thickness, it appears as a thickness and slope dependent addition to the convective velocity. Its origin, however, is in the unbalanced diffusive flux caused by the thickness variation. This effect can be seen from an analysis of Figure IV-16. Here J(x) refers to the vertically-averaged horizontal diffusive flux. The net rate of change of material in the trapezoidal region as a result of diffusion is given by:

$$\frac{\Delta Q}{\Delta t} = J(x)H - J(X+\Delta x)(H+\Delta H) \qquad \text{(IV-23)}$$

Substituting the Taylor series expansion for $J(x+\Delta X)$

$$J(x+\Delta x) = J(x) + \frac{\partial J(x)}{\partial x} \cdot \Delta x + \text{higher order terms in } \Delta x,$$

Equation IV-23 reduces to the following:

$$\frac{\Delta Q}{\Delta t} = -\frac{\partial J(x)}{\partial x}\Delta x H - J(x)\Delta H - \frac{\partial J(x)}{\partial x}\Delta x \Delta H \qquad \text{(IV-24)}$$

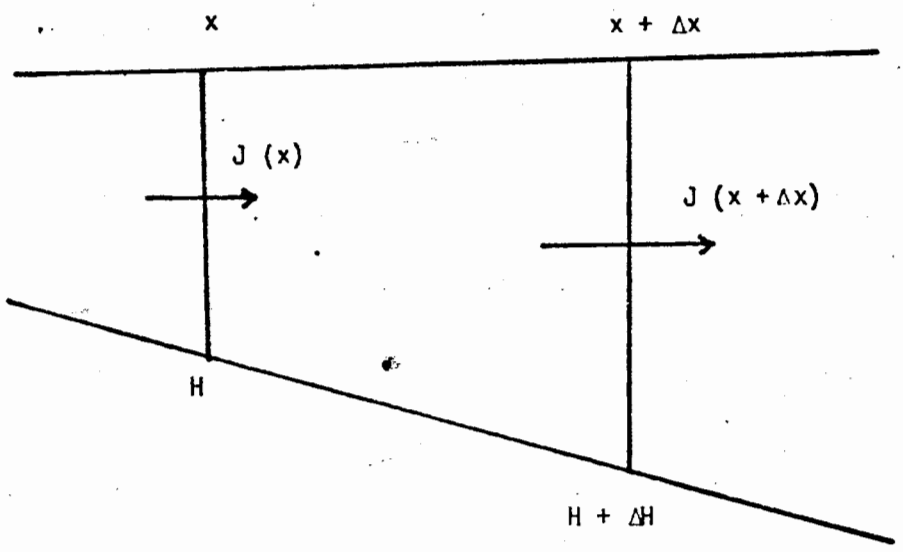

J (x) = vertically averaged flux at x

H = thickness

FIGURE IV-16. Diagram Used in Deriving One-Dimensional Vertically Averaged Transport Equation

The concentration $\rho = \frac{Q}{\Delta x(H+\Delta H/2)}$, making this substitution and taking the limit as Δx, $\Delta t \to 0$ yields the equations:

$$\frac{\partial \rho}{\partial t} = - \frac{\partial J(x)}{\partial x} - \frac{J(x)}{H} \frac{dH}{dx} \qquad \text{(IV-25)}$$

Then, since the diffusive flux is proportional to the concentration gradient, $J = -D \frac{\partial \rho}{\partial x}$, the equation can be written in the form:

$$\frac{\partial \rho}{\partial t} = \frac{\partial}{\partial x} \left(D \frac{\partial \rho}{\partial x}\right) + \frac{D}{H} \frac{dH}{dx} \frac{\partial \rho}{\partial x} \qquad \text{(IV-26)}$$

The last term in this equation is of particular interest. This term results from the unequal transfer area across the trapezoid in Figure IV-16. The convective flux will only add the expected term $v \frac{\partial \rho}{\partial x}$ since v is conservative and in one dimension inversely proportional to the thickness H. These results were checked by reformulating Equation IV-24 slightly to produce the following difference equation in ρ:

$$\frac{H_i \Delta x^2}{D} \frac{\Delta \rho}{\Delta t} = H_{i-1/2}\, \rho_{i-1} - (H_{i-1/2} + H_{i+1/2})\, \rho_i + H_{i+1/2}\, \rho_{i+1} \qquad \text{(IV-27)}$$

Here H_i, ρ_i are the thickness and concentration, respectively, in a node centered finite difference scheme.

If the usual Crank-Nicolson approximation is made in time the result is a tri-diagonal system of equations:

$$A_i\, \rho_{i-1}^{n+1} + B_i\, \rho_i^{n+1} + E_i\, \rho_{i+1}^{n+1} = F_i \qquad \text{(IV-28)}$$

where

$$A_i = -H_{i-1/2}$$

$$B_i = 2[H_i + \alpha] \;,\; \alpha = \frac{H_i \Delta x^2}{D \Delta t}$$

$$E_i = -H_{i+1/2}$$

$$F_i = H_{i-1/2}\, \rho_{i-1}^n - 2(H_i - \alpha)\, \rho_i^n + H_{i+1/2}\, \rho_{i+1}^n$$

Here the subscript i refers to horizontal position at the node centers and the superscript n refers to the time step. These equations were solved with 500 nodes for two cases, Figures IV-17 and IV-18. The first case has a uniform thickness of 50 ft and the second a uniformly varying thickness with $\frac{dH}{dx} = .1$. For each case the mean position and variance of the solution were calculated at each time step and stored. A least squares straight line fit was made for each set of points to obtain the slopes. These slopes were used to compute the convection and dispersion from the equations.

$$v = \frac{d}{dt} M(x) \text{ and } D = \frac{1}{2} \frac{d}{dt} VAR(x) \qquad \text{(IV-29)}$$

where

v = effective convective velocity
$M(x)$ = mean position of the solution $\rho(x,t)$
D = effective dispersion coefficient
$VAR(x)$ = variance of the x coordinate of the solution $\rho(x,t)$

The listed velocities and dispersion coefficients were obtained from the above equations. The effect of the slope term can be seen in Figure IV-18. This term produces the slight drift of the solution in the positive x direction. The velocity obtained from the drift of the mean of the solution .0209 ft/day compares favorably with the value .019 ft/day found by evaluating the term:

$$v = -\frac{D}{H}\frac{dH}{dx} = -\frac{10 \text{ ft}^2/\text{day}}{51.8 \text{ ft}} \times -.1 \text{ ft/ft} = .0193 \text{ ft/day}$$

The small difference is mainly caused by the slight skewing resulting from the higher drift rate with decreasing thickness. This differential velocity increases the effective diffusion coefficient from 10. to 10.26.

The same case was solved with a two-dimensional random walk model. The dimensions are in the x and z directions. The normal component of flux = 0 conditions was simulated by making the upper and lower boundaries act as perfect reflectors. The vertically averaged concentrations are computed

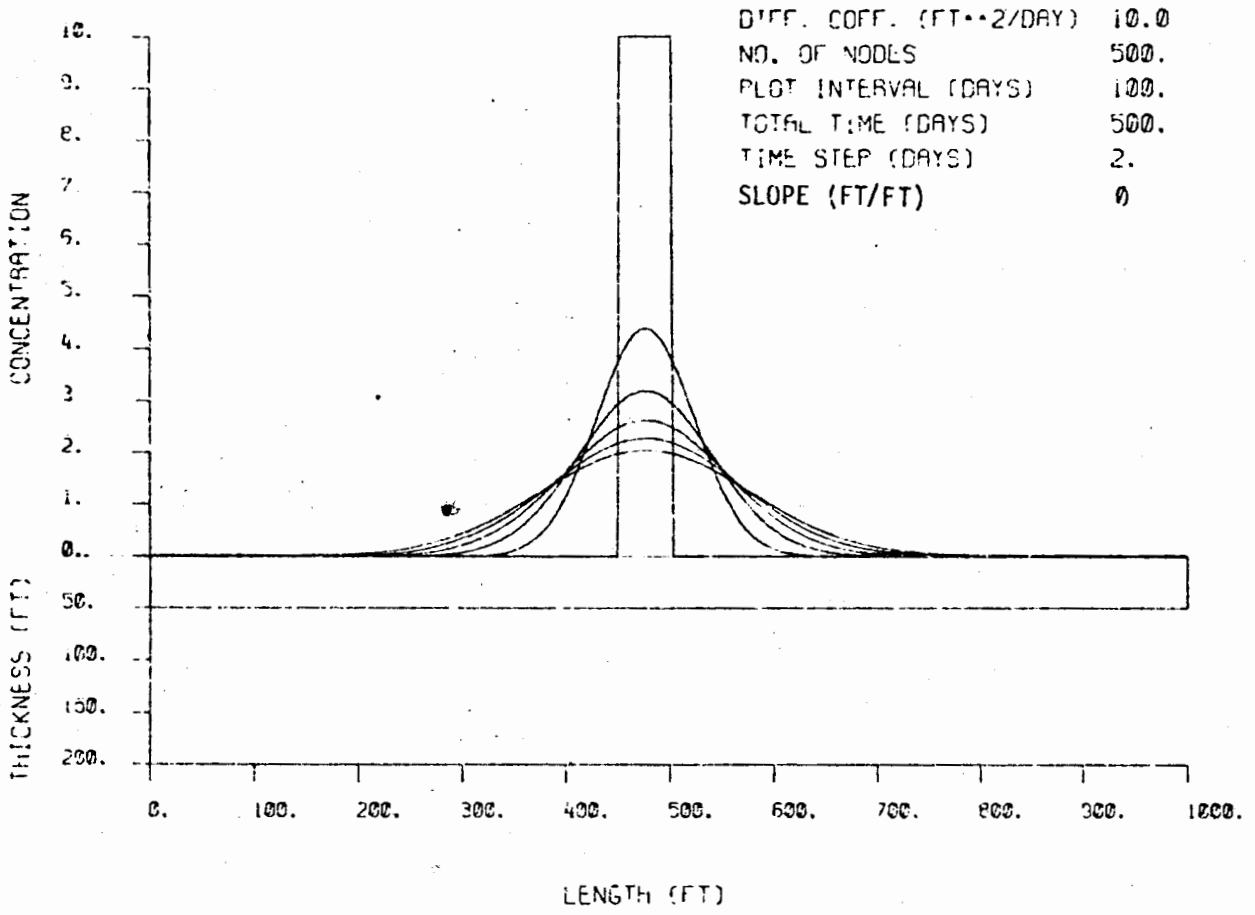

TIME (DAYS)	MEAN POSITION (FT)	VARIANCE (FT^2/DAY)
100	476.	2225.9
200	476.	4226.2
300	476.	6225.9
400	476.	8225.8
500	476.	10225.4

From least squares fit:
Velocity (FT/DAY) = 0
Diffusion Coeff. (FT^2/Day) = 10.(

FIGURE IV-17. Finite Difference Solution to Uniform Thickness Case

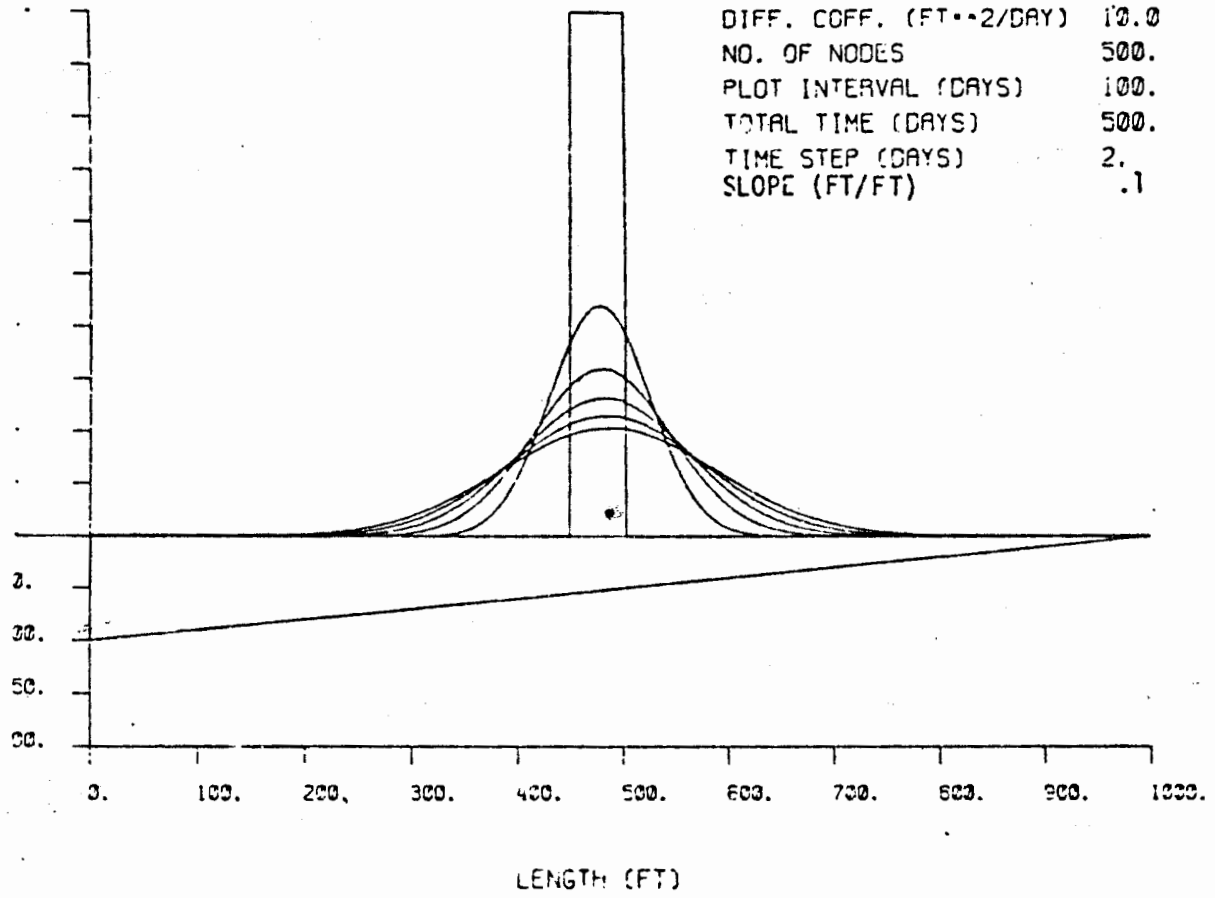

TIME (DAYS)	MEAN POSITION (FT)	VARIANCE (FT^2/DAY)
100	477.9	2235.5
200	479.9	4261.4
300	482.0	6305.8
400	484.1	8372.8
500	486.3	10466.5

From least squares fit
Velocity (FT/DAY) - 0209
Diffusion Coeff. (FT^2/DAY) = 10.26

FIGURE IV-18. Finite Difference Solution to Variable Thickness Case

and plotted in Figure IV-19. The mean and variance were calculated as in the finite difference case and also appear in Figure IV-19. The results agree with the finite difference solution as well as would be expected for 3000 parcels. By examining a number of runs, it was determined that the average velocity error was about $\pm$.0024 ft/day, for the random walk solution. The main object of this simulation was to establish that the simple random walk diffusion with a reflecting boundary condition would lead to the same result obtained from the vertically averaged differential equation. In the direct simulation the additional velocity term comes about naturally from the particle reflections off the sloping boundaries.

The most practical way to incorporate this term, however, is to simply modify the convective velocity field by the amount $\Delta v = -\frac{D}{R}\frac{dH}{dx}$, for one dimension. The two-dimensional case is given by Equation II-9. A one-dimensional case of this type was solved and plotted in Figure IV-20. Here the ambient velocity field was 1 ft/day. The average slope contribution to the velocity was about .01 ft/day. The calculated diffusion constant is somewhat large but the accuracy could be improved by increasing the number of particles.

Examples of the application of the model to two-dimensional cases of realistic complexity can be found in References 7 and 28.

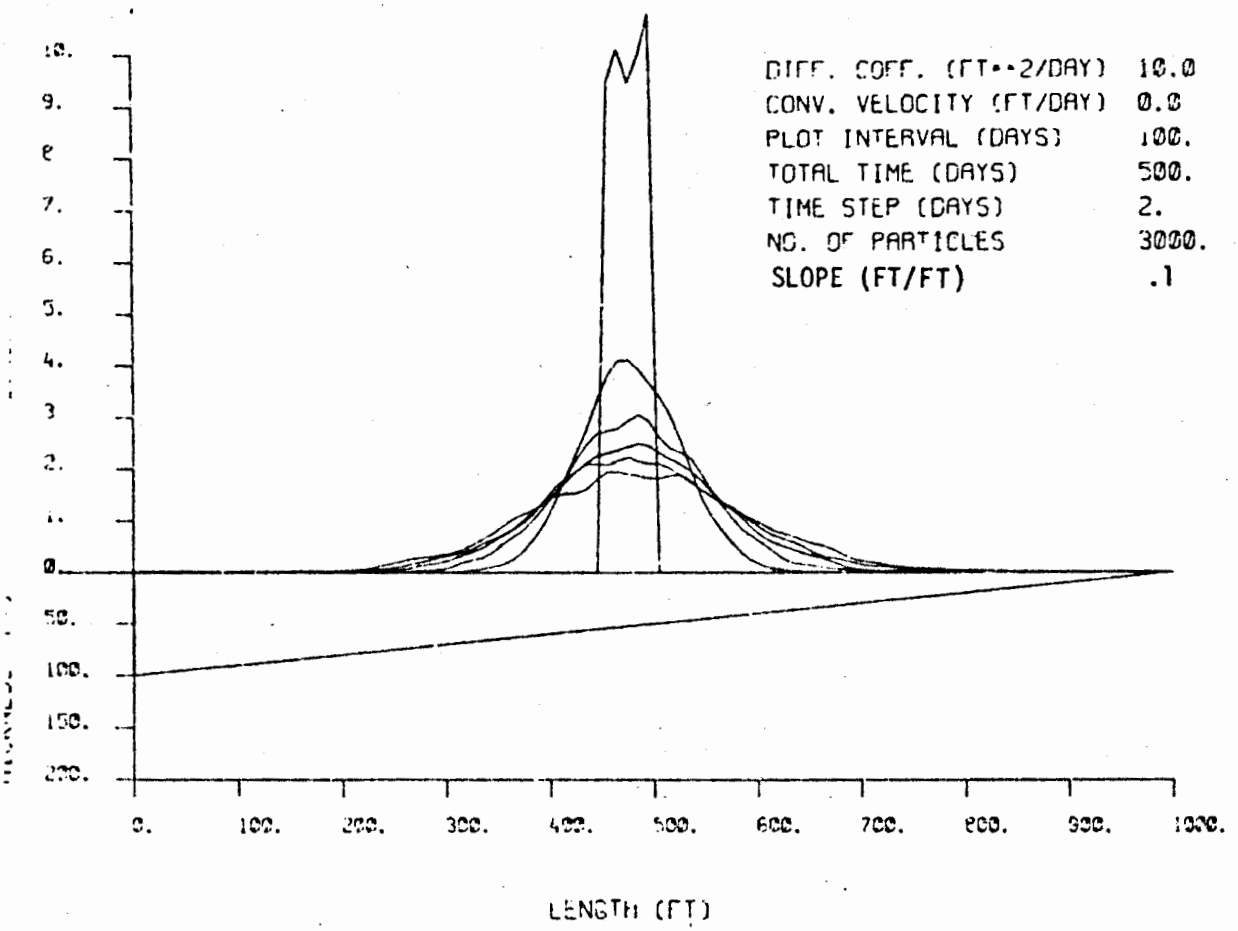

TIME (DAYS)	MEAN POSITION (FT)	VARIANCE (FT^2/DAY)
100	476.9	2163.8
200	479.5	3923.5
300	479.9	6114.8
400	481.6	8256.8
500	484.5	9791.3

From least squares fit:
Velocity (FT/DAY) = .0174
Diffusion Coeff. (FT^2/DAY) = 9.71

FIGURE IV-19. Vertically Averaged Two-Dimensional Random Walk Solution to the Variable Thickness Case

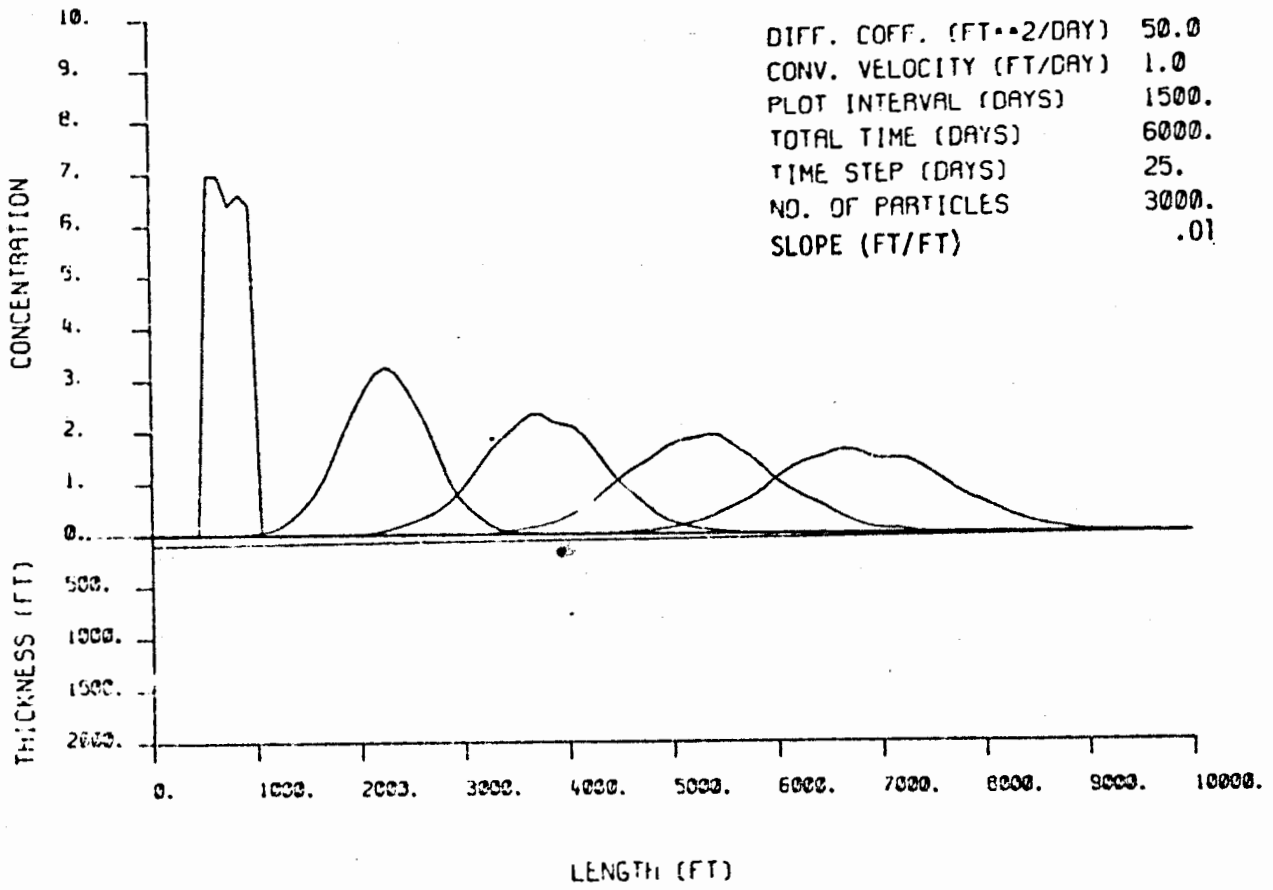

TIME (DAYS)	MEAN POSITION (FT)	VARIANCE (FT^2/DAY)
1500	2247.	162634.
3000	3756.	326436.
4500	5272.	488214.
6000	6798.	652688.

From least squares fit:
Velocity (FT/DAY) = 1.011
Diffusion Coeff. (FT^2/DAY) = 54.4

FIGURE IV-20. One-Dimensional Random Walk Solution to Vertically Average Transport Equation

BLANK PAGE

V. PRELIMINARY APPLICATION OF THE MMT-DPRW MODEL

A preliminary application of the MMT-DPRW model consisted of simulating tritium movement in the Hanford unconfined aquifer between 1968 and 1976. The purpose of this simulation was to test the model with existing Hanford field data in order to determine any insufficiencies in the present hydrological data base and/or in the model formulation. Tritium was chosen for this application for several reasons:

- Several tritium concentration measurements have been made throughout the Hanford unconfined aquifer. These data are the most complete data set now available to provide initial conditions and also to check the model results.
- The current extent of measurable tritium levels defines a plume that lies beneath a substantial portion of the Hanford Site.
- It can be assumed that tritium will not chemically interact with the porous medium or with other dissolved species. Consequently, except for dispersion phenomena and radioactive decay, tritium can be considered water coincident. This property avoids introducing the additional uncertainties associated with sorption and other chemical reactions during this preliminary application.

The starting point or "initial condition" for the MMT-DPRW Hanford runs was supplied by preparing a hand-interpreted concentration contour map of the tritium plume as of January 1968 (Figure V-1). Tritium values were then read from this interpreted map and entered into the initial condition file of the model. The 1968 tritium concentration contour map was considered the earliest adequate map that could be prepared with reasonable accuracy from historical data. Tritium was not recognized as a fission product until 1958[24] and analysis of tritium in Hanford groundwater did not begin until 1962.[25] A second manually interpreted tritium concentration contour map for January 1976 was constructed using data collected during the last quarter of 1975 (Figure V-2).

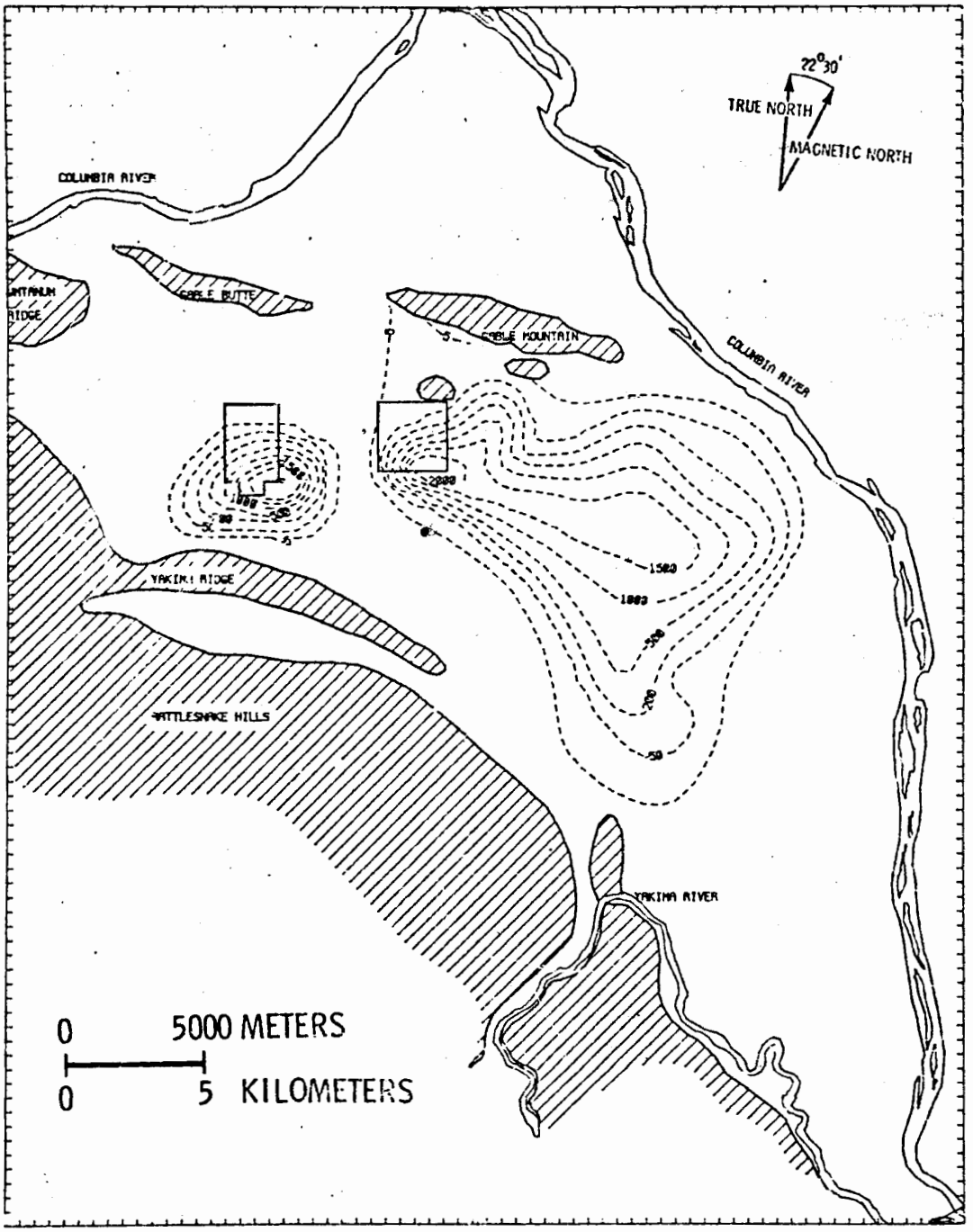

FIGURE V-1. Tritium Simulation Initial Conditions - January 1968 (pCi/ml)

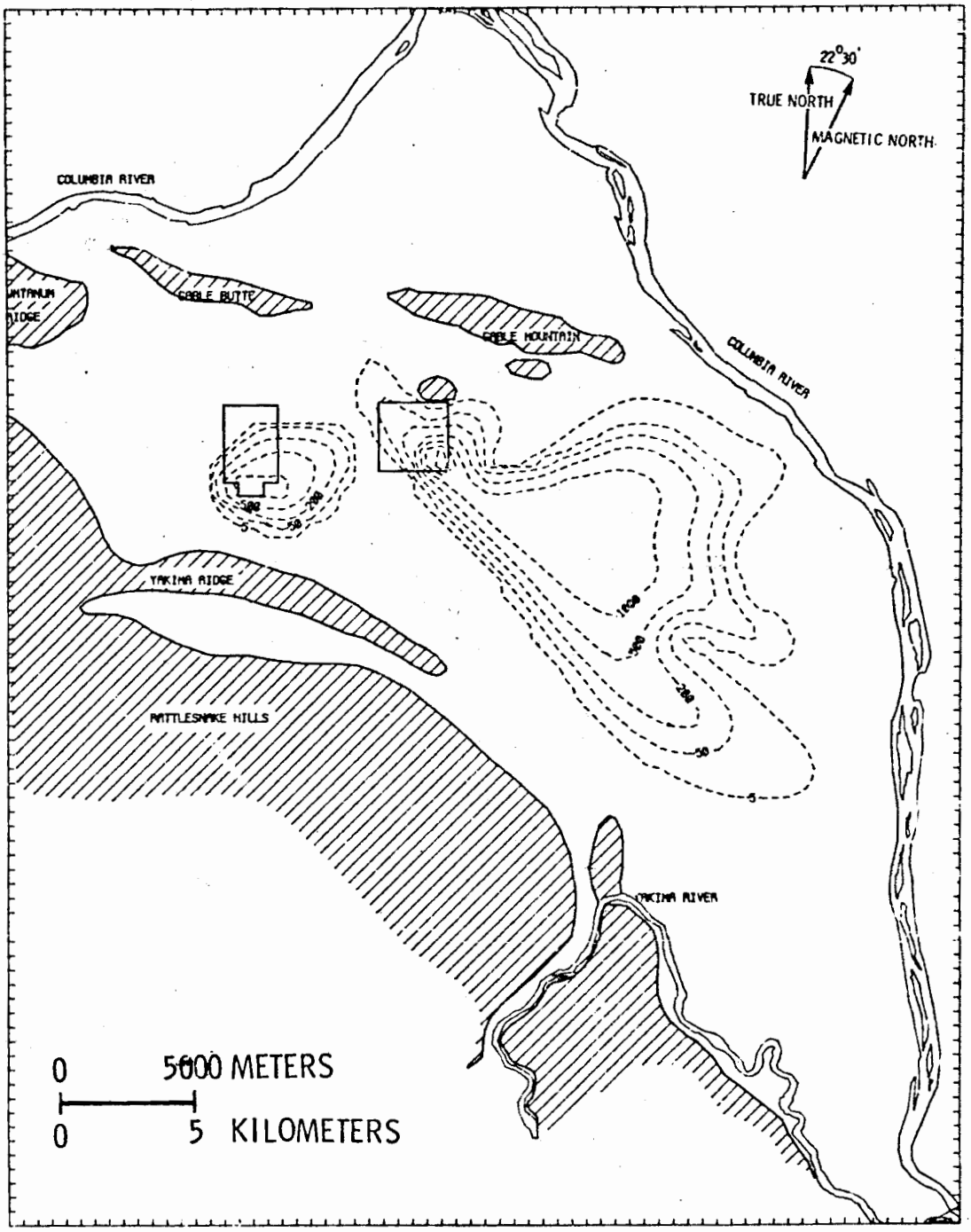

FIGURE V-2. Tritium Simulation Final Conditions - January 1976 (pCi/ml)

It is important to point out that Figures V-1 and V-2 are interpreted maps based upon available analyses of samples from approximately 250 wells. Although the sample density for the radioactive contaminants is probably greater at Hanford than for other comparably sized groundwater systems, considerable judgment and extrapolation is still required to prepare these maps. The result of a model simulation such as that presented in this section is particularly sensitive to inaccuracies, misinterpretations or data gaps in the initial condition distribution (Figure V-1).

For the purposes of this initial application, tritium in the groundwater in the reactor areas north of Gable Mountain and Gable Butte was ignored. The volumes and concentration of significant tritium discharges to groundwater for the 1968-1976 period were obtained from direct measurements wherever possible. It was necessary in some cases to estimate tritium concentrations from an empirical relationship between fuel exposure time and tritium content. Before presenting the model runs, it should be pointed out that the groundwater velocity field is represented by its vertical average value, and the tritium is assumed to be completely mixed over a variable aquifer depth so that the tritium concentration as predicted by the model is also a vertical average. If the groundwater velocity fields are supplied by the VTT flow model, a vertically integrated version of the MMT-DPRW model must be used. This version is necessary because the VTT model is formulated as a vertically integrated model which assumes that the properties of the porous medium as well as the flow field can be adequately represented by their respective vertical averages.

The first MMT-DPRW simulation starting with the 1968 initial condition (Figure V-1) was performed assuming that the tritium from the various near-surface discharge sites was transmitted to the groundwater without delay in the zone between the water table and land surface (vadose zone). The depth to groundwater from the land surface is approximately 300 ft in the southeast portion of the 200 East Area where the most significant tritium discharges were located. The model-predicted tritium plume for January 1976 is shown in Figure V-3. Comparing Figure V-3 with Figure V-2 shows some qualitative agreement but clearly indicates that the predicted tritium plume

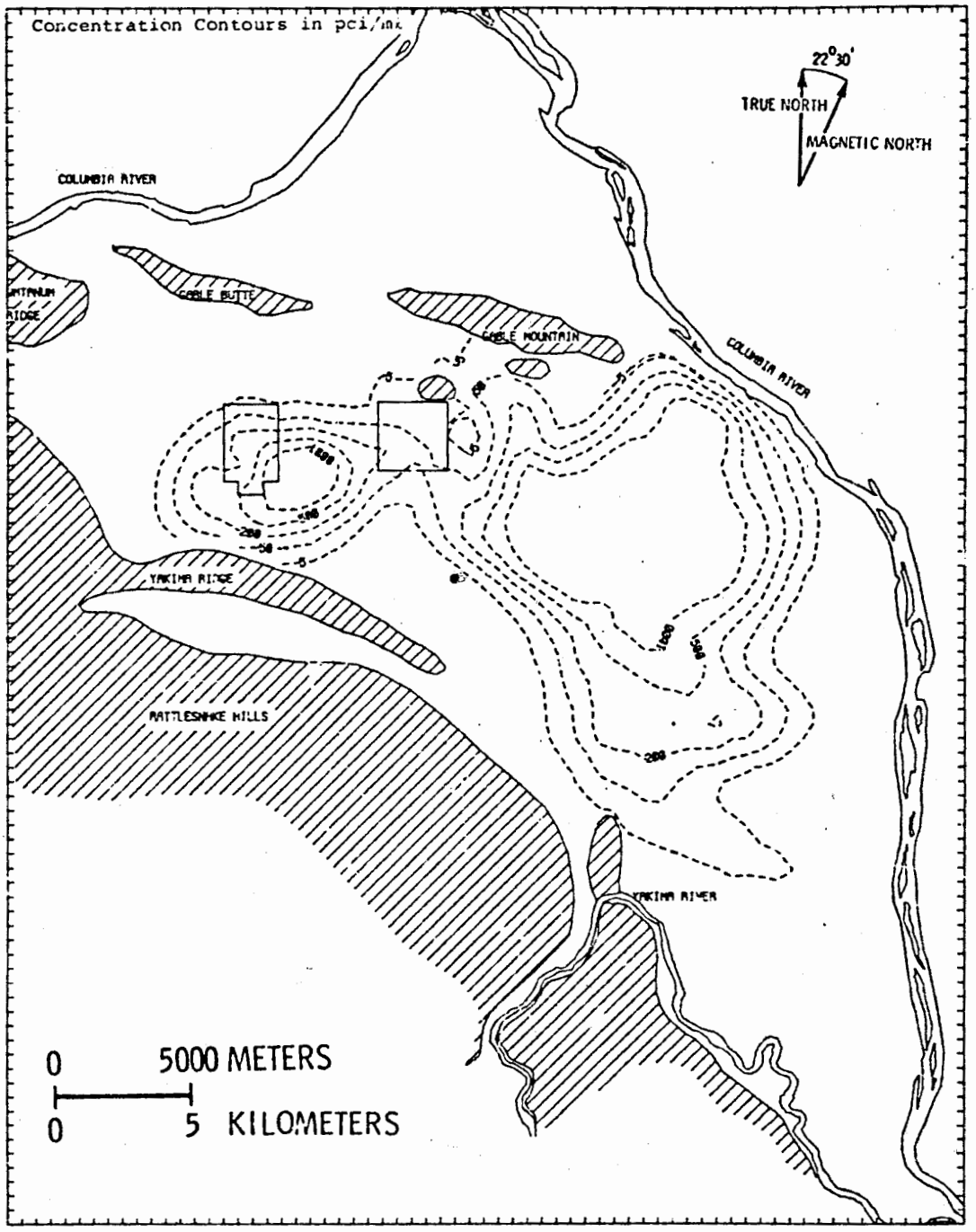

FIGURE V-3. Computed Tritium Concentration Patterns (January 1976) (Estimated 1968-1975 Discharges, with Initial Conditions, No Delay)

is moving too rapidly towards the Columbia River, particularly in the northeast direction. It therefore appears that the approximation of no delay in tritium transit time from the near-surface waste discharge sites to groundwater is probably invalid.

In order to obtain a preliminary evaluation of the effect of the vadose zone delay, a second series of simulations were performed using various delay periods between waste discharge and its appearance in the groundwater. The most satisfactory match was obtained with a delay of 3 years. The results of the 1968-1976 tritium simulation with the 3-year delay in the vadose zone are shown in Figure V-4 and the combined contours from Figure V-2 and Figure V-4 are shown in Figure V-5.

During the course of the model runs, it was determined through trial-and-error procedures that dispersion scalars of 100 ft in the longitudinal and 60 ft in the lateral directions seemed to give the best results relative to the 1976 interpreted map. These values are high compared to typical laboratory values; field values of dispersivity are likely to be much higher than laboratory measurements as a result of unidentified variations in the porous media properties. The lateral dispersivity used herein is much larger relative to the longitudinal dispersivity than has been suggested by de Jong.[22] This may also be due to the unidentified inhomogeneities present in the aquifer system.

Although the model results indicate some qualitative agreement as to the directions of flow, examination of Figure V-5 shows that some important differences between the 1976 interpreted and model-predicted tritium plumes remain. As pointed out earlier, one of the most likely reasons for these differences lies in the preparation of the initial condition surface (Figure V-1). It should also be noted that most of the groundwater samples were collected near the water surface of the unconfined aquifer by lowering a glass bottle enclosed in a steel bail into the water.[26] Thus, the data used in preparing Figures V-1 and V-2 of this report represent at best the surface tritium concentrations and not the vertical average values as calculated by the model (Figures V-3 and V-4).

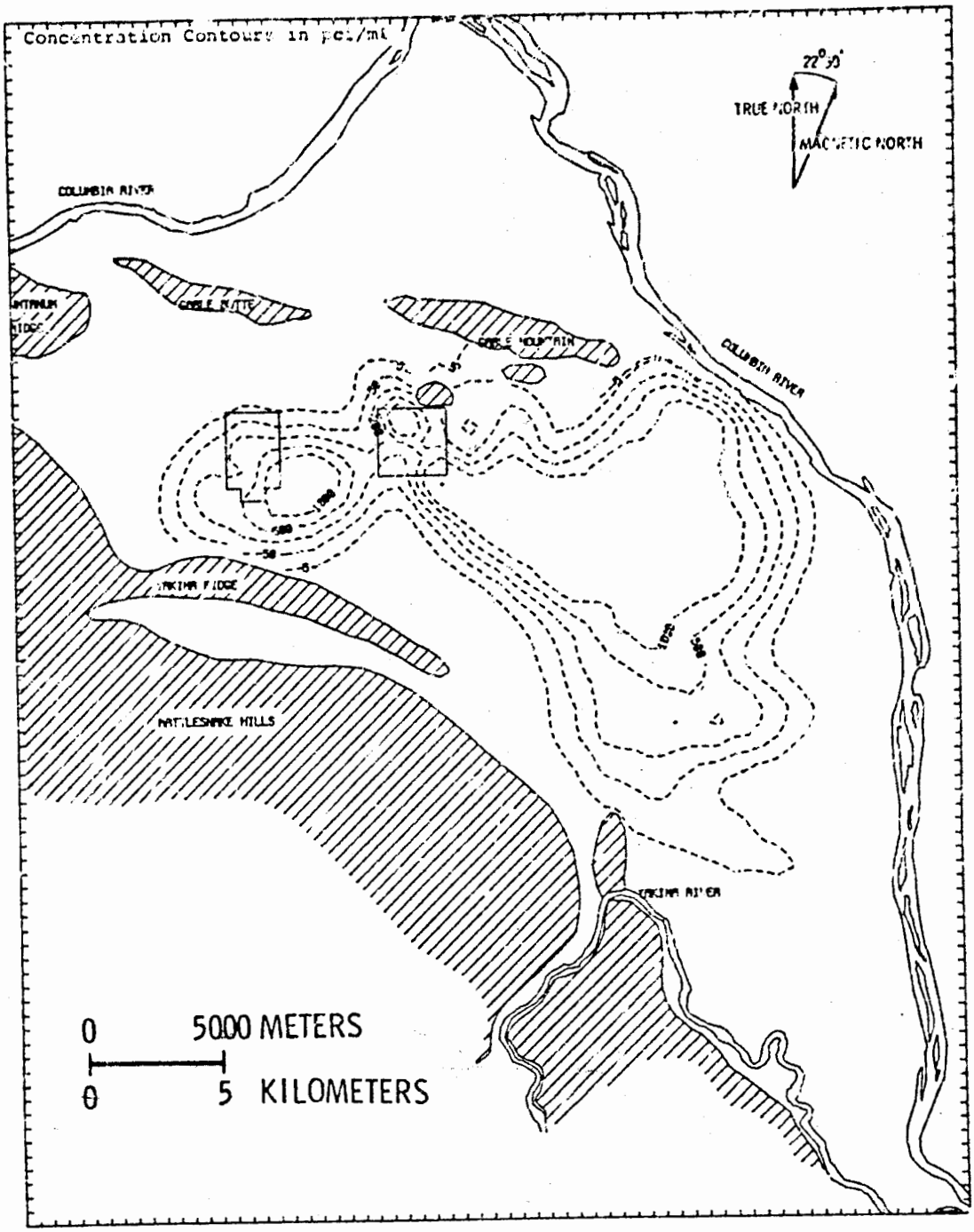

FIGURE V-4. Computed Tritium Concentration Patterns (January 1976) (Estimated 1968-1975 Discharges, with Initial Conditions, 3 Year Delay)

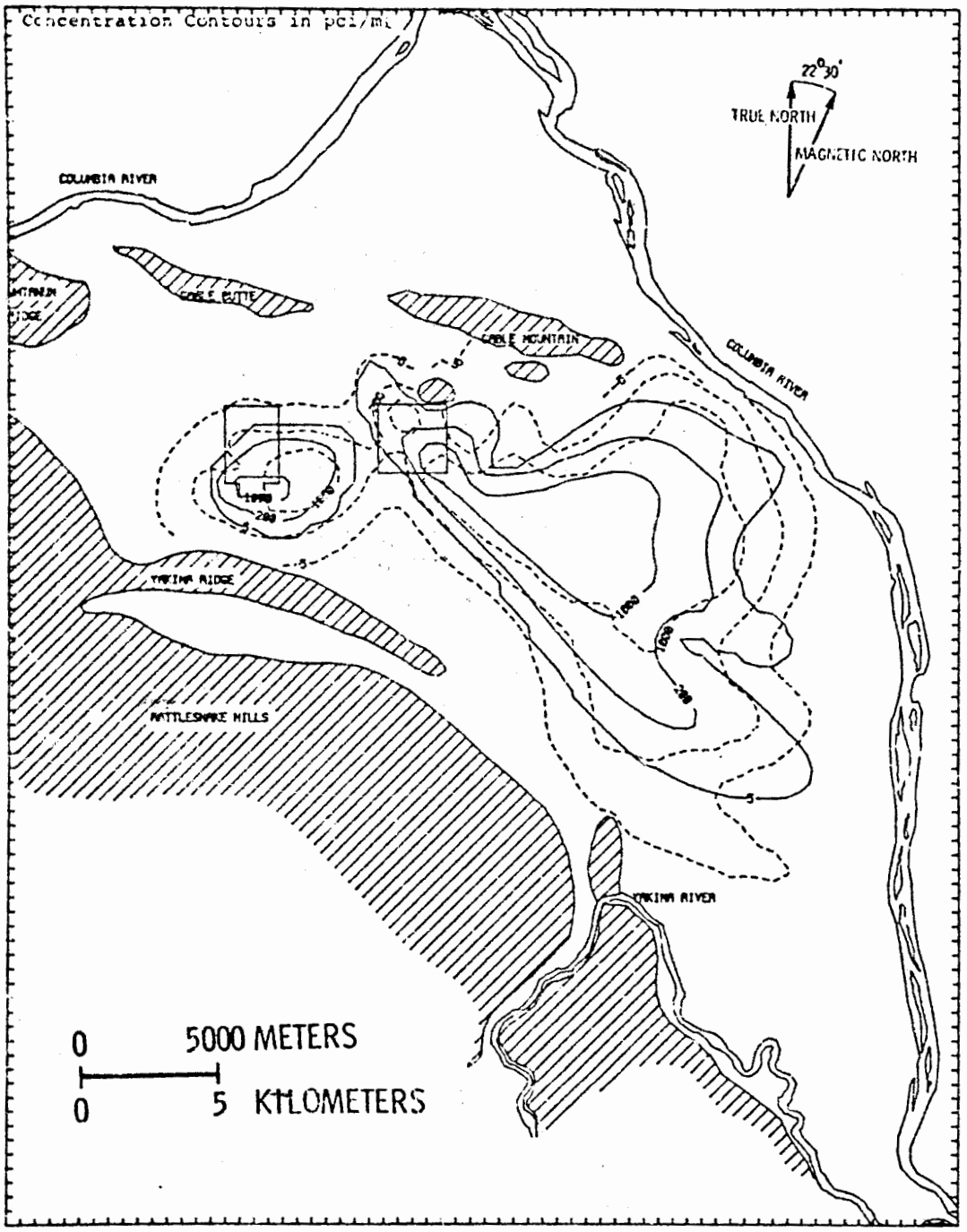

FIGURE V-5. Computed Vs. Estimated Tritium Concentration Patterns (January 1976) (Dotted Line Computed, Solid Line Estimated)

A high degree of vertical mixing may occur near the 200 East Area waste discharge sites where the bulk of the post 1967 tritium has been discharged. However, there is a strong possibility that vertical contaminant stratification exists throughout most of the Hanford groundwater system covered by the tritium plume. A limited study using three-dimensional groundwater models indicates that vertical velocity components may be important in predicting contaminant movement.[27] Vertical velocity components currently are not considered by the VTT flow model[5] and the VTT compatible form of the MMT-DPRW.

Other likely causes for the differences between the model-predicted results and the January 1976 interpreted tritium map are:

- uncertainties in the definition of the system properties such as hydraulic conductivity and porosity,
- uncertainties in the period of delay within the vadose zone,
- uncertainties in the contaminant concentrations of the Hanford plant discharges, and
- uncertainties in the interpretation of the unconfined aquifer bottom.

The Hanford contractor responsible for radioactive waste management, presently the Atlantic Richfield Hanford Company (ARHCO), is proceeding with a comprehensive field data collection program designed to improve characterization and modeling of the Hanford groundwater system. A series of piezometers are being installed to obtain information on vertical groundwater potentials and contaminant distributions. An extensive drilling and pump testing program together with geologic and lithologic studies will allow improved definition of aquifer medium properties and boundaries. Efforts are also being conducted to improve the measurement of both liquid quantities and contaminant concentrations of the active discharges to groundwater recharge sites. In addition, ARHCO is proceeding with a program to adapt three-dimensional flow and transport models to predict vertical groundwater and contaminant movement and to simulate vertical variations in the contaminant distributions.

BLANK PAGE

REFERENCES

1. R. A. Deju, R. E. Gephart, "Hydrologic Management at the Hanford Nuclear Waste Facility," ARH-SA-235, Atlantic Richfield Hanford Company, Richland, WA, 1975.

2. D. A. Myers, et al., Environmental Monitoring Report on the Status of the Groundwater Beneath the Hanford Site, January 1976 - December 1976. BNWL-2199, Battelle, Pacific Northwest Laboratories, Richland, WA, April 1977.

3. R. C. Arnett, et al., Conceptual and Mathematical Modeling of the Hanford Groundwater Flow Regime. ARH-ST-140, Atlantic Richfield Hanford Company, Richland, WA, October, 1976.

4. A. E. Reisenauer, et al., Partially-Saturated Transient Groundwater Flow Model: Theory and Numerical Implementation. BNWL-1713, Battelle, Pacific Northwest Laboratories, Richland, WA, 1975.

5. K. L. Kipp, et al., Variable Thickness Transient Groundwater Flow Model: Theory and Numerical Implementation. BNWL-1703, Battelle, Pacific Northwest Laboratories, Richland, WA, 1972 (updated 1976).

6. G. F. Pinder and H. H. Cooper, Jr., "A Numerical Technique for Calculating the Transient Position of the Saltwater Front," Water Resources Research. 6(3), June 1970.

7. J. R. Eliason and H. P. Foote, Long Beach Generating Station Thermal Transport Modeling Study. Prepared for the Southern California Edison Company, 212B01337, Battelle, Pacific Northwest Laboratories, November 1972.

8. R. B. Bird, W. E. Stewart, and E. N. Lightfoot, Transport Phenomena. John Wiley & Sons, New York, 1966.

9. J. Bear, Dynamics of Fluids in Porous Media. American Elsevier Publishing Co., New York, 1972.

10. F. W. Swartz, "Macroscopic Dispersion in Porous Media: The Controlling Factors." University of Alberta, Edmonton, Canada, submitted to Water Resources Research, June 1976.

11. R. C. Routson, and R. J. Serne, One-Dimensional Model of the Movement of Trace Radioactive Solute Through Soil Columns. BNWL-1718, Battelle, Pacific Northwest Laboratories, Richland, WA, 1972.

12. G. L. Guyman, Mathematical Modeling Movement of Dissolved Constituents in Groundwater Aquifers by the Finite-Element Method. Ph.D. Thesis, Department of Civil Engineering, University of California, Davis, California, 1970.

13. W. Feller, An Introduction to Probability Theory and Its Applications. John Wiley and Sons, New York, 1957.

14. H. Cramer, Mathematical Methods of Statistics. Princeton University Press, Princeton, NJ, 1946.

15. M. S. Bartlett, An Introduction to Stochastic Processes. Cambridge Univ. Press, London, 1956.

16. A. E. Scheidegger, "Statistical Hydrodynamics in Porous Media," J. Appl. Phys. No. 25, 1954.

17. S. Chandrasekhar, "Stochastic Problems in Physics and Astronomy," Rev. Mod. Phys. 15, 1943.

18. G. T. Csanady, Turbulent Diffusion in the Environment. D. Reidel Publishing Co., Boston, 1973.

19. Kai Lai Chung, Elementary Probability Theory with Stochastic Processes. Springer-Verlag, New York, 1974.

20. H. S. Carslaw and J. C. Jaeger, Conduction of Heat in Solids. Oxford University Press, London, 1959.

21. J. Crank, The Mathematics of Diffusion. Oxford University Press, London, 1956.

22. J. De Jong, "Longitudinal and Transverse Diffusion in Granular Deposits," Trans. Amer. Geophysical Union. 39, 1958.

23. D. S. Trent, "Mathematical Modeling of Transport Processes In Aquatic Systems." BNWL-SA-5379, Battelle, Pacific Northwest Laboratories, Richland, WA, April, 1975.

24. E. L Albensivs, "Tritium as a Product of Fission," Physics Review Letters. 3, 1958.

25. W. A. Haney, D. J. Brown, and A. E. Reiserauer, Fission Product Tritium in Separation Wastes and in the Groundwater. HW-74536. August 1962. Available through the National Technical Information Service.

26. D. A. Meyers, et al., Environmental Monitoring Report on the Status Groundwater Beneath the Hanford Site, January-December 1975, BNWL-2034, Battelle, Pacific Northwest Laboratories, Richland, WA, 1976.

27. Hydrology Model Evaluation at the Hanford Nuclear Waste Facility, ARH-C-00017, Intera Environmental Consultants, Inc., Report to Atlantic Richfield Hanford Company, October 1976.

28. Physical and Chemical Oceanographic Characterization of the Cherry Point Site and Vicinity. Battelle, Pacific Northwest Laboratories, Richland, WA, April 1974.

BLANK PAGE

APPENDIX

THE SOIL-WASTE REACTION CHEMICAL SUBMODEL

The current version of the soil-waste reaction submodel that is used by the MMT-DPRW Model embodies an equilibrium constraint approach very similar to that proposed by Routson and Serne.[1] The following discussion is based on their chemical model description given in BNWL-1718. Reaction types considered include ion exchange, precipitation-dissolution, and aqueous complex formation.

Ongoing programs at Hanford[2] have indicated that radionuclides reaching the accessible environment are present only in very minute (trace) amounts. A trace solute, hereafter, referred to as a microion or microsolute, is defined as one whose presence does not measurably affect the chemical behavior of any other species present. In contrast, the appreciable concentrations of some species (macroions or macrosolutes) may affect the sorption of trace radionuclides.

The first-order chemical reactions which mathematically describe the chemical submodel are separately discussed in macrosolute and microsolute categories. Division into these two categories was made for two reasons. First, mathematical simulation of the chemistry of the common macrosolutes in natural (Na, K, Ca, and Mg) soil systems requires successive iterations to calculate the equilibrium states. In contrast, the sorption of a microsolute can be adequately calculated empirically without iteration; thus, computer time is saved by separating the two systems. Secondly, the sorption of trace radionuclides is often so complex that theoretical methods have not been developed to account for all different types of sorption which may occur. The method selected empirically solves the microion sorption reactions.

Macrosolute Chemistry

The macrosolute chemical model represents a mathematical description of the soil-solution interactions between three phases: a cation exchangeable

solid phase, a solution phase, and a crystalline salt phase. Interactions which may occur between these three phases are sorption, ion exchange, complexation, dissolution, and precipitation.

Below the zone of root penetration the finely divided mineral surfaces of the soil solid phase are generally negatively charged. The negative charge results largely from the isomorphous replacement of Al^{+3} for Si^{+4} ions and/or Mg^{+2} and Fe^{+2} for Al^{+3} and to a lesser extent, by hydrolysis of hydroxyl groups which are structurally a part of the soil matrix. To maintain electroneutrality, positively charged ions counter the net negative charge of the soil and are susceptible to exchange with other species in the percolating solution.

Mathematical descriptions of the cation exchange reactions between soil and solution used in the model are a combination of theoretical exchange equations and empirical results. It is assumed that multicomponent exchange reactions can be approximated as a system of binary reactions.

The mass action equation for a general heterogeneous reaction such as:

$$aA^{+m} + B_b{}^{+n}X \rightleftarrows bB^{+n} + A_a{}^{+m}X$$

at constant temperature and pressure can be written as:

$$K = \frac{[B^{+n}]^b \; [A_a{}^{+m}X]}{[A^{+m}]^a \; [B_b{}^{+n}X]} \qquad \text{(A-1)}$$

where

A,B = exchangeable ions in solution or on the soil,

n,m = ionic charge of A or B

X = total solid phase soil matrix,

[ ] = activities of constituents.

Since no direct means currently exists for estimating solid phase soil activities, an empirical approach has been utilized.[3] Data from

batch system experiments for binary exchange reactions were analyzed and found to approximate a linear relationship when plotted as a log-log function. The log of the solute activity ratio:

$$\frac{[B^{+n}]^b}{[A^{+m}]^a}$$

was plotted on the ordinate and the log of the ratio of the concentrations in the soil solid phase,

$$\frac{(B_b{}^{+n}X)}{(A_a{}^{+m}X)}$$

was plotted on the abscissa. The slope of the line yields a solid phase activity correction and the antilog of the intercept yields the empirical selectivity constant. The general empirical exchange expression obtained by this method is:

$$K^* = \frac{[B^{+n}]^b}{[A^{+m}]^a} \left\{ \frac{(A_a{}^{+m}X)}{(B_b{}^{+n}X)} \right\}^p \qquad \text{(A-2)}$$

where

( ) = concentrations of constituents
K^* = selectivity constant
p = empirical activity correction

The activities of the solution phase are defined as:

$$[A] = \gamma_A(A) \qquad \text{(A-3)}$$

where

γ_A = activity coefficient of ion A

The activity coefficient is calculated from Davies' extension of the Debye-Hückel theory at 25°C.[4]

$$-\log \gamma_A = .509\, Z_A^2 \left[\left(\frac{\sqrt{I}}{1+\sqrt{I}} \right) - .2I \right] \qquad \text{(A-4)}$$

where

Z_A = valence of ion A

I = ionic strength of solution.

The ionic strength of the solution is calculated from the expression:[4]

$$I = \frac{1}{2} \sum_{i=1}^{N_i} C_i Z_i^2 \qquad \text{(A-5)}$$

where

C_i = molal concentration of ion i

N_i = number of ionic species in solution.

Dissolution-precipitation reactions in the soil-solution system are represented by their heterogeneous equilibria:

$$A_x B_y(s) \rightleftarrows xA^{+y} + yB^{-x}$$

Slightly soluble salt and complex ion formation reactions are based on the solubility product rule in which the solid phase activity is assumed to be one, so that:

$$K_{sp} \geq [A^{+y}]^x [B^{-x}]^y \qquad \text{(A-6)}$$

The solubility product, K_{sp}, is defined as the product of the activities of the interacting ions at the point of first precipitation. At this point the product reaches its maximum value. Consequently, in solutions devoid of precipitate the product of activities is always less than K_{sp} which necessitates the inequality representation of Equation A-6.

Presently, the submodel considers the effect of binary cation exchange of four species (K^+, Ca^{+2}, Na^+, Mg^{+2}) and the surrounding soil matrix. The effect can be described in terms of a set of any three independent exchange expressions. For example:

$$K^+ + NaX \rightleftharpoons Na^+ + KX$$

$$2Na^+ + CaX \rightleftharpoons Ca^{+2} + Na_2X$$

$$M^{+2} + CaX \rightleftharpoons Ca^{+2} + MgX$$

The empirical equations for calculating the equilibrium concentrations are then: (see Equation A-2)

$$K^*_{Na-K} = \frac{(Na^+)}{(K^+)} \left\{\frac{(KX)}{(NaX)}\right\}^{P_1} \tag{A-7}$$

$$K^*_{Ca-Na} = \frac{\gamma_{Ca}(Ca^{+2})}{\gamma_{Na}{}^2(Na^+)^2} \left\{\frac{(Na_2X)}{(CaX)}\right\}^{P_2} \quad \text{and} \tag{A-8}$$

$$K^*_{Ca-Mg} = \frac{(Ca^{+2})}{(Mg^{+2})} \left\{\frac{(MgX)}{(CaX)}\right\}^{P_3} \tag{A-9}$$

It should be noted that the activity coeffficients of like valenced ions in the same ionic strength solution are equal and thus cancel out in Equations A-7 and A-9. A careful examination of these equations reveals that all other binary exchanges, i.e., K-Ca, can be represented as a linear combination of the above (A-7, A-8, A-9) expressions, and consequently do not constitute additional independent relationships.

Two slightly soluble salts and one complex ion formation are also included in the present chemical submodel. These are gypsum ($CaSO_4 \cdot 2H_2O$), limestone ($CaCO_3$), and undissociated calcium sulfate $(CaSO_4)_{aq}$.

The equilibrium concentrations for the gypsum reaction,

$$CaSO_4 \cdot 2H_2O\downarrow \rightleftarrows Ca^{+2} + SO_4^{-2} + 2H_2O$$

are determined using the solubility product rule and assuming the activity of water to be one. The mass action equation is then:

$$K_{Sp} = \left[Ca^{+2}\right]\left[SO_4^{-2}\right] = \gamma_{Ca}(Ca^{+2})\ \gamma_{SO_4}(SO_4^{-2}) \qquad \text{(A-10)}$$

The reaction of the aqueous complex calcium sulfate,

$$CaSO_4(aq) \rightleftarrows Ca^{+2} + SO_4^{-2}$$

is modeled using the dissociation constant as follows:

$$K_{diss} = \frac{\left[Ca^{+2}\right]\left[SO_4^{-2}\right]}{[CaSO_4]\ aq} = \frac{\gamma_{Ca}(Ca^{+2})\ \gamma_{SO_4}(SO_4^{-2})}{(CaSO_4)_{aq}} \qquad \text{(A-11)}$$

The activity coefficient of the undissociated species, γ_{CaSO_4}, is one as predicted by Equation A-4.

The solubility of limestone is calculated using the solubility product rule and carbonic acid equilibria relationships. Since bicarbonate (HCO_3^-) is more easily measurable in the soil-solution system than carbonate (CO_3^{-2}), it is convenient to consider the overall reaction:

$$Ca^{+2} + 2HCO_3^- \rightleftarrows CaCO_3\downarrow + H_2CO_3$$

The equilbrium equation is:

$$K = \frac{\left[CaCO_3\right]_s\left[H_2CO_3\right]}{\left[Ca^{+2}\right]\left[HCO_3^-\right]^2} \qquad \text{(A-12)}$$

The activity of carbonic acid is a constant if the partial pressure of carbon dioxide is constant:

$$CO_{2\ (g)} + H_2O_{(\ell)} \rightleftarrows H_2CO_3$$

yielding,

$$\frac{[H_2CO_3]}{[H_2O][CO_2]} = \frac{[H_2CO_3]}{P_{CO_2}(g)} = K_o \qquad \text{(A-13)}$$

where K_o is an equilibrium constant, and $P_{CO_2}(g)$ is the partial pressure of CO_2 in the ambient atmosphere. The partial pressure of CO_2 in the earth's atmosphere at sea level is relatively constant at $10^{-3.5}$ atm., hence the activity of H_2CO_3 can be assumed to be a constant, K_o':

$$[H_2CO_3] = K_o\ (P_{CO_2}) = K_o' \qquad \text{(A-14)}$$

The first and second ionization constants of carbonic acid, K_1 and K_2, are given by:

$$\frac{[H^+]\ [HCO_3^-]}{[H_2CO_3]} = K_1 \qquad \text{(A-15)}$$

$$\frac{[H^+]\ [CO_3^{-2}]}{[HCO_3^-]} = K_2 \qquad \text{(A-16)}$$

Combining Equations A-13, A-14, and A-15 gives:

$$\left[CO_3^{-2}\right] = \frac{K_2}{K_1 K_o'}\ [HCO_3^-]^2 \qquad \text{(A-17)}$$

The solubility product constant of limestone is given by:

$$K_{sp}' \geq [Ca^{+2}]\ [CO_3^{-2}] \qquad \text{(A-18)}$$

assuming again that the activity of the solid phase is unity. Substituting Equation A-17 for $[CO_3^{-2}]$, yields the final carbonate equilibria relationship:

$$\frac{K'_{sp} K_1 K'_o}{K_2} \geq \gamma_{Ca}(Ca^{+2}) \quad \gamma^2_{HCO_3} (HCO_3^-)^2 \qquad \text{(A-19)}$$

In the soil-waste model, anion exchange is considered negligible. Anions other than those involved in slightly soluble salt or complex ion formation are considered to be non-reactive.

It should be noted that inherent in the model is the assumption that the influent seepage velocity is slow enough to allow chemical equilibria to be attained continuously throughout the system. Percolation velocities have generally been found to be slow enough to justify the use of this assumption at Hanford.

Microsolute Chemistry

Microions species are assumed to be present in such small quantities that they do not measureably affect the macroion chemistry or the behavior of other microions. The sorption of micro constituents is modeled as a specialized exchange reaction.

A general expression for ion exchange of a trace species (microion) in a macroion environment may be formulated as a replacement reaction:

$$xC_{micro} + A_{macro} \rightleftharpoons yC_{macro} + A_{micro}$$

where C indicates a fluid phase consituent and A indicates the presence of the constituent in the soil matrix. This expression indicates the competition between the micro and macroions for sorption sites on the soil. The mass action relationship for this system at equilibrium is:

$$K = \frac{[C_{macro}]^y \; [A_{micro}]}{[A_{macro}] \; [C_{micro}]^x} \qquad \text{(A-20)}$$

Several approximations can be made to simplify Equation A-20 for a system consisting of simple binary exchange of like valenced (x=y) macro and trace constituents. Because of the very minute quantities of microion present, the soil concentration of macroions (A_{macro}) can be assumed to be essentially independent of microion concentration. Similarly, the small amount of macroions displaced by sorbed microions will not significantly alter the liquid phase macroion concentration (C_{macro}) that is present in the absense of micro constituents. With these assumptions Equation A-20 can be rewritten as:

$$K\frac{(A_{macro})}{(C_{macro})}\gamma' = \frac{(A_{micro})}{(C_{micro})} \qquad \text{(A-21)}$$

where $\gamma' = \dfrac{\gamma_{A_{macro}}\ \gamma_{C_{micro}}}{\gamma_{C_{macro}}\ \gamma_{A_{micro}}}$

which is also assumed to be constant with respect to microion concentration. When written in this form it is apparent that the expression on the left side of Equation A-21 represents a microion distribution (or sorption) coefficient which can be represented by K_d. The sorbed microion concentration can then be expressed as:

$$A = K_d\ C \qquad \text{(A-22)}$$

where the micro subscripts have been dropped for convenience.

Obviously, in the above formulation K_d is a function of the type of macroion that is being displaced. In more complex (three or more component) systems the observed K_d becomes a function of all of the macro constituents in solution. It then becomes necessary to experimentally determine the distribution coefficient, K_d, for each microion of interest as a function of macroion concentrations.

The investigation of the effects of the macroion variables on K_d is amenable to factorial experimentation. Factorial experiments allow the study of the effects of several variables and their interactions in one experimental design. The experimental procedures and multiple regression techniques used to quantify the functional relationship of K_d and macroion concentrations for some Hanford soil-waste systems are detailed in BNWL-1721.[5]

As an example, the following procedure was used to calculate an empirical K_d function for the radionuclide strontium (^{85}Sr). It was determined that the macroions in a typical Hanford soil solution which compete with strontium in the cation exchange-sorption reactions include Ca^{+2}, K^+, Na^+, and H^+ (pH). A 2^4 factorial, batch system, sorption experiment was set up to determine the effects of the above four variables on strontium sorption. Two levels of concentration for each variable, high (H) and low (L), were permuted to yield sixteen observations (see Table A-1).

TABLE A-1. Permutation Used in the Factorial Design Experiment

Experiment Number	Ca^{+2}	K^+	Na^+	pH
1	H	H	H	H
2	H	H	H	L
3	H	H	L	H
4	H	H	L	L
5	H	L	H	H
6	H	L	H	L
7	H	L	L	H
8	H	L	L	L
9	L	H	H	H
10	L	H	H	L
11	L	H	L	H
12	L	H	L	L
13	L	L	H	H
14	L	L	H	L
15	L	L	L	H
16	L	L	L	L

The observed K_d values were statistically analyzed to yield the four main and twelve interaction effects of the variables studied. These sixteen effects are used as the multiple linear regression coefficients in an equation describing K_d as a function of the four variables studied. Within the range of pH investigated (5-8) this variable was found to have little influence on strontium sorption and was neglected in further calculations.

The K_d predictor equation becomes:

$$K_{d(Sr)} = aX_{Ca}+bX_{Na}+cX_K+dX_{Ca}X_{Na}+eX_{Ca}X_K+fX_{Na}X_K+gX_{Ca}X_{Na}X_K \qquad \text{(A-23)}$$

where a,..., g are the coefficients derived from the factorial design experiment and $X_{(i)}$ are normalized concentration variables covering the range of concentration (H-L) used in the factorial experiment. For example:

$$X_{Ca} = \frac{(Ca) - \frac{1}{2}(H_{Ca} + L_{Ca})}{\frac{1}{2}(H_{Ca} - L_{Ca})} \qquad \text{(A-24)}$$

where

H_{Ca} = high calcium concentration used in the factorial design experiment

L_{Ca} = low calcium concentration used in the factorial design experiment

(Ca) = value of calcium concentration for which K_d is being calculated

The $X_{(i)}$ variables will lie between ±1 for any concentration within the range used in the factorial design experiment.

Equation A-23 is an approximation of a phenomenon which is complex and often nonlinear. Therefore, to obtain a more accurate fit, the variables' concentration ranges were subdivided and separate factorial experiments were performed for each smaller range. Additional details of the experimental studies can be found in BNWL-1719.[6]

Computation of Radionuclide Sorption

As seen above, the chemical submodel in current use by the MMT-DPRW model is a semi-empirical equilibrium constraint type of formulation with the built in assumption that the soil-waste reactions occur rapidly with respect to the flowrate of the groundwater system so that the system is essentially always at equilibrium.

The model divides the subsurface into a finite number of rectangular solids referred to as cells (Figure III-1). At the end of each time step the material that has been transported into each cell is required to be in chemical equilibria. The mass of each macro element is redistributed among the species present as specified by the equations that describe the equilibirum state. When the macroion equilibria has been determined, the sorption coefficient for each micro species present is evaluated from an expression of the form of Equation A-23. The change in microion concentration as a result of sorption processes is then calculated as follows.

For simplification a single cell in a system with only one trace contaminant is considered. At the end of time step n the concentration of the fluid and solid phases of this tracer within the cell are C^n and A^n, respectively. Advection and dispersion then take place and the fluid concentration changes to the intermediate value, C^*. After this cell has equilibrated, the concentrations at the n+1 time level will be given by:

$$A^{n+1} = A^n + \Delta A^{n+1} \qquad \text{(A-25)}$$

$$C^{n+1} = C^* + \Delta C^{n+1} \qquad \text{(A-26)}$$

From Equation A-22 we know that:

$$A^{n+1} = K_d^{n+1} C^{n+1} \qquad \text{(A-27)}$$

or

$$\Delta A^{n+1} = K_d^{n+1} (C^* + \Delta C^{n+1}) - A^n \qquad \text{(A-28)}$$

From quation A-22 we also know that:

$$A^n = K_d^n C^n \tag{A-29}$$

The change of mass of tracer in the fluid phase must equal the change of mass in the solid phase if mass is to be conserved. If soil concentrations are expressed in terms of mass of microion/mass of soil and the fluid concentration are given in terms of mass of microion/volume of fluid, the changes in concentrations in each phase are related by:

$$\Delta C^{n+1} = -\beta \Delta A^{n+1} \tag{A-30}$$

where

β = the soil-to solution ratio $[M/L^3]$

Substituting A-29 and A-30 into A-28 solving for ΔC^{n+1} gives:

$$\Delta C^{n+1} = \frac{\beta(K_d^n C^n - K_d^{n+1} C^*)}{1 + \beta K_d^{n+1}} \tag{A-31}$$

Using the results of A-31, Equation A-26 can now be rewritten as:

$$C^{n+1} = \frac{C^* + \beta K_d^n C^n}{1 + \beta K_d^{n+1}} \tag{A-32}$$

Using the nomenclature of Section III, Equation A-32 would be expressed as:

$$\rho_{ijl}^{k,n+1} = \frac{\rho_{ijl}^{k,*} + \beta K_d^n \rho_{ijl}^{k,n}}{1 + \beta K_d^{n+1}} \tag{A-33}$$

The new parcel weights as a result of sorption can then be computed by Equation III-20.

APPENDIX

REFERENCES

1. R. C. Routson, and R. J. Serne, One-Dimensional Model of the Movement of Trace Radioactive Solute Through Soil Columns. BNWL-1718, Battelle, Pacific Northwest Laboratories, Richland, WA, 1972.

2. B. F. Hajek, "Trace Strontium and Cesium Equilibirum Distribution Coefficients: Batch and Column Determinations." BNWL-SA-843, 1968.

3. R. M. Garrels and C. L. Christ, Solutions, Minerals, and Equilibria. Harper and Row, NY, pp. 267-276, 1965.

4. J. N. Butler, Ionic Equilibrium. Addison-Wesley, Reading, MA, p. 48, 1964.

5. R. J. Serne, et al., Experimental Methods for Obtaining PERCOL Model Input and Verification Data. BNWL-1721, Battelle, Pacific Northwest Laboratories, Richland, WA, 1973.

6. R. C. Routson and R. J. Serne, Experimental Support Studies for the PERCOL and Transport Models. BNWL-1719, Battelle, Pacific Northwest Laboratories, Richland, WA, 1972.

APPENDIX SYMBOLS

A,B	exchangeable ions in solution or on the soil matrix
A^i	soil phase concentration of tracer at time level i $[m/L^3]$
Ca^{+2}	calcium ion
CO_2	carbon dioxide gas
CO_3^{-2}	carbonate ion
C^i	fluid phase concentration of tracer at time level i $[m/L^3]$
C_i	molal concentration of ion i $[m/L^3]$
H_2O	water
HCO_3	bicarbonate ion
H_i	high concentration of species i in factorial $[m/L^3]$ experiment
I	total ionic strength of solution
K^+	potassium ion
K_d	sorption coefficient $[L^3/m]$
K_{sp}	solubility product
K^*_{ij}	selectivity constant of i-j exchange
K_o, K, K_2	equilibrium constants
L_i	low concentration of species i in factorial $[m/L^3]$ design experiment
Mg^{+2}	magnesium
m,n	ionic charge of A and B
Na^+	sodium ion
N_i	number of ionic species in solution
P_i	emperical activity correction parameter of i^{th} exchange
SO_4^{-2}	sulfate ion
X	total solid phase soil matrix
X_i	normalized concentration variable of species i in factorial design experiment

x,y	stoichiometric coefficients of A and B
Z_i	Valance of ion i
[ ]	enclosed quantity is an activity
( )	enclosed quantity is a concentration
B	soil to solution ratio $[m/L^3]$
γ_i	activity coefficient of ion i

END

DATE FILMED

1/26/78